FINAL REPORT

PROJECT NO. RSCH010-983
VERMONT DEPARTMENT OF TRANSPORTATION

"Full-Scale Pilot Study to Reduce Lateral Stresses in Retaining Structures Using GeoFoam"

by

Alan J. Lutenegger
Professor of Civil & Environmental Engineering

and

Matt Ciufetti
Graduate Research Assistant

Department of Civil & Environmental Engineering
University of Massachusetts
Amherst, Ma. 01003

5/31/09

1. Report No.	2. Government Accession No.	3. Recipient's Catalog No.
2009-3		

4. Title and Subtitle	5. Report Date
Full-Scale Pilot Study to Reduce Lateral Stresses in Retaining Structures Using GeoFoam	June 2009
	6. Performing Organization Code

7. Author(s)	8. Performing Organization Report No.
Alan J. Lutenegger, Matt Ciufetti	2009-3

9. Performing Organization Name and Address	10. Work Unit No.
Department of Civil & Environmental Engineering University of Massachusetts Amherst, Ma. 01003	11. Contract or Grant No.

12. Sponsoring Agency Name and Address	13. Type of Report and Period Covered
Vermont Agency of Transportation Materials and Research Section National Life Building Drawer 33 Montpelier, VT 05633-5001	Final
	14. Sponsoring Agency Code

15. Supplementary Notes

16. Abstract

A field study was performed during the construction of a full-scale bridge of the influence of GeoFoam backfill to study the lateral earth pressures on the back of the rigid concrete abutments developed using the GeoFoam as an alternative to conventional granular backfill. Both abutments of a single span bridge were instrumented and were monitored for approximately 16 months. The results of the instrumentation showed that the use of GeoFoam reduced the lateral earth pressures substantially. In addition, the GeoFoam absorbed vertical stresses from the overlying granular fill and approach slab.

17. Key Words	18. Distribution Statement
Earth Pressures, GeoFoam, Abutment	Document available to the public through the sponsoring agency

19. Security Classif. (of this report)	20. Security Classif. (of this page)	21. No. Pages	22. Price
Unclassified	Unclassified	142	

ABSTRACT

A field study was performed during the construction of a full-scale bridge of the influence of GeoFoam backfill to study the lateral earth pressures on the back of the rigid concrete abutments developed using the GeoFoam as an alternative to conventional granular backfill. Both abutments of a single span bridge were instrumented and were monitored for approximately 16 months. The results of the instrumentation showed that the use of GeoFoam reduced the lateral earth pressures substantially. In addition, the GeoFoam absorbed vertical stresses from the overlying granular fill and approach slab.

CHAPTER 1. INTRODUCTION AND SCOPE OF WORK

The design of earth retention structures represents a complex balance of load versus resistance. The design must be approached systematically in order to achieve the necessary factors of safety against both internal (structural capacity) and external (soil shear resistance) failure. In the design of bridge approaches, internal stability of the bridge abutment requires adequate resistance to the lateral earth pressures acting upon the abutment due to the approach embankment. External stability of the system requires that the foundation soils have adequate shear strength to support the bearing pressures of the abutment and approach embankment and result in minimal settlements. A common approach to achieving the desired factors of safety against internal and external failures is to base the design upon load combinations that exceed the predicted maximum loads. This can result in considerable increases in construction costs, as adequate resistance to the larger loads may require increased quantities of building materials to provide internal stability and complicated foundation designs to provide external stability.

An alternative approach is the use of an alternative lightweight fill material for the construction of the approach embankment, which can effectively achieve the desired factors of safety by reducing the actual loads within the system rather than by increasing the resistance. One such lightweight fill material is expanded polystyrene (EPS) in block form, or GeoFoam. The extremely low density of GeoFoam in comparison with that of conventional backfill soil significantly reduces both vertical and lateral stresses on the system while the durability of the material makes it ideal for fill applications. GeoFoam has been successfully used on several major projects, including the Central Artery Project in Boston, MA, and has been the subject of several previous studies to determine the engineering behavior of the material when functioning as a fill material. As additional research is conducted, a further understanding of the advantages of GeoFoam as a lightweight fill material may result in its more widespread use.

The primary objective of this research was to evaluate the performance of EPS GeoFoam in reduction of lateral and vertical earth pressures by conducting a full-scale pilot study. EPS GeoFoam was used to construct the approach embankments of a single span bridge. Instrumentation installed during construction provided direct measurements of vertical stresses within the approach embankments and lateral stresses acting upon the abutment walls.

This project represents a collaborative effort between the University of Massachusetts Amherst Department of Civil and Environmental Engineering and the Vermont Agency of Transportation (VTrans). The laboratory testing program was conducted between 2006 and August 2007 at the University of Massachusetts Amherst Geotechnical Engineering Laboratories. The field study was conducted in Leicester, Vermont, from July 2006 to August 2007.

A laboratory testing program consisting of soil classification and composition analysis, one-dimensional consolidation tests, and laboratory vane undrained shear tests was conducted on undisturbed tube samples obtained from the field site prior to construction of the bridge. Logs from five boreholes containing Standard Penetration Test (SPT), Field Vane Test (FVT), and laboratory soil classification data obtained by VTrans were also provided. The data obtained from both laboratory and in situ tests were used to present a characterization of the site.

The field study consisted of oversight of the construction of the bridge as well as an instrumentation program. Various stages of the construction process were documented including excavation, installation of pile foundations, abutment construction, and installation of the GeoFoam fill. Following the removal of the abutment concrete two total earth pressure cells were mounted flush with the face the back wall of each abutment into order to measure lateral pressures. During the placement of the GeoFoam fill, one total earth pressure cell was placed horizontally to measure vertical pressures at the bearing elevation of each GeoFoam embankment and three total earth pressure cells were placed horizontally to measure vertical pressures at acting upon each GeoFoam embankment. A total of 12 total earth pressure cells were installed and wired into jumper boxes located on the front wall of each abutment footing. During the remainder of the construction process periodic pressure and temperature measurements were recorded. After completion of the bridge, monthly pressure and temperature measurements were recorded until the conclusion of the field study.

CHAPTER 2 BACKGROUND – GEOFOAM IN GEOTECHNICAL CONSTRUCTION

2.1 EPS GeoFoam

The manufacture of rigid plastic foams dates back to the 1950s, with adaptation for geotechnical use occurring in the early 1960s. In 1992, the category of "GeoFoam" was proposed as an addition to the variety of geosynthetics already in existence. The most commonly used GeoFoam material is a polymeric form called expanded polystyrene (EPS), also known as expanded polystyrol outside of the United States. Such widespread use can be attributed to global availability, significantly lower cost than other materials, and the absence of post-production long-term release of gases such as formaldehyde or CFC, a behavior observed with other polymeric forms (Horvath 2004).

The most common method of producing EPS GeoFoam is block molding, in which a mold is used to create a prismatic rectangular block. Depending upon the application, other mold shapes can be used, however it is more common to shape the blocks post-production (Horvath 1994). The raw material used to create GeoFoam is referred to as expandable polystyrene, or often resin, and is composed of small beads with diameters similar to medium to coarse sand (0.2 to 3 mm). The bead size chosen will not ultimately affect the engineering properties of the completed block (Horvath 1994). The beads are composed of polystyrene and a dissolved petroleum hydrocarbon, usually pentane or rarely butane, which acts as the blowing agent. The beads may also contain other additives to affect certain properties of the completed block (flammability, etc.), however this is dependent upon the application in a similar fashion to the addition of admixtures in concrete (Stark et al. 2004).

The density of EPS GeoFoam is controlled primarily through regulation of the manufacturing. It has been found that even with a well-controlled manufacturing process, there will still be variability in density between blocks from the same production run, as well as a density gradient within each block. This can affect the geotechnical properties of the material, as density has been found to be a controlling factor in the performance of the GeoFoam (Horvath 1994). The actual range of densities that EPS blocks can be manufactured is between approximately 10 kg/m^3 (0.6 lb/ft^3) and 100 kg/m^3 (6 lb/ft^3) (Stark et al. 2004). The low density of EPS GeoFoam results in the development of uplift forces when submerged in water, and therefore for many design situations an anchor system or adequate surcharge load (e.g. soil cover) is required (Negussey 1997).

The dimensions of GeoFoam blocks affect only cost and construction layout, and not the engineering properties of the blocks. There are no standard sizes for EPS block molds and given the numerous applications of GeoFoam blocks and abundant manufacturers (over 100 in the United States), there is much variability in dimensions of raw GeoFoam blocks. Typically designers attempt to use full-sized blocks and when necessary blocks can be cut to shapes in-situ with a hot wire or, less effectively, a chainsaw. An alternative to in situ shaping of the blocks is custom manufacture of the block mass, in which the EPS producer uses the construction plans to develop an efficient layout for the block mass, however this is usually reserved for complex projects due to the associated increases in cost (Stark et al. 2004).

EPS GeoFoam has proven to be quite durable when exposed to common natural elements. Polystyrene is non-biodegradable, and is inert in both soil and water (Horvath 1994). Exposure to ultraviolet (UV) radiation from sunlight causes only cosmetic discolorations, and only after an extended period of time, allowing for a window of exposure time during the construction period. Exposure to water may result in a small amount of absorption, the magnitude of which is inversely proportional to the density of the GeoFoam and is dependent upon numerous factors such as GeoFoam block thickness, surrounding hydraulic gradients, and the phase of the water. Water absorption does not affect the volume of the EPS, and there is no effect on mechanical properties (Horvath 1994).

Exposure to certain substances and conditions can result in damage to the polystyrene. The use of polystyrene in transportation projects risks the material coming into contact with common fuels, which polystyrene will readily dissolve in, or road salts, however this risk is usually eliminated through the proper installation of a barrier such as an impermeable membrane (Horvath 1994). Polystyrene can be flammable when exposed to an ignition source, as is the blowing agent used in production. An additive, usually consisting of a bromine-based chemical, added to the expandable polystyrene causes the material to become flame retardant. The issue of ignition of the flammable blowing agent is resolved by allowing adequate seasoning time of the EPS block in order to allow outgassing to occur. Flame retardant EPS can still melt when exposed to extreme temperatures between approximately 150 and 260°C, however maximum exposure temperatures for design conditions are usually considerably lower (Stark et. al. 2004).

The thermal conductivity of dry EPS GeoFoam is affected by the density of the material, which can be controlled during the manufacturing stage, and the ambient temperature. Generally, the thermal conductivity of dry EPS GeoFoam is approximately 30 to 40 times less than that of soil, making it a very efficient insulator. The effect of absorbed water upon thermal conductivity is more difficult to quantify, given the numerous factors affecting the volume of water uptake (Stark et. al. 2004). As water has a higher thermal conductivity than dry EPS GeoFoam, moisture absorption is expected to result in an increase in thermal conductivity. Even under extreme cases of moisture absorption, EPS GeoFoam serves as a better insulator than soil (Horvath 1994).

2.2 Engineering Properties of EPS GeoFoam Blocks

In addition to material properties such as density, a variety of other factors must be considered when selecting the appropriate EPS GeoFoam material for a project. It should be noted that, in a similar fashion to soil, small specimens of EPS GeoFoam are often used to determine material behavior as it is difficult if not impossible to test the entire block. Given internal variations within each block, it is very possible that there will be some error in predicting the performance of an entire block based upon such small test specimens. However, this associated error may not be detrimental to the project (Stark et. al. 2004). Generally, the most important aspects of GeoFoam block behavior involve performance under compression loading in both short-term and long-term durations. Other modes of loading such as tension, flexure, and especially shear may be of importance when analyzing the overall stability of a project.

General compressive behavior of EPS is usually determined by laboratory testing of 50mm (2 in.) cubes under strain-controlled unconfined axial loading at rates of up to 20% strain per minute, with 10% being the most common within the current literature (Horvath 1994). Other forms of testing may be performed to determine differences in behavior under varied test conditions such as cyclic loading and the application of confining pressures, which will be covered in subsequent sections.

A typical stress-strain curve is shown in Figure 2.1. It is obvious that the traditional definitions of failure of EPS GeoFoam do not apply. Solid material failure is defined by rupture along a plane, as in concrete or steel. Particulate material failure occurs in the form of inter-particle slippage and the development of steady-state or residual strength. EPS failure consists of crushing of the material in one dimension back to the original solid polystyrene state (Stark et. al., 2004). The stress-strain response of EPS GeoFoam can be divided into four zones consisting of initial linear response (Zone 1), yielding (Zone 2), post-yield linear work hardening (Zone 3), and post-yield nonlinear work hardening (Zone 4) (Stark et. al. 2004).

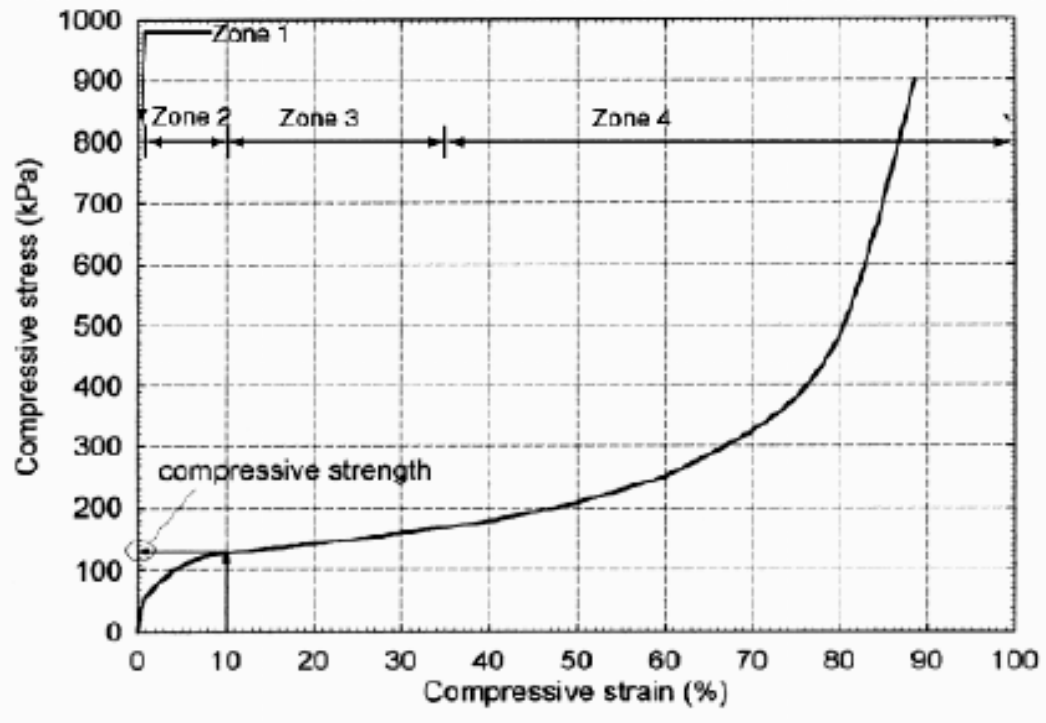

Figure 2.1. Typical Stress-Strain Response of 21 kg/m^3 EPS Geofoam at 10% strain per minute (from Stark et. al. 2004).

Most studies have found the extent of the initial linear-elastic portion of the curve to be up to 2% strain, however some researchers have reported slight downward concavity of the curve in a range of up to 1%. It has now been commonly accepted that the elastic limit stress, σ_e, corresponds to a compressive strain of 1%. This is because at such a small strain time-dependent effects are generally negligible, and the resulting stress value will be fairly conservative. The elastic limit stress increases with increasing EPS density (Horvath 1994). The slope of the linear

elastic range is defined as the initial tangent Young's modulus, E_{ti}. Most data display a correlation between EPS density and E_{ti}.

Following the initial linear elastic behavior is a zone of yielding as yield of EPS GeoFoam occurs over a range rather than a single point (Horvath 1994). The upper and lower strain boundaries for the zone of yielding, as well as the radius of curvature within the zone, are dependent upon the density of the EPS, with most data indicating a decrease in both radius of curvature and upper boundary strain with increase in density. Given the yielding behavior of EPS GeoFoam, the compressive strength is also arbitrarily defined based upon strain level. Much of the world defines the compressive strength as σ_{c10}, indicating a strain level of 10%, however in other parts of the world other strain levels may be selected (Stark et. al. 2004).

An additional parameter referred to as the yield stress (σ_y) is used to define the stress at the onset of yielding. Graphically, the yield stress occurs at the intersection of construction lines representing extensions of the initial linear elastic range (Zone 1) and the post-yield linear work-hardening range of the stress-strain curve. The yield stress generally corresponds to a strain of approximately 1.5% and is approximately 75% of the magnitude of the compressive strength (Horvath 1995).

Poisson's ratio, ν, of EPS GeoFoam in block form is typically measured using undrained triaxial testing, and is generally found to be small (0.1 to 0.2) within the elastic range where its magnitude is greatest. This has led to the assumption that ν is equal to zero in many design applications (Stark et. al. 2004). An empirical equation relating the density of EPS GeoFoam to Poisson's ratio has also been determined in an attempt to obtain a numerical value:

$$\nu = 0.0056\rho + 0.0024$$

where EPS density has units of kg/m^3. This relationship indicates an increase of ν with increasing density. Beyond the elastic range, data indicate that Poisson's ratio will decrease, in some instances resulting in a negative value and thus necking of the material (Stark et. al. 2004).

Poisson's ratio is directly related to the coefficient of lateral earth pressure at rest, K_0, through the relationship:

$$K_0 = \frac{\nu}{1-\nu}$$

Given the range of values for Poisson's ratio in the elastic range, the resulting range of K_0 values is between .1 and .25. As K_0 is valid under at-rest (confined) conditions, its magnitude is also affected by confining pressure, as will be discussed subsequently.

The use of EPS GeoFoam in geotechnical engineering applications often requires that it be placed below the ground surface. Increasing depth of embedment results in increased initial pressures upon the material, and therefore the behavior of EPS GeoFoam under various initial confining pressures is of importance. Undrained triaxial compression testing of EPS GeoFoam specimens permits both the application of initial confining pressures, as well as measure of volume change during testing. The effects of confining pressures upon volume change can be

determined, and therefore the ultimate effect upon Poisson's ratio and K_0. Although current data are limited for such testing, existing results indicate that Poisson's ratio will decrease with increasing confining pressures (Preber et. al. 1994).

The application of initial confining pressure also affects the overall stress-strain behavior of EPS GeoFoam. Data obtained from undrained triaxial tests on cylindrical specimens of the same density indicate that the compressive strength, σ_{c10}, and initial tangent modulus, E_{ti}, both decrease with increasing confining pressure (Athanasopoulous et. al. 1999). Similar testing of various densities of EPS GeoFoam obtained similar results, noting also an increase in the slope of the post-yield linear work-hardening portion of the stress-strain curve. This slope is sometimes referred to as the plastic tangent modulus, E_p.

Although there have been relatively few experiments investigating the effect of strain rates on EPS GeoFoam behavior, it can be concluded that compression behavior is rate dependent (Negussey, 1997). The observed behavior under small strains (approximately 1%) has varied, with some data indicating more significant effects on the initial tangent Young's modulus (Horvath 1995), and other data indicating that the behavior is not significantly affected until beyond a strain of 1%. The behavior at larger strains is more clearly defined, with an increase in compressive strength as strain rate increases. Tests performed with variable strain rates in which the rate is suddenly reduced or increased have shown that the stress-strain curves will shift appropriately. (Negussey 1997).

EPS GeoFoam compressive strength varies dynamically with temperature such that strength may remain constant or change depending on the range of temperatures the material is exposed to. Table 2.1 summarizes the behavior over appropriate temperature ranges. Compressive strength will remain fairly consistent to extremely low temperatures, not becoming brittle at -196°C (-321°F) (Stark et. al. 2004).

Table 2.1. Change in Compressive Strength of EPS GeoFoam with Varying Temperature (from Stark et. al. 2004).

Temperature Range	Rate of Change	Comments
Less than 0°C (+32°F)	0%	Approximately Constant
0°C (+32°F) to +23°C (73 °F)	-7% per 10°C (18°F)	Decreases Linearly with Increasing Temperature
+23°C (+73°F) to +60°C (+140°F)	+7% per 10C (18°F)	Increases Linearly with Increasing Temperature

Application and removal of loads in a cyclic fashion will affect the behavior of EPS GeoFoam to a varying degree depending upon the magnitude of the applied stresses. The application of cyclic stresses of magnitude not exceeding the elastic limit stress will cause no permanent axial strain upon stress removal (Stark et. al. 2004). Therefore there will be no change in the initial tangent Young's modulus, indicating that the resilient modulus and elastic

modulus are approximately equal (Preber et. al. 1994). The application of stresses of magnitude exceeding the elastic limit will result in both permanent, plastic deformation as well as reduction of the initial tangent Young's modulus. As strain increases, the slope of the stress strain curve increases dramatically due to work hardening of the EPS (Stark et. al. 2004).

The strain behavior of EPS GeoFoam under an applied stress of constant magnitude over an extended period of time, known as creep, is of interest for applications requiring a considerable design life. It should be noted that there is no standard creep test method for EPS GeoFoam, and therefore quantitative differences in test data due to varying specimen dimensions and testing conditions are common within existing research (Stark et. al. 2004). However, it is useful to describe the general behavior of EPS GeoFoam under long-term compression. EPS GoFoam exhibits three stages of creep behavior similar to other materials. These stages are referred to as primary, secondary, and tertiary.

As limited data exist for creep tests performed on EPS GeoFoam at test temperatures above normal ambient laboratory temperatures, it is generalized that creep rate will increase with elevated temperatures, which is a typical behavior of polymeric materials (Stark et. al. 2004). This is supported by the available data, as shown in Table 2.2 for tests conducted on 20 kg/m^3 (1.25 lb/ft^3) EPS GeoFoam for 2,400 hours (approx. 3 months).

Table 2.2. Results of Temperature Controlled Creep Tests Performed on 20 kg/m^3 (1.25lb/ft^3) EPS GeoFoam (from Horvath, 1995).

Stress	Temperature	Strain	Strain Increase
30 kPa (626 lb/ft^2)	+23 C (+73 F)	0.8%	-
	+ 60 C (+140 F)	1.5%	88%
40 kPa (835 lbs/ft^2)	+23 C (+73 F)	1.1%	-
	+ 60 C (+140 F)	3.25%	195%

Given the various applications of EPS GeoFoam for geotechnical use, it is necessary to analyze shear behavior under different conditions. Shear strength of EPS GeoFoam must be considered both for an intact block (internal shear strength) as well as for an arrangement of blocks, and therefore sliding resistance (external shear strength) is also of great interest for design purposes. As arrangements of blocks involve contact between blocks as well as between blocks and other materials, prediction of shear behavior along various interfaces is important. Internal shear strength of EPS GeoFoam is often determined according to ASTM C 273 through the use of structural sandwich core testing. The EPS specimen is attached to plates using either a pinning system or bonding adhesive and rapidly loaded in compression with the direction of load parallel to the sandwich surfaces. Shear strength is defined as the maximum shear stress reached during loading, with a rupture failure not necessarily occurring during the test (Stark et. al. 2005). Internal shear strength increases with increasing EPS GeoFoam block density.

EPS GeoFoam blocks are often arranged in stacked or layered configurations when used in geotechnical applications. Therefore, the prediction of shear strength along each block-to-block interface is often necessary when significant lateral loading may occur. There is no

specific standard procedure for EPS GeoFoam, but the preferred method of determining interface shear strength between EPS GeoFoam blocks is similar to the procedure used to determine the shear strength of soil using a direct shear apparatus (ASTM Standard D 5321). Two specimens of EPS GeoFam are placed in contact along a horizontal surface and a normal stress is applied to the top specimen on the horizontal plane. The specimens are then sheared while instrumentation records the magnitude of horizontal displacement and loading in order to determine the maximum required shearing force. Given the manufacturing process of EPS GeoFoam blocks, the outer surfaces previously in contact with the block mold will generally be smoother than surfaces exposed after trimming of the block. Therefore specimens are often trimmed from the external surface of a block and placed into the apparatus with the smooth surfaces in contact with each other, thus yielding the most conservative estimate of shear strength (Stark et. al. 2004).

The interface shear resistance between EPS GeoFoam blocks can be defined by Coulomb's dry friction equation:

$$\tau = \sigma_n \times (\mu) = \sigma_n \times (\tan\delta)$$

where:
τ = interface shear resistance
σ_n = applied normal stress
μ = coefficient of friction = $\tan\delta$
δ = interface friction angle

Classical Coulomb behavior will occur as the interface shear resistance, τ, will increase with increasing normal stress in a linear relationship. Given the low density of the EPS GeoFoam blocks, actual conditions in the field may result in very low vertical stresses and corresponding low interface shear resistance. Due to the lack of a standard testing procedure and therefore variability in test parameters and specimen requirements, typical values of the coefficient of friction, μ, and the interface friction angle, δ, are given as ranges. The coefficient of friction between EPS GeoFoam blocks ranges from 0.5 to 0.7, and the interface friction angle ranges between 27° and 35° (Stark et. al. 2005).

The use of EPS GeoFoam blocks in transportation projects will often involve contact between the blocks and an external dissimilar material such as geotextiles or impermeable membranes for isolating the blocks from potential gasoline spills and Portland cement or soil for fill applications. Current published data are restricted to interface between either soil or a geosynthetic material (Stark et. al. 2004). Direct shear tests conducted on specimens of EPS GeoFoam block sheared along a contact interface with Ottawa sand (a common fill material) indicate that the interface friction angle (and therefore coefficient of friction) between EPS GeoFoam and sand is approximately equal to the internal friction angle (Φ) of sand (Negussey 1997). Values of the interface friction angle between EPS GeoFoam and sand (and the internal friction angle of sand) range between 27° and 33°, corresponding to a friction coefficient of between 0.5 and 0.65 (Stark et. al. 2004).

The shear resistance between EPS GeoFoam and various types of geosynthetic is determined according to ASTM Standard D 5321, which requires the use of a large scale direct

shear box test performed on 305 mm (12 in.) by 356 mm (14 in.) specimens of EPS GeoFoam. However, a provision within the standard allows for the use of alternative testing techniques provided the results are comparable. Testing using a ring shear apparatus on annular specimens with an inside diameter of 20mm (0.8 in.) and an outside diameter of 160 mm (6.3 in.) produced similar results to the large-scale direct shear testing, in addition to allowing shear and displacement to continue into the residual range, whereas the direct shear box terminates prior to this range. The use of the ring shear apparatus for project-specific testing of EPS GeoFoam to geosynthetic interface shear resistance is recommended both for this reason as well as due to a small specimen size requirement. Available data for tests conducted using nonwoven polypropylene geotextile and gasoline containment geomembrane suggest that the interface between the smooth geomembrane and exterior surface of the EPS GeoFoam will produce extremely high peak friction angles (average 52°), whereas the interface between the nonwoven geotextile and the EPS GeoFoam block will produce lower peak friction angles (average 25°). This is due to the EPS GeoFoam bonding or sticking to the geomembrane. As there are different manufacturers and types of geosythetics, project-specific testing is still recommended for design purposes (Stark et. al., 2004).

There are virtually no applications of EPS GeoFoam that require tensile loading and tensile strength is of interest only for quality control purposes in order to verify proper fusion of the expandable polystyrene beads. Given the nature of EPS GeoFoam and methods of specimen preparation for laboratory testing, normal tensile strength tests according to ASTM Standard C 1623 performed on hour-glass shaped specimens are rarely performed due to difficulty obtaining an acceptable specimen. An alternative to tensile testing is flexural testing of a 100 mm (4 in.) by 300 mm (12 in.) by 25 mm (1 in.) beam as specified in ASTM Standard C 203. Transverse loading of the beam produces the maximum bending moment at the extreme fiber, from which the maximum tension can be determined. As shown in Figure 3.15, tensile and flexural strength increase with increasing density. As flexural and tensile strengths are used more for quality control than for design purposes, there is no existing data correlating with temperature or load duration (Stark et. al. 2004).

2.3 Applications of EPS GeoFoam

Given the engineering properties of EPS GeoFoam, there is great potential for the material as an alternative to conventional materials in geotechnical applications. The most common use of EPS GeoFoam is the function of lightweight fill due to the very low unit weight of EPS when compared with typical backfill soils. As a result of increased research in recent years, the range of possible functions of EPS GeoFoam has been expanding as response behavior to certain loading conditions is further understood. There is increasing interest in the use of EPS GeoFoam as a compressible inclusion, which in alone can serve a number of possible functions. Due to inherent material properties, EPS GeoFoam can provide thermal insulation, vibration damping, and drainage when a project requires any or all of these functions. In order to simplify the following discussion of EPS GeoFoam applications, focus will be upon lightweight fill and compressible inclusion functions.

2.3.1 EPS GeoFoam as Lightweight Fill

The concept of the use of lightweight fill relies upon the basic principle of capacity or load resistance vs. applied loads. Reducing the applied loads or increasing the load resistance results in an increased factor of safety. One method of reducing applied loads is the use of lightweight fill to decrease gravity loads. Lightweight fills in various forms in addition to EPS GeoFoam are already in current use, primarily in situations where soft ground conditions pose a potential problem. EPS GeoFoam has been used in a variety of projects, with the most frequent being embankment construction, earth retention structure backfill, and slope stabilization. The following sections will briefly discuss the use of the material in each basic function.

2.3.2 Embankment Construction

A typical design configuration for EPS GeoFoam use in embankment construction is shown in Figure 2.2.

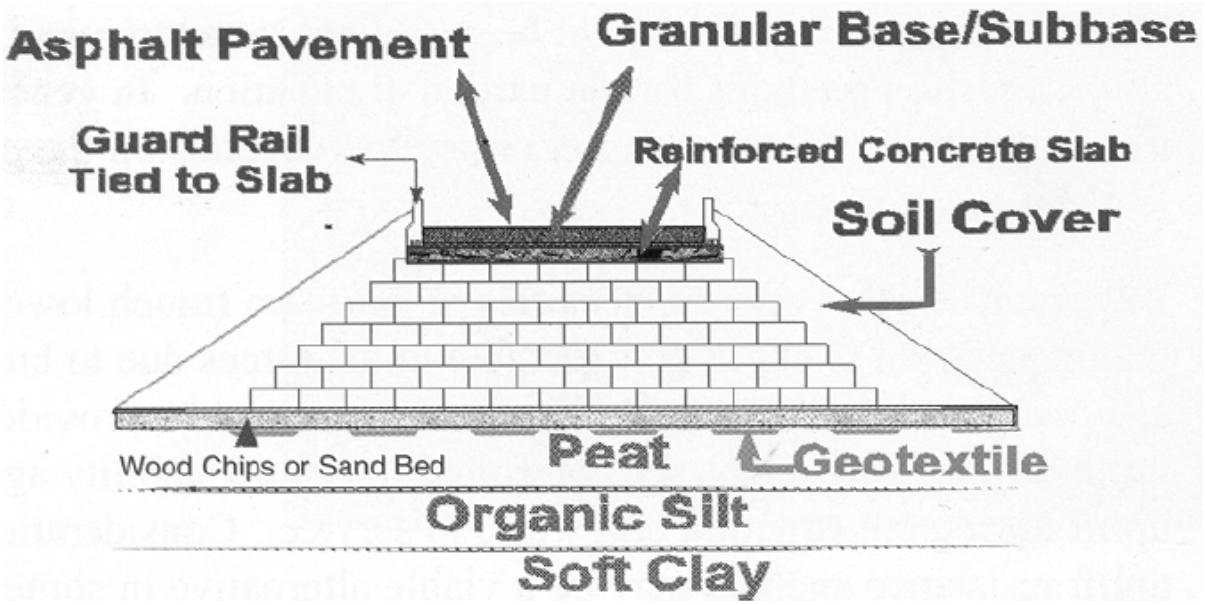

Figure 2.2. Typical Construction Detail for EPS GeoFoam Embankment (from Negussey 1997).

There are a variety of possible solutions allowing construction to occur over soft soils. Depending upon the thickness and properties of the soft soil layer(s), excavation of the soil may be possible, or for thicker layers there are ground improvement techniques such as surcharge preloading and the installation of wick-drains in order to consolidate the underlying soil and reduce settlements while increasing strength. A downside to excavation or surcharge loading is the time required for preparation of the ground prior to the actual construction of the embankment. Of course, this time represents additional cost for the project. An alternative is the use of EPS GeoFoam blocks as a fill material in the embankment, as the decreased loading of the underlying soils reduces settlements and decreases vertical stresses, eliminating or reducing the

need for surcharge loading and thus greatly reducing construction time. Construction time is further reduced as block placement in layers by hand eliminates the need for placement of soil in lifts with subsequent compaction. A typical (simplified) EPS GeoFoam embankment construction usually consists of placement of a leveling course (usually sand fill), construction of the stepped-side EPS GeoFoam embankment, placement of a protective cover over the EPS blocks (either a membrane or soil cap), and placement of a concrete slab over the EPS blocks in order to distribute loads and allow the construction of a road structure (Negussey 1997).

2.3.3 Earth Retention Structure Backfill

Construction of retaining walls and bridge approach fills can require fairly complex designs in order to achieve required levels of stability. In the case of retaining walls, loading upon the wall as well as vertical stresses within the retained soil must be evaluated. Approach fills require similar analysis, with the additional consideration of differential settlement between the approach and the bridge deck. This is especially challenging in cases where soft soils dominate subsurface conditions. The use of EPS GeoFoam as a lightweight fill material, as shown in Figure 2.3, provides a number of advantages over conventional fill. The low Poisson's ratio and coefficient of lateral earth pressure of EPS GeoFoam in conjunction with a lower unit weight than soil results in greatly reduced lateral pressures on the wall. The low unit weight of the EPS GeoFoam blocks also results in lower vertical stress within the retained soil mass and, in situations where soft soils prevail, reduced settlements.

In such soft ground situations, the concrete abutment structure may by supported by deep foundations such as drilled shafts or piles driven to a competent soil layer. EPS GeoFoam block backfill is often placed in a wedge configuration as shown in Figure 2.3. A sand layer is usually used to allow a level base for the lowest layer of blocks near the abutment, and additional fill material is used to fill gaps between blocks and the sloping soil onto which the blocks are stepped. This fill material also serves as a drainage path in order to eliminate standing water behind the retention structure which will cause buoyancy effects within the EPS blocks (Negussey 1997). The blocks are often capped with a slab for load distribution as well as additional granular fill in order to provide additional normal stress in order to increase frictional strength between blocks (Snow 2004).

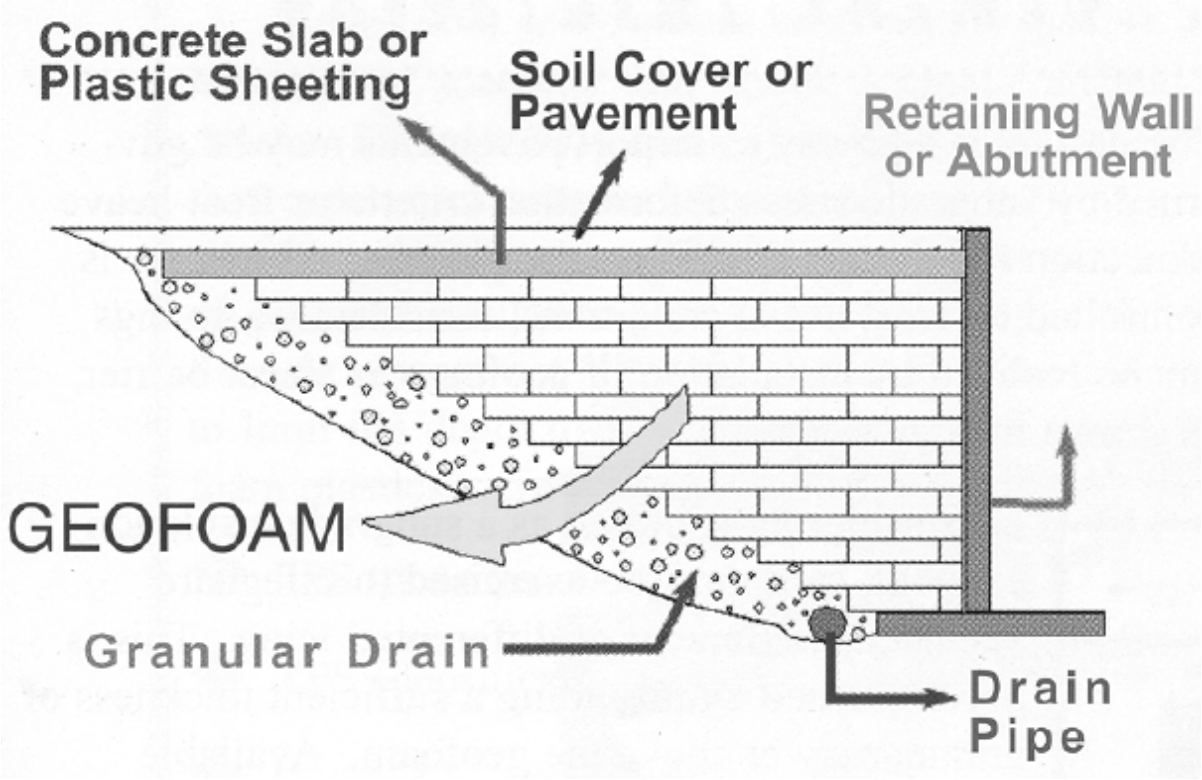

Figure 2.3. Typical Construction Detail for EPS GeoFoam Backfilled Earth Retention Structure (from Negussey 1997)

2.3.4 Slope Stability

Transportation projects requiring safety factors against slope failure may require a combination of earthwork and ground improvement in order to achieve the proper balance of driving forces to resisting forces. Techniques such as increasing effective stress through groundwater lowering and reinforcing the resisting portion of the slope can be complicated and require a considerable amount of time. An alternative is the use of EPS GeoFoam as a substitute for the soil within the driving block in order to decrease the driving forces due to gravity-based loads. This is a case-sensitive concept, and therefore designs may differ considerably from project to project due to soil conditions and the intended function of the slope. Typical design considerations are the placement of granular fill for drainage and concrete slabs for load distribution, as is common in other EPS GeoFoam applications (Negussey 1997).

2.3.5 EPS GeoFoam as a Compressible Inclusion

While the low unit weight and compressive strength of EPS GeoFoam make it an ideal lightweight fill material, its compressive properties can also make it useful as a boundary material between a structure and backfill soil. This is known as the compressible inclusion function, also referred to as controlled yielding or displacement (Horvath 2005). EPS GeoFoam is not the first material to be used as a compressible inclusion; materials used in such applications have included hay bales, cardboard, and loose granular fill soils. As problems of

biodegradability and unpredictable stress-strain material are nonexistent through the use of polystyrene, its use as a compressible inclusion material represents great potential. Similarly to the lightweight fill function, this use of EPS GeoFoam reduces the loads upon the structure. Rather than designing for minimal deformation of the EPS GeoFoam blocks, the designer selects a material with properties such that it will be the most compressible in comparison with the fill soil and the structure. Given the previously discussed relationship between EPS block density and compressive strength, a lower density is selected to yield greater compressibility, however the lowest density possible is not used due to durability issues resulting from improper fusion of the polystyrene beads. An additive during manufacturing can produce elasticized EPS GeoFoam, which affects the initial modulus and compressive strength of the material at relatively low stresses. The density of EPS GeoFoam selected must also be based upon creep behavior, as most projects that would benefit from compressible inclusions involve long-term loading. Currently more research into the creep behavior of elasticized EPS GeoFoam is necessary. Possible applications for compressible inclusions are in earth retaining structures, as boundaries for basement structures, and as protection for structures such as pipes and conduits (Horvath 1997).

2.3.6 Compressible Inclusions in Earth Retaining Structures

Although full-scale test results are limited for this type of application, based upon numerical modeling with finite-element solutions two separate design alternatives are identified for using EPS GeoFoam as a compressible inclusion in earth retention structures. These are referred to as the Reduced Earth Pressure (REP) concept and the Zero Earth Pressure (ZEP) concept. An example of a retaining wall based upon the REP concept is shown in Figure 2.4. The application in its most basic form consists of a rigid or non-yielding structure with a compressible zone of EPS GeoFoam separating the structure from the backfill material. The ground conditions and application control the estimated stress-strain behavior of the soil, just as the properties of the EPS GeoFoam inclusion control compressibility and deformation behavior. Shear strength can be mobilized by selecting EPS GeoFoam properties and inclusion thickness such that the necessary displacement required to transition from at-rest earth pressure state to an active earth pressure state occurs (Horvath 2005).

The ZEP concept shares a common basis with the REP concept, however in addition the structure is essentially designed with a similar reinforcement to a Mechanically Stabilized Earth (MSE) wall using reinforcement material for tensile loading, as shown in Figure 3.22. The ZEP concept allows for simultaneous use both a rigid wall and deformation-dependent reinforcement which become active due to deformation of the compressible inclusion rather than movement of the structure. Theoretically this could mean that the soil mass would be completely supported by the reinforcement material and therefore lateral earth pressures on the wall would be zero. In reality, the compressible inclusion would have to be of zero-stiffness in order to result in such stress-strain behavior (Horvath 1997).

Both the REP and ZEP concepts require further investigation in order to develop a reliable numerical model. Based upon current research there are additional benefits to using a compressible inclusion to overcome project-specific problems involving such elements as soil volume change (freeze/thaw, etc.), compaction stresses, seismic force reduction, and structural

movements. Structural movement, as in the case of an integral abutment bridge, is possibly the most complex problem which a compressible inclusion may potentially solve, and therefore a considerable amount of research is necessary before a solution can be reached. The REP and ZEP concepts also represent potential rehabilitation and upgrade alternatives for structures that are not adequately designed or which will require increased load capacity (Horvath 2005).

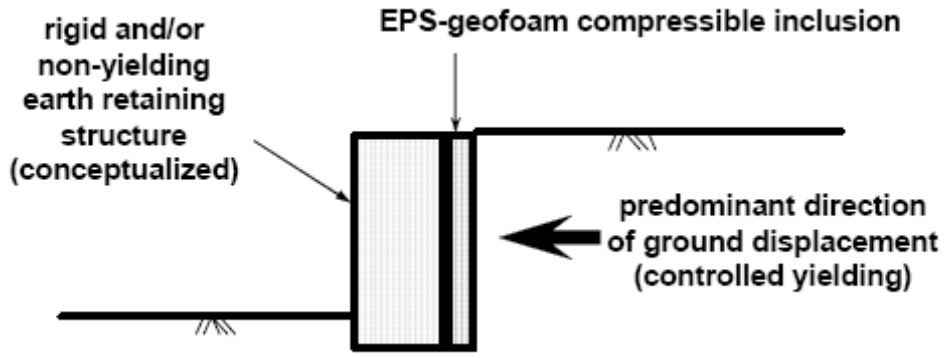

Figure 2.4. Reduced Earth Pressure (REP) EPS Geofoam Compressible Inclusion Concept (from Horvath 2005).

2.3.7 Compressible Inclusions in Basement Structures

Typical methods of constructing foundations on soft soils involve the use of a structural base (slab) supported by grade beams connected to deep foundations such as piles or drilled shafts. Projects located in regions where expansive soils are common must overcome the problem of upward swell pressures and volumetric expansion (heave). The use of a compressible inclusion in a fashion very similar to that of REP earth retention structures results in a reduction of vertical swell pressure as well as volumetric expansion of the soft soil. As shown in Figure 3.23, the compressible inclusion is placed as a horizontal zone between the structural slab and the deep foundation supports. This use of a compressible inclusion is already very popular in regions dominated by expansive soils, and typical design criteria consist of a similar displacement and swell pressure (force) relationship as found in Figure 3.21, however as shear strength is not being mobilized there is no particular displacement required for effectiveness of the inclusion. Therefore, design is usually based upon data from either confined or free swell tests on the underlying soil, slab design requirements (affecting the weight of the slab), and the economic impact of compromising between slab design and inclusion thickness (Horvath 2005).

2.3.8 Compressible Inclusions in Pipes and Conduits

The use of EPS GeoFoam as a compressible inclusion for structural protection of underground pipes and conduits is merely an updated form of an already standard concept. Traditionally, compressible inclusion materials such as bales of hay have been used to reduce the vertical loads on such structures. The use of EPS GeoFoam, represents a more modern alternative, with the advantages of non biodegradability and negligible effects of water on

performance. Research has shown that EPS GeoFoam can successfully be used for such a purpose, however much of the research is based upon numerical methods for design purposes rather than the simple design charts used for other materials.

2.4 Design Method for EPS GeoFoam Embankment Construction/Abutment Fill

The most up-to-date source of information on the use of EPS GeoFoam as a fill material in embankment and abutment construction is the 2004 National Cooperative Highway Research Program report entitled "GeoFoam Applications in the Design and Construction of Highway Embankments." Included in the report is a comprehensive literature review including information on the history of the development of EPS GeoFoam as a construction material, engineering properties, and case studies on the uses of EPS GeoFoam. This information is supplemented by additional research, with the objective of the report being the creation of a design guideline and a material and construction standard (Stark et. al. 2004).

2.4.1 Lateral Pressure (Abutment Design)

According to Stark et al. (2004) embankments constructed as bridge approach fills require the design of an abutment/soil system which consists of a 7 step process:

1. Select preliminary wall proportions
2. Determine loads and earth pressures
3. Calculate the magnitude of the reaction force on the base
4. Check stability and safety criteria:
    a. Location of normal component of reactions
    b. Adequacy of bearing pressure
    c. Safety against sliding
5. Revise proportions of wall, iterating until stability and safety criteria are satisfied; then check:
    a. Settlement within tolerable limits
    b. Safety against deep-seated foundation failure
6. If proportions become unreasonable, foundation may be supported on driven piles or drilled shafts
7. Compare economics of completed design with other wall systems

The second step described above must incorporate the EPS GeoFoam into the design process, as the sources of earth pressures consist of the EPS dead load, W_{EPS}, the pavement system load, W_P, the soil dead load, W_{SOIL}, and the active earth pressure transferred to the abutment through the GeoFoam by the retained soil, P_A. These loads are illustrated in Figure 2.5.

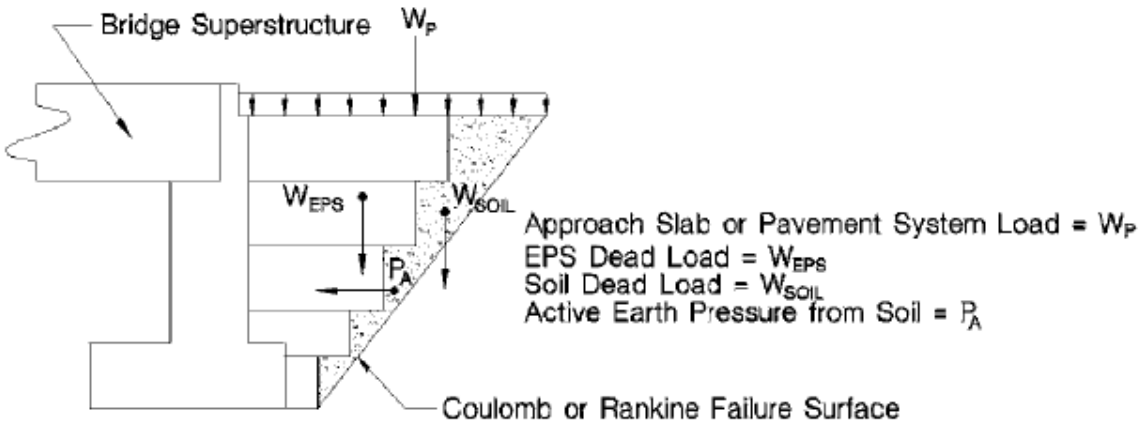

Figure2.5. Loads on an EPS-block GeoFoam Bridge Approach System (from Stark et. al. 2004).

The actual magnitude of the loads can vary depending on if the project requires additional design for seismic load resistance. In the case of simple gravity loading, design is based upon several assumptions regarding the components. The horizontal pressure resulting from the vertical stress caused by the pavement loads is assumed to be equal to 1/10 the magnitude of the vertical stress. The horizontal stress from the EPS blocks is assumed negligible. The vertical pressure applied by the pavement system to the top of the EPS GeoFoam blocks contributes a uniform horizontal pressure acting over the depth of the blocks. The lateral earth pressure is conservatively assumed to be fully transmitted to the GeoFoam blocks; any dissipative effects of the EPS GeoFoam blocks are ignored. It is also assumed sufficient lateral deformation will occur to result in active earth pressure conditions, and the earth pressure is calculated using Coulomb's theory:

$$K_A = \left[\frac{\sin(\theta - \phi)\left(\frac{1}{\sin\theta}\right)}{\sqrt{\sin(\theta+\delta)} + \sqrt{\frac{\sin(\theta+\delta)\sin(\phi)}{\sin(\theta)}}} \right]^2$$

and

$$P_A = \frac{1}{2}\gamma_{soil} H^2 K_A$$

where:

δ = Friction angle of the EPS/soil interface (°), assumed equal to ϕ.
γ_{soil} = Unit weight of soil (kN/m^3)
ϕ = Soil friction angle (°)
θ = Slope angle of stepped GeoFoam blocks (°)
H = Height of interface (m)

K_A = Coefficient of active lateral earth pressure

The gravity load components are shown in Figure 2.6. It is assumed that the displacement required to mobilize passive earth pressure conditions will be too large, and therefore passive pressures of the soil in front of the abutment are ignored.

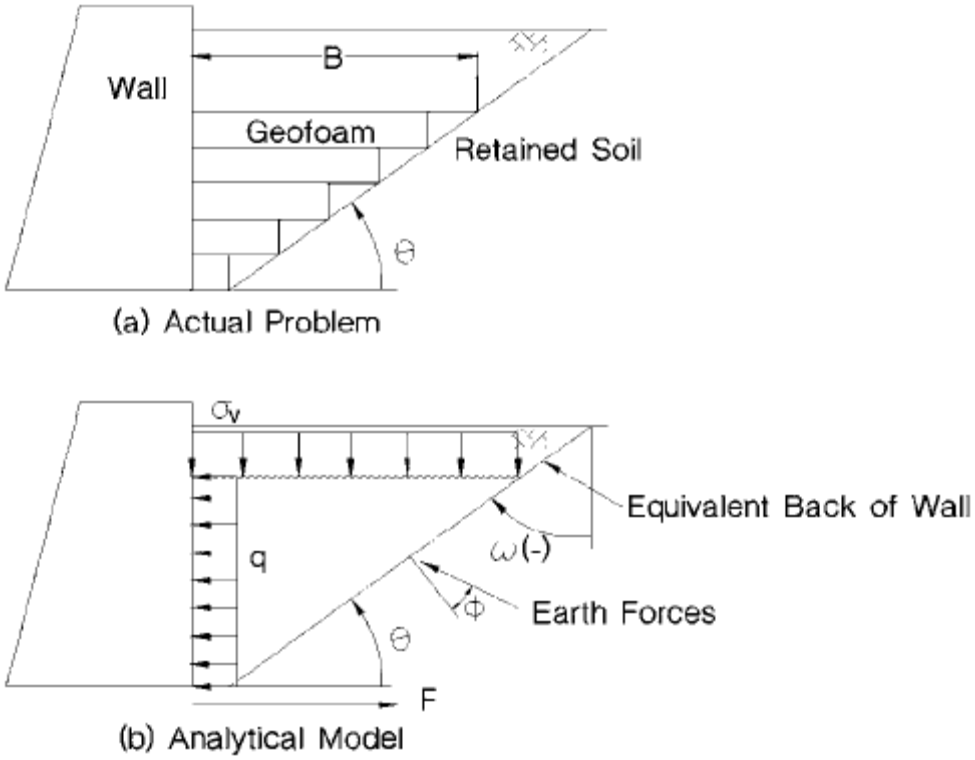

Figure 2.6. Gravity Load Components on a Vertical Wall (from Stark et. al. 2004).

2.4.2 Vertical Pressure (External Stability)

In projects founded on soft, saturated cohesive soils, EPS GeoFoam presents several advantages, including a reduction in stresses to the foundation soil due to self-weight gravity loads when compared to traditional fill soils, and also dissipation of normal stresses applied to the top of the constructed approach fill through the height of the EPS GeoFoam array. Stress transfer of pavement and traffic stresses applied at the top of the array to the foundation soil is determined using the 2:1 distribution method:

$$\sigma_{n,pavement@0m} + \sigma_{n,traffic@0m} = \frac{\left(\sigma_{n,pavement} + \sigma_{n,traffic}\right) \times T_W}{\left(T_{w+} T_{EPS}\right)}$$

where:

$\sigma_{n,pavement@0m}$ = normal stress applied by the pavement at the ground surface, kPa

$\sigma_{n,traffic@0m}$ = normal stress applied by traffic surcharge at the ground surface, kPa

$\sigma_{n,pavement}$ = normal stress applied by pavement at top of embankment, kPa

$\sigma_{n,traffic}$ = normal stress applied by traffic surcharge at top of embankment, kPa

T_W = top width of embankment, m

T_{EPS} = thickness of EPS GeoFoam block, m

The Boussinesq stress distribution theory is used to incorporate the normal stress at the ground surface due to the weight of the EPS GeoFoam embankment:

$$\sigma_{n@0m} = \sigma_{n,pavement@0m} + \sigma_{n,traffic@0m} + \frac{(\gamma_{EPS} \times T_{EPS})}{2}$$

where:

$\sigma_{n@0m}$ = normal stress applied by total embankment at the ground surface, kPa

γ_{EPS} = unit weight of EPS GeoFoam, kN/m^3

2.5 Case Studies

The following case studies are presented in order to provide a basis of comparison between data obtained in this study and existing published data regarding the measurement of stresses in structures utilizing EPS GeoFoam blocks as a fill material. For the purpose of comparing theoretical results with data measured in the field, data predicted using computer numerical analysis will be considered as well as data obtained from pilot studies.

2.5.1 Case I

The first case study was reported by Negussey and Sun (1996). Both a field observation program as well as computer finite element analysis were used to study the effectiveness of the use of EPS GeoFoam as a backfill material for a basement wall. The site for the field observation program was a large shopping mall being constructed over deep deposits of compressible fill and soft lake bottom settlements in Syracuse, New York. The first stage of construction consisted of excavation of existing soil from the building plan area (mat foundation) and placement adjacent to the building perimeter wall. The unloading on the inside of the building and loading on the outside of the building represented high potential for differential settlements. In addition to extending the mat foundation area by 2.1m beyond the perimeter of the superstructure, 28,000 m^3 of EPS GeoFoam was placed around the perimeter. During the second stage of construction the GeoFoam was excavated along with conventional fill that served as preloading for an expansion of the building.

The foundation for the new expansion was supported on deep piles. Adjacent to the pile-supported exterior columns was a parking area, with the basement wall backfilled using 2.7 m (8.9 ft) of EPS GeoFoam. Adjacent to the GeoFoam wedge was recent fill, with a concrete cap and pavement placed over the GeoFoam and extending over the fill. Three earth pressure cells were installed flush with the outer face of the basement wall at the GeoFoam/concrete interface.

One cell was located at a depth of 0.70 m (2.3 ft) from the top of the wall, while the other two cells are located at a depth of 1.60 m (5.2 ft) with a center to center offset of 7.32 m (24.0 ft). The stress cells were zeroed in place prior to placement of the GeoFoam backfill and periodic readings were taken.

A finite element analysis was performed using the Soilstruct program to create a simplified representation of the wall, backfill, and foundation soil. The backfill was modeled as both EPS GeoFoam as well as conventional sandy soil backfill. The basement wall was restrained from lateral movement by the concrete deck, therefore lateral pressures were modeled based upon at-rest (K_0) conditions. Values chosen for K_0 were 0.1 and 0.5. Other engineering properties for the EPS GeoFoam were chosen based upon the nominal values of the material density.

The use of GeoFoam as the backfill material resulted in a reduction of vertical stress from approximately 42 kPa to 4 kPa. The upper cell registered a negligible stress, while the lower cells indicated stresses of 2 and 2.6 kPa. Therefore the upper cell was consistent with low K_0 behavior, however the lower cells agreed with the analysis for K_0 of 0.5. Under the field conditions, this may be due to differential settlement causing a rotation of the GeoFoam wedge away from the wall, which would result in low or negligible pressures high in the wall and measurable pressures lower in the wall near the anchor point.

2.5.2 Case II

The second case study was presented by Stuedlein et al. (2004). A newly constructed bridge replacing the Route 85 Bridge over Normans Kill Creek in Albany, NY, was built over weak and compressible lacustrine deposits. EPS GeoFoam was used as a lightweight fill to construct the approach fills in order to mitigate settlements and reduce lateral stresses and downdrag. The wingwall abutments were founded on steel H-piles, and GeoFoam approach fills were constructed using Type VIII EPS 19 GeoFoam blocks placed on a granular leveling course. Fine to medium sand was used as a chimney drain material between the GeoFoam and abutment. A 100 mm reinforced concrete load distribution slab was poured in place over the GeoFoam surface and chimney drain, over which 0.6 m each of sub-base and base for the approach slab were placed. A 305 mm thick Portland Cement Concrete approach slab and asphalt pavement were placed over the base. Five total stress cells were placed within the approach fill. Two cells were oriented to register vertical stresses directly below the GeoFoam base, while another registered vertical stresses at the base of the chimney drain. Two stress cells were placed to register horizontal stresses at heights of 0.6 m and 2.4 m above the base of the chimney drain.

A numerical model of the GeoFoam fill was also created using FLAC (Fast LaGrangian Analysis of Continua) software, with varying Young's Modulus values (4.1 and 11 MPa) and Poisson's Ratio (0.2 and 0.3). The use of a higher Young's Modulus value and Poisson's ratio of 0.2 to 0.3 resulted in agreement between field performance and computer modeling. This configuration was used in Trial 3, however it should be noted that in all cases the model trials over predicted the stresses compared with those recorded by the stress cells located at the base of the chimney drain and the upper location.

CHAPTER 3. DESCRIPTION OF BRIDGE and BRIDGE CONSTRUCTION

3.1 Introduction

The bridge selected for this study was the replacement for Bridge No. 6 located on TH I (FAS 160), a major collector connecting the towns of Leicester and Whiting. The existing bridge was a 3-span steel beam bridge with a concrete deck constructed in 1932. In order to maintain an uninterrupted traffic flow at this crossing point of Otter Creek a temporary bridge was constructed adjacent to the existing bridge prior to demolition and traffic over the bridge was maintained until the completion of the project. The newly constructed bridge is a single span steel girder bridge with a concrete deck. Given the soft soil conditions, the abutments were founded on battered and vertical piles driven to bedrock. The approach embankments were constructed using lightweight EPS GeoFoam blocks in order to reduce settlements and reduce vertical and lateral earth pressures.

3.2 Bridge Dimensions

Plan and elevation views of the replacement bridge are shown in Figures 3.1 and 3.2. The total length of the structure is 34.8 m (114.2 ft), with a clear span of 32.7 meters (107.3 ft) normal to the stream. The maximum vertical clearance above the streambed is 6.7 m (22.0 ft), with a waterway opening of 174.0 m^2 (1872.9 ft^2). The reinforced concrete deck is approximately 9.3 m (30.5 ft) wide and is supported on five 13X1220 WEB plate girders as shown in Figure 3.2. The super elevation of the deck is due to the 5^0 skew of the roadway centerline with the normal centerlines of the abutment front walls. An expansion joint located at Abutment 1 allows the superstructure to expand and contract with seasonal temperature changes.

3.3 Abutment Details

Elevation and plan views of the bridge abutments are shown in Figures 3.3 and 3.4. Abutments are reinforced concrete asymmetrical cantilever type wingwall abutments resting on spread footings. Reinforced concrete footings are founded at an elevation of 101.5 m (333.0 ft) and have a height of 0.9 m (3.0 ft). The concrete was poured onto a granular backfill leveling base. The front sides of the footings are 13.8 m (42.3 ft) long and the back sides are 8.3 m (27.2 ft) long. The footings are approximately 2.7 m (8.9 ft) thick along the centerline. The footing wingwalls are 2.7 m (8.9 ft) wide and are parallel with the 5^0 skewed roadway centerline. The inner length of the footing wingwalls is 2.0 m (6.6 ft) and the outer length is 4.7 m (15.4 ft).

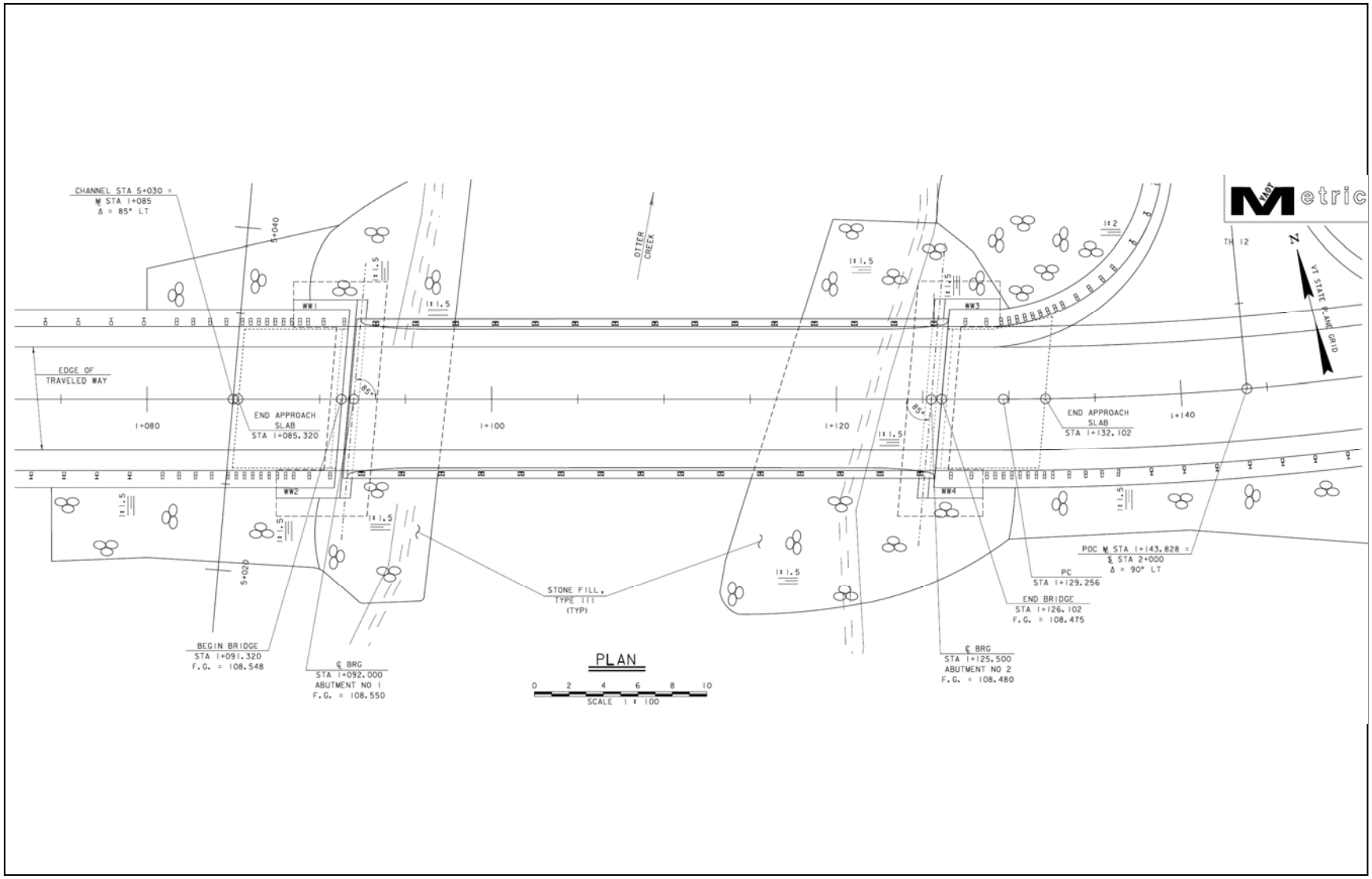

Figure 3. 1 Plan View of Bridge.

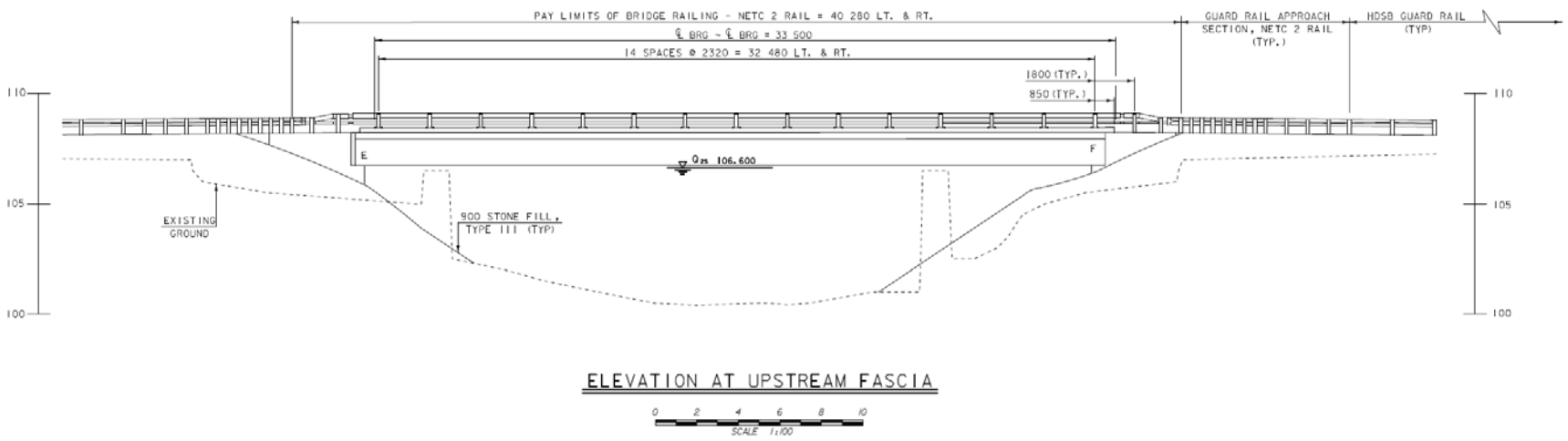

Figure 3.2 Elevation View of Bridge

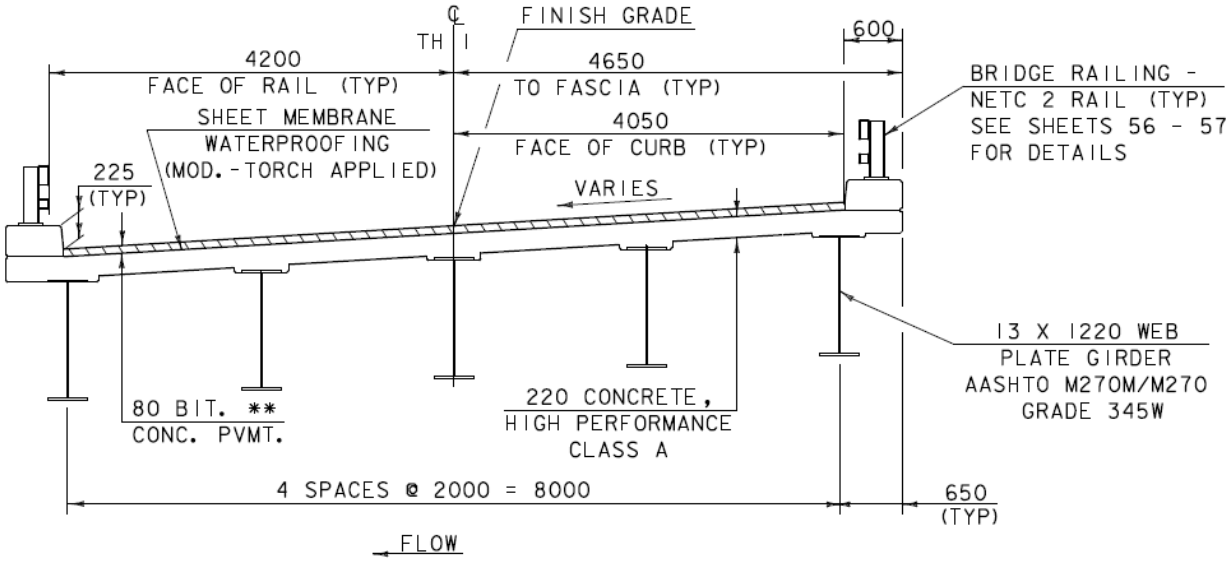

Figure 3.3 Bridge Deck Cross Section.

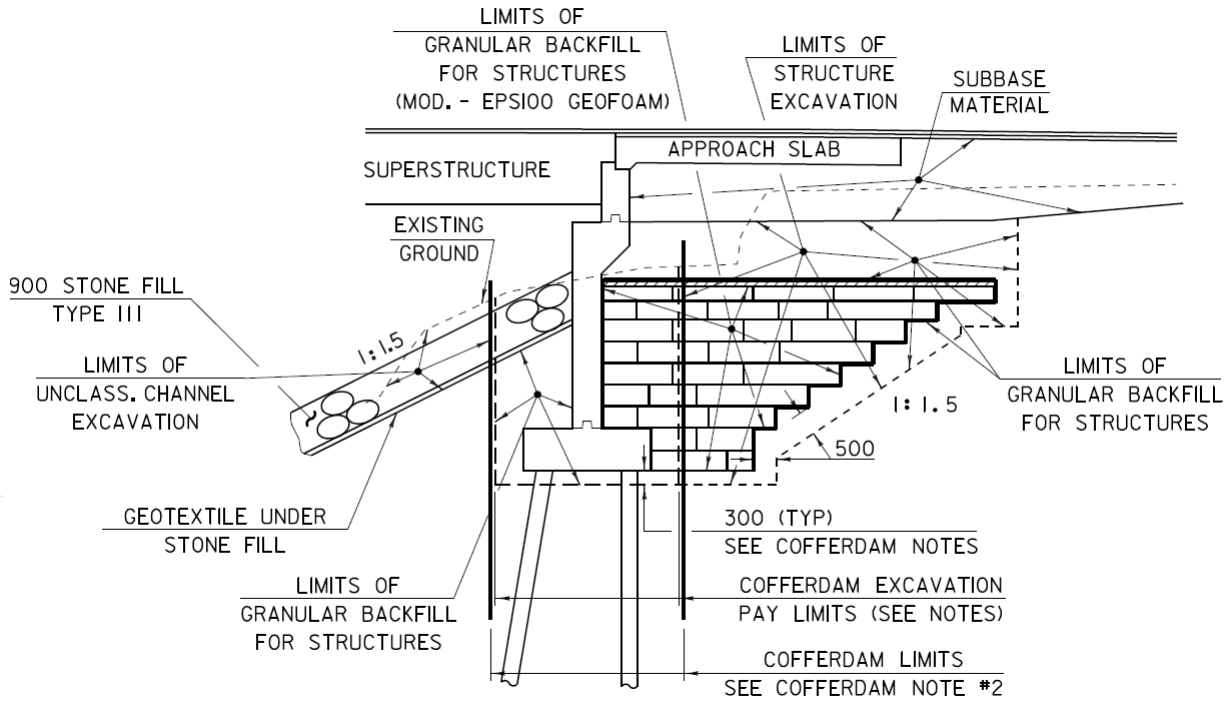

Figure 3.4 Typical Abutment Section.

The abutment walls are approximately 6.2 m (20.3 ft) high and 0.6 m (2.0 ft) thick. The front side of the abutment wall is 11.7 m (38.4 ft) long and the back side is 10.5 m (34.4 ft) long. The abutment wingwalls are 0.6 m (2.0 ft) thick with an inner length of 2.8 m (9.2 ft) and an outer length of 3.8 m (12.5 ft). The footings rest on twenty-one (21) driven HP 360X108 piles consisting of eight (8) vertical piles along the backside and inner wingwalls and thirteen (13) battered piles along the front side and outer wingwalls as shown in Figure 3.5. The battered piles were driven at a 1:6 slope.

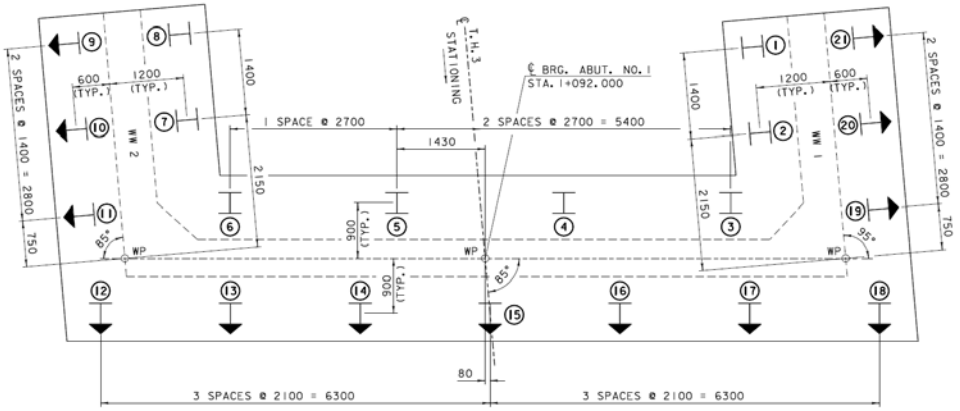

Figure 3.5 Typical Abutment Pile Layout.

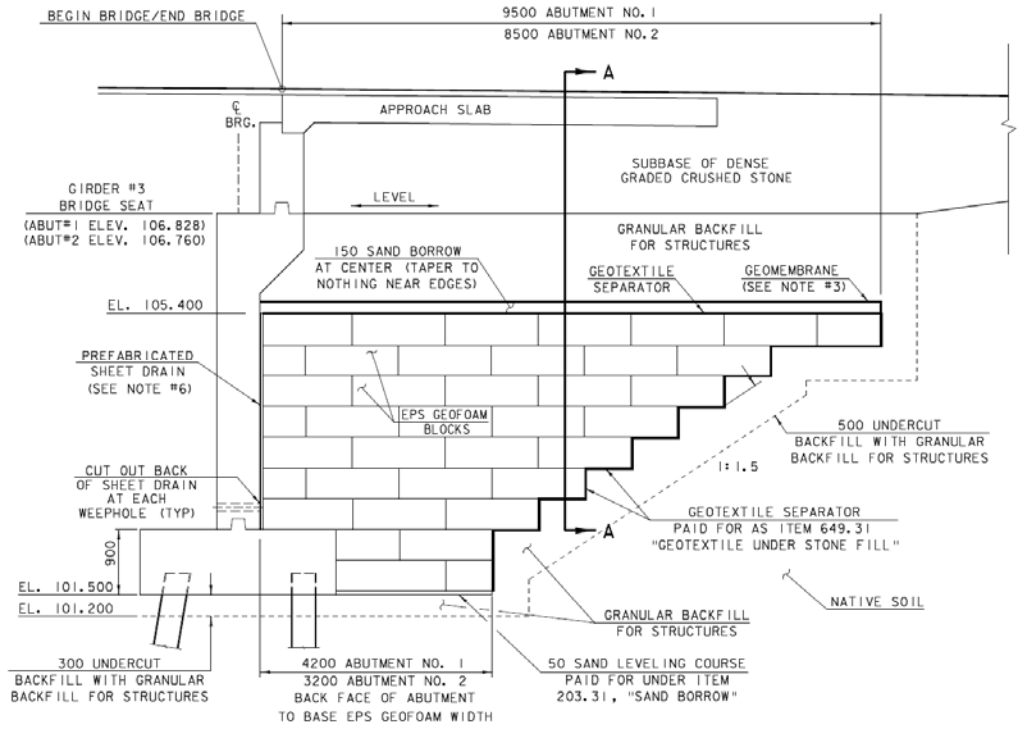

Figure 3.6 Typical Abutment Cross Section (Facing Perpendicular to Centerline).

3.4 Approach Embankment and GeoFoam Backfill Details

Approximately 450 m^3 (588.6 $yard^3$) of EPS100 GeoFoam were used behind the abutments to construct the approach embankments. Block shapes varied in order to fit the geometry of the abutment; typical construction details can be found in the Appendix. A typical cross section of the approach embankments perpendicular to the roadway centerline is shown in Figure 3.6. A typical cross section of the approach embankment facing towards the back face of the abutment along the roadway centerline is shown in Figure 3.7.

GeoFoam blocks were placed by hand in an overlapping configuration, with metal interlock plates used to secure face-to-face contact. Modifications to block geometry were made on site using a hot wire as necessary as shown in Figure 3.8. The lowest layer of blocks was of equal height with the abutment footing and was placed on a sand leveling course at even elevation with the base of the abutment footing as shown in Figure 3.9. The layer was then wrapped in a geotextile separator and backfilled with granular fill material as shown in Figure 3.10. Subsequent layers were placed with the rear limit of each layer increasing to create a stepped configuration of 1:1.5 slope as shown in Figure 3.11. A prefabricated sheet drain was placed between the GeoFoam blocks and the back face of the abutment. The lateral limit of the GeoFoam (perpendicular to the abutment centerline) was the inside of the abutment wingwalls. The sides of the EPS GeoFoam embankment are vertical, with a maximum height of the blocks of 3.9 m (12.8 ft). The uppermost layer of the EPS GeoFoam blocks extends 9.5 meters (31.2 feet) along the approach at Abutment 1 and 8.5 meters (27.9 feet) along the approach at Abutment 2.

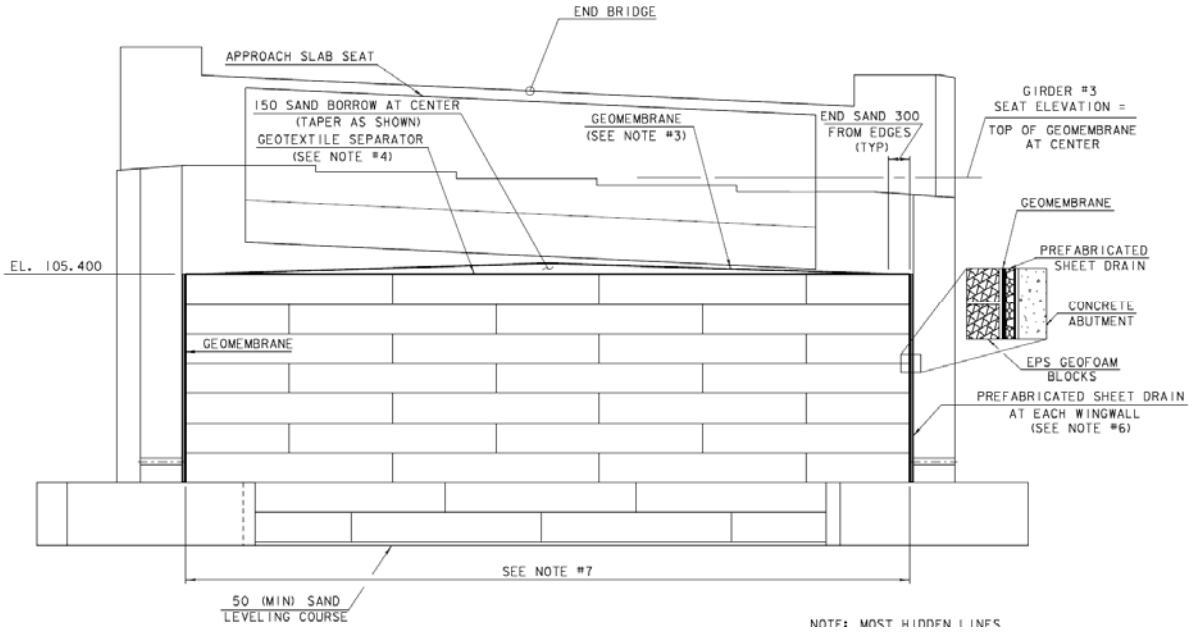

Figure 3.7 Typical Abutment Cross-Section (Facing Back Abutment Along Centerline).

Geotextile separator was placed over the top layer of blocks, with a tapered layer of sand borrow placed over the top of the blocks as shown in Figure 3.12. A flexible PVC geomembrane

was placed over the tapered sand layer as shown in Figure 3.13 to create a drainage path to divert water and protect the GeoFoam from potential exposure to gasoline. Compacted granular backfill was placed adjacent to and on top of the GeoFoam in order to create a leveling course for the asphalt approach roadway as shown in Figure 3.14. Beyond the width of the roadway the embankment sides were sloped downward at 1:1.5 and 1:1.75 reflecting the super elevation of the bridge deck. A 0.7 m (2.3 ft) thick reinforced concrete approach slab was placed over the roadway sub-base extending 6.0 m (19.7 ft) from the end limit of the structure. The roadway pavement was placed directly over the approach slab.

Figure 3.8 Trimming a GeoFoam Block.

Figure 3.9 Placement of GeoFoam Blocks Adjacent to Abutment Footing.

Figure 3.10 Wrapping GeoFoam Blocks with Geotextile Separator and Backfilling.

Figure 3.11 Placement of GeoFoam Blocks in Stepped Layers.

Figure 3.12 Placement of Geotextile Separator and Tapered Sand Layer.

Figure 3.13 Installation of Flexible PVC Geomembrane.

Figure 3.14 Placement of Granular Backfill.

CHAPTER 4. METHODS AND RESULTS OF SITE INVESTIGATION

4.1 Introduction

A geotechnical site investigation and field instrumentation program were conducted as part of this project. The test drilling was performed by VTrans and the laboratory testing program was conducted at the University of Massachusetts Amherst Geotechnical Laboratory. The field instrumentation program was conducted at the construction site in Leicester, VT. Laboratory testing consisted of general soil classification and indexing, consolidation, and laboratory vane undrained shear strength tests performed on Shelby tube samples collected at Borehole B201. Field instrumentation consisted of the installation of vibrating wire total earth pressure cells during the construction of the bridge as well as monitoring of earth pressures following completion of the bridge.

4.2 Laboratory Tests

Table 4.1 summarizes the laboratory tests and corresponding test standards used. A brief outline of each procedure follows. All tests were conducted on samples extracted from Shelby tube samples collected from Borehole B201 over a depth range of 10.7 m (35 ft) to 30.5 m (100 ft). The Shelby tubes were sealed at each end with rubber caps and paraffin wax. Samples of soil were then removed for various classification and index testing.

Table 4.1 Summary of Laboratory Testing Procedures.

Procedure	Test Standard
Moisture Content	ASTM D2216-92
Atterberg Limits	ASTM D4318-95a
Shrinkage Limits	Head (1980); Briaud et. al. (2003)
Specific Gravity	ASTM D854-06
Grain-Size Distribution (Hydrometer)	ASTM D422-63
Clay Dispersion by Double Hydrometer	ASTM D4221-99
Carbonate Content	Dreimanis (1962)
Free Swell Index	Lutenegger (2008)
Specific Surface Area	Cerato and Lutenegger (2002)
One-Dimensional Consolidation	ASTM D2435-04
Undrained Shear Strength	ASTM D4648-05

Table 4.2 summarizes the results of index and classification tests, including water content, Atterberg Limits, shrinkage limit, free-swell index tests, and dispersion. Table 4.3 summarizes results of grain-size analysis, specific gravity tests, carbonate content determination, and specific surface area determination.

Table 4.2 Summary of Index and Classification Tests.

Depth (m)	Depth (ft)	w_n (%)	Atterberg Limits						
			PL	LL	PI	LI	SL_{Lin}	SL_{Diam}	SL_{Vol}
15.5	51.0	80	39	89	50	0.8	22	23	28
17.1	56.0	57	31	75	44	0.6	20	24	29
18.9	62.0	52	29	72	43	0.5	20	18	26
20.4	67.0	71	33	76	43	0.9	22	25	26
21.9	72.0	61	30	74	44	0.7	21	23	21
23.5	77.0	61	29	73	44	0.7	21	24	26
24.7	81.0	50	20	39	19	1.5	21	35	21
26.2	86.0	56	26	58	32	0.9	19	30	22
27.7	91.0	45	22	52	30	0.8	21	20	21
29.6	97.0	41	23	56	33	0.5	23	20	23

Depth (m)	Depth (ft)					USCS Classification
		FSI	RFSI	Swelling Severity	Dispersion (%)	
15.5	51.0	72	1.72	Medium/Slight	40.6	CH
17.1	56.0	79	1.75	Medium/Slight	34.4	CH
18.9	62.0	65	1.65	Medium/Slight	37.2	CH
20.4	67.0	60	1.60	Medium/Slight	33	CH
21.9	72.0	78	1.73	Medium/Slight	30.7	CH
23.5	77.0	70	1.70	Medium/Slight	29.6	CH
24.7	81.0	95	1.90	Medium/Slight	34.1	CL
26.2	86.0	68	1.73	Medium/Slight	30.9	CH
27.7	91.0	49	1.45	Low/Negligible	31.1	CH
29.6	97.0	45	1.45	Low/Negligible	14.8	CH

4.2.1 Water Content

Water content of the soil was determined in general accordance with ASTM Standard D2216-92, *Standard Test Method for Determination of Water (Moisture) Content of Soil and Rock*. Two specimens were obtained from each sample and were placed into aluminum tares and weighed to obtain the total mass of soil and water. The tares were then placed into an oven at an operating temperature of 110 °C for twenty-four hours.

Figure 4.1 presents the variation in water content as a function of depth. Water content in the upper alternating layers of sand and silt range between approximately 20% and 100%. At greater depth to the boundary with the clay layer there is evidence of spatial variation at the site; the data corresponding to Boreholes B-1 and B-4 are grouped, as are the data corresponding to

B-201, B-5, and B-7, which are located on the opposite side of Otter Creek. Within the clay layer the data are less scattered and indicate a general reduction in water content with depth into the clay layer.

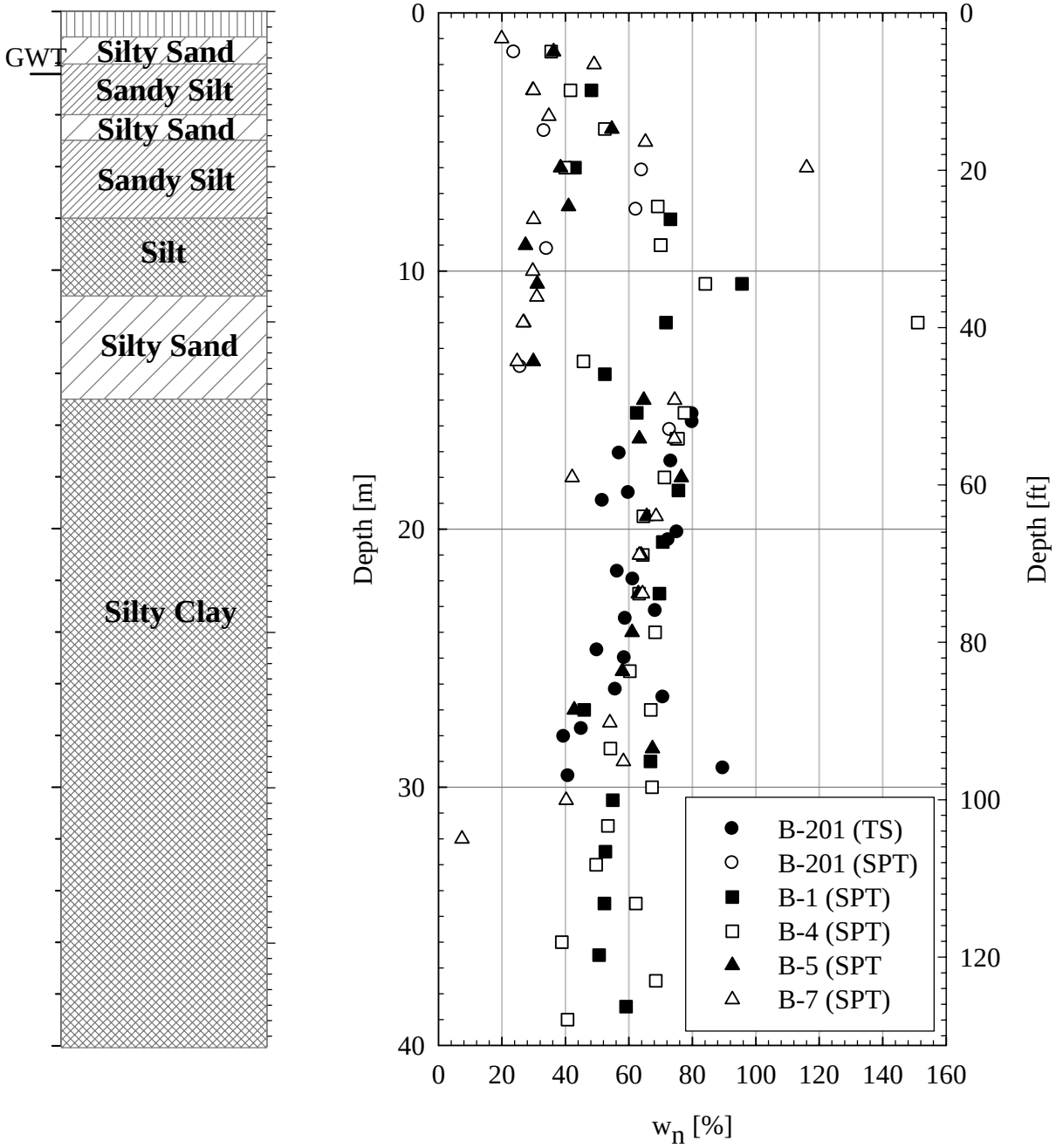

Figure 4.1. Water Content Variation with Depth.

Table 4.3 Summary of Soil Composition Analyses.

Depth (m)	Depth (ft)	Grain Size			Specific Gravity	Carbonates			Specific Surface Area (m^2/g)
		Sand (%)	Silt (%)	Clay (%)		Calcite (%)	Dolomite (%)	Total (%)	
15.5	51.0	0.0	6.4	93.6	2.76	2.4	2.1	4.5	149.3
17.1	56.0	0.0	13.8	86.2	2.77	3.9	3.3	7.2	127.2
18.9	62.0	0.0	18.8	81.2	2.76	5.6	4.2	9.8	101.1
20.4	67.0	0.0	7.4	92.6	2.74	5.6	2.3	7.9	117.5
21.9	72.0	0.0	10.3	89.7	2.75	10.4	4.9	15.3	138.5
23.5	77.0	0.0	9.4	90.6	2.75	6.5	3.4	9.9	119.8
24.7	81.0	0.0	46.9	53.1	2.76	3.5	6.2	9.7	87.6
26.2	86.0	0.0	17.5	82.5	2.73	8.1	4.6	12.7	77.9
27.7	91.0	0.0	31.9	67.1	2.78	6.7	5.1	11.8	81.1
29.6	97.0	0.0	28.1	71.9	2.78	8.5	5.1	13.6	128.0

4.2.2 Atterberg Liquid and Plastic Limits

Atterberg Limits tests were performed in general accordance with ASTM D 4318-95a, *Standard Test Method for Liquid Limit, Plastic Limit, and Plasticity Index of Soils*. Approximately 200 g of soil was required to perform both the liquid and plastic limit tests. The soil was first air-dried and hand-pulverized with a rubber-tipped mortar and pestle and passed through a #40 sieve. Distilled water was added to the samples to bring the water content to a point where the blow count equaled 15 or less and the sample was covered and placed in a humid room for 24 hours to temper. The liquid limit test was performed using a Casagrande cup.

Figure 4.2 presents the results of Atterberg limit tests performed on samples obtained from Boreholes B-4, B-7, and B-201 versus depth. The liquid limit, plastic limit, and natural water content are plotted together with liquid limit and plastic limit indicated using error bars. The corresponding plasticity and liquidity indices are also presented. The plastic limit values remain fairly consistent throughout the profile for all boreholes, with a range of approximately 15% to 40%. The liquid limits range from approximately 25% to 89%, with an overall trend of decreasing with depth. The resulting plasticity indices range from approximately 9% to 50% and also decrease with depth. Values remain consistent around an average of approximately 40% to a depth of 25.0 m (82.0 ft). At a depth of 25.0 m (82.0 ft) there is a slight decrease in values to approximately 30%, and at depths exceeding 35.0 m (114.8 ft) there is a sharp decrease to a minimum value of 9%. The in situ water contents tend to be close to and in some cases exceed the liquid limit values, which is typical for normally consolidated to slightly overly consolidated clays. The resulting liquidity indices range from approximately 0.5 to 2.8, indicating a range of behavior under shearing from that of a plastic solid to that of a viscous fluid.

Figure 4.3 shows plasticity index and liquid limit data on Casagrande's Plasticity Chart. Most of the data points plot in the high plasticity clay (CH) region corresponding, however several data points from Boreholes B-201, B-5, and B-7 with liquid limits of less than 50% plot in the low plasticity clay (CL) region.

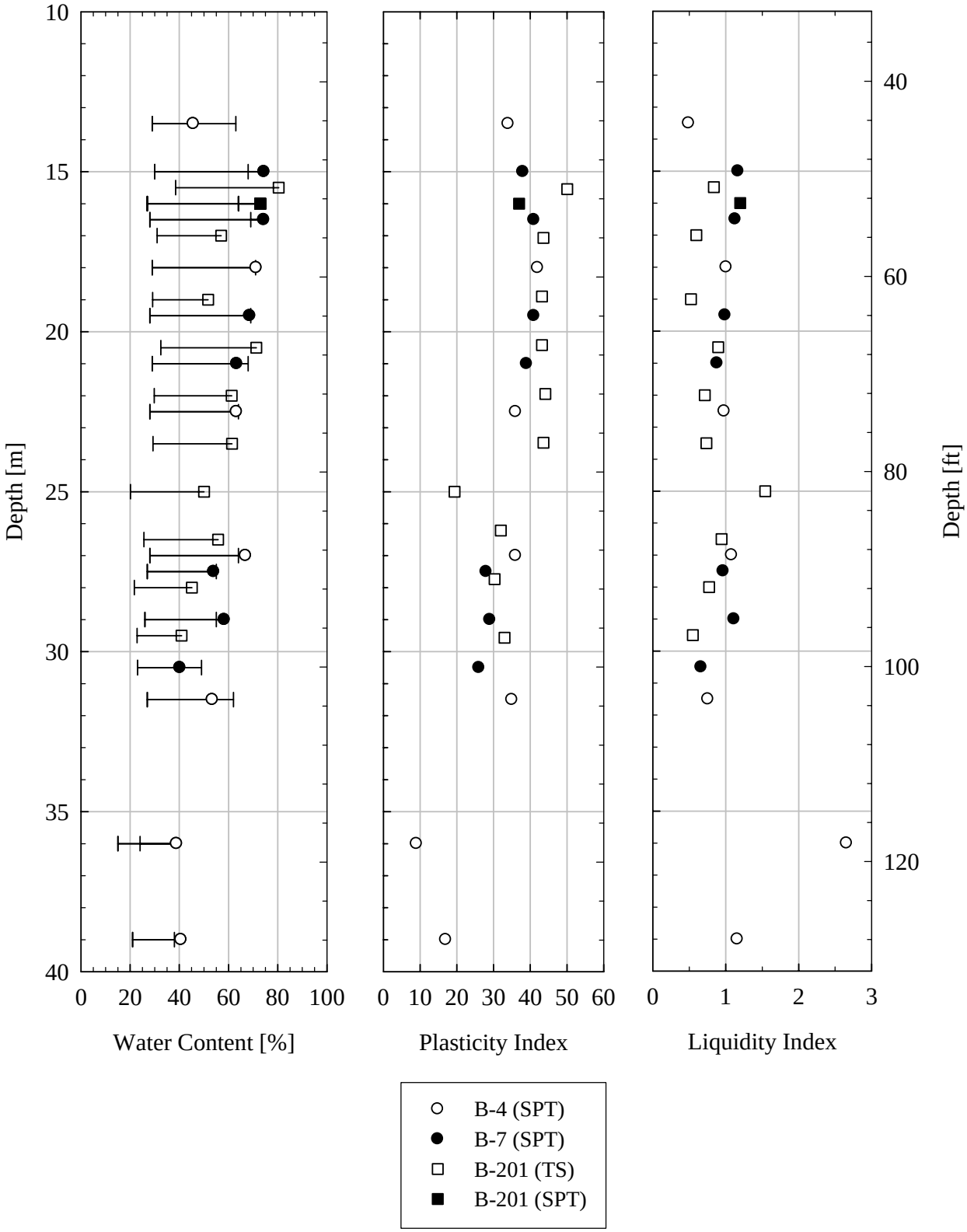

Figure 4.2 Variation in Atterberg Limits with Depth.

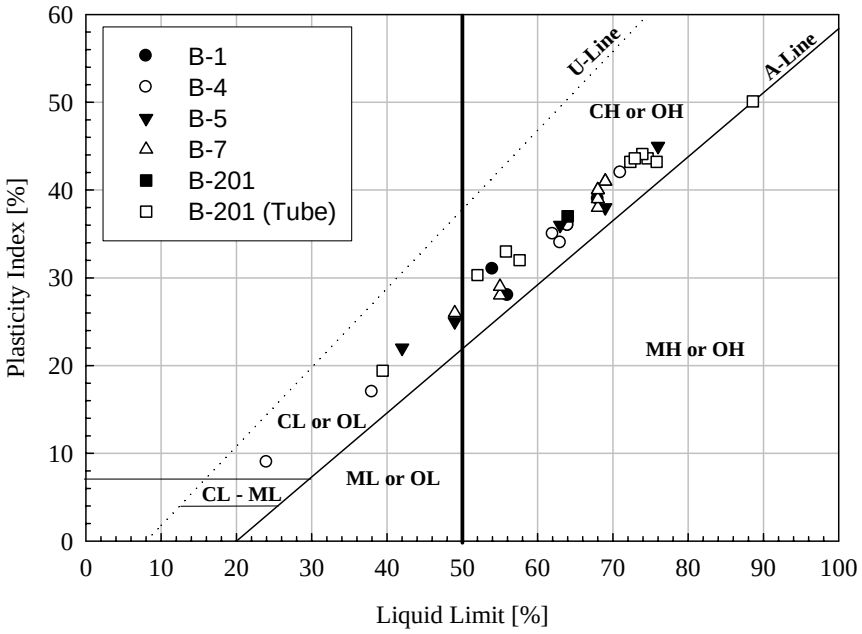

Figure 4.3. Casagrande Plasticity Chart.

4.2.3 Shrinkage Tests

Shrinkage tests were performed using the procedures presented by Head (1980) and Briaud et al. (2003). Approximately 150 g of soil was required to perform the linear shrinkage limit test as presented by Head (1980). The specimen was prepared prior to the liquid limit test using the same soil sample. A shrinkage mold consisting of a semi-cylindrical trough 140 mm (5.5 in) long and 15 mm (0.6 in) diameter was cleaned and the inside coated with a thin film of vacuum grease and weighed. The soil sample was then placed into the mold and worked in order to ensure that no air is entrapped. The specimen length was measured and recorded periodically using a digital caliper and the mass of the specimen and mold was measured using a digital scale. Once the specimen length became constant with time, the specimen was oven dried and the mold and specimen weighed to obtain the dry mass of the specimen. A similar procedure was also adapted to measure diametric shrinkage limit using the Shrinkage Limit dish. Approximately 20 g of soil was required to perform the diametric shrinkage limit test using a circular mold with an internal diameter of 42 mm (1.65 in) and depth of 11.5 mm (0.45 in).

Shrinkage tests on undisturbed samples were performed using the procedure described by Briaud et al. (2003). Specimens approximately 74 mm (2.9 in) in diameter and 32 mm (1.25 in) in height were obtained from the extruded soil using a wire saw. Each specimen was placed on a Plexiglas plate of known mass and allowed to air dry at room temperature. The specimens were placed upright in order to expose the maximum amount of surface area. Specimen diameter and height were measured periodically using a digital caliper and mass including Plexiglas plate

measured using a digital scale. Specimens were oven dried in porcelain dishes and weighed once shrinkage ceased.

The linear shrinkage limit results are very consistent with a range of 19% to 23%. The volumetric shrinkage limit results show a trend of decreasing shrinkage limit with depth, with an overall range of 21% to 28%. The volumetric shrinkage limit is greater than or equal to the linear shrinkage limit throughout clay layer, most likely due to the destruction of existing soil structure when preparing the linear shrinkage limit specimens.

4.2.4 Specific Gravity Tests

Specific gravity was determined in general accordance with ASTM D854 *Standard Test Method for Specific Gravity of Soils* using approximately 20 g of soil. The soil was first air-dried and hand-pulverized with a rubber-tipped mortar and pestle and passed through a #40 sieve. Specific gravity is reported based upon water at 20°C using a conversion factor, K, based upon the temperature at the time of the test. The specific gravity data range from 2.73 to 2.78 and are very uniform throughout the soil layer with an average value of 2.76.

4.2.5 Grain-Size Distribution

Grain-size distribution was determined using the hydrometer method described in ASTM 422-63 *Standard Test Method for Particle-Size Analysis of Soils*. The hydrometer analysis was performed on approximately 50 g specimens using sodium hexametaphosphate as the dispersing agent. After the hydrometer readings were complete, the soil suspension was passed through a #200 sieve to obtain the percentage of sand.

General grain-size composition ranges are 0% sand, 6.4% to 46.9% silt, and 53.1% to 93.6 % clay-sized particles. The lack of sand within the soil is in agreement with grain-size distribution data provided by VTrans in which a negligible percentage of sand is reported. The soil is fairly uniform over depth, with a slight increase in the percentage of silt particles at depths below 27.7 m (91.0 ft). The presence of a thin layer of low plasticity clay at a depth of 24.7 m (81.0 ft) is shown as a sudden increase in silt particles and decrease in clay-sized particles within the layer.

4.2.6 Dispersion by Double Hydrometer

The percent dispersion of the soil samples was determined using the double hydrometer method described in ASTM D4221-99 *Standard Test Method for Dispersive Characteristics of Clay Soils by Double Hydrometer*. The procedure for determining the dispersive characteristics of the fine-grained soils is identical to the procedure for determining grain-size distribution by hydrometer analysis as described above, however the dispersing agent is omitted. The dispersion is expressed as a percentage and was determined as:

$$\text{Dispersion} = \frac{\%\ \text{finer than}\ 5\ \mu\text{m (Method D}-4221)}{\%\ \text{finer than}\ 5\ \mu\text{m (Method D}-422)} \times 100\%$$

The values range from 14.6% to 40.8% with most of the values falling into the range of 30% to 50%, indicating a moderately dispersive soil.

4.2.7 Carbonate Content

The carbonate content was determined using the Chittick Apparatus and procedure presented by Dreimanis (1962). The Chittick Apparatus measures the amount of carbonates in soil by measuring the amount of carbon dioxide that evolves from the reaction between the carbonates and a dilute hydrochloric acid solution. The percentages of calcite and dolomite are calculated separately based upon the data. The carbonate content data show an increase in total carbonate content with depth with an overall range of 4.5% to 15.3%. The percentages of calcite and dolomite are approximately equal at the top of the clay layer however with increasing depth the data show a greater increase in calcite than dolomite. The overall range of calcite content is 2.4% to 10.4%. The range of dolomite content is 2.1% to 5.1%.

4.2.8 Free Swell Index

Free swell index tests were performed according to the recommended procedures as outlined by Lutenegger (2008). Free swell tests were performed in water on specimens consisting of approximately 10 g of oven dried soil crushed to pass a #40 sieve. Each specimen was then placed into a 25 ml graduated cylinder and the initial volume of soil recorded. Each specimen was then transferred to a graduated cylinder filled with 100 ml of water and stirred to remove air pockets. The specimens were allowed to swell for 24 hours, after which the final volume of soil and water was recorded. The Free Swell Index, FSI, and Relative Free Swell Index, RFSI, were determined as:

$FSI = (V_F - V_O)/V_O \times 100\%$

and

$RFSI = (V_F/M_S)$

where:

M_s = mass of soil, g
V_O = initial volume of soil, ml
V_F = final volume of soil, ml

Free swell index tests were also performed using kerosene in place of distilled water. Specimens identical to those described above for the distilled water procedure were placed into graduated cylinders containing 40 ml of kerosene and mixed using a glass stirring rod. The specimens were then permitted to swell for 24 hours. The volume of kerosene and soil was then recorded. The Differential Free-Swell Index, DFSI, and Free-Swell Ratio, FSR, were determined as:

$DFSI = (V_W - V_K)/V_K \times 100\%$

and

$$FSR = (V_W/V_K)$$

where:

V_K = volume of soil in kerosene, ml
V_W = volume of soil in water, ml

Free Swell Index (FSI) values range from 45% to 90%, with values of less than 50% indicating a low swelling severity and within the range of 50% to 100% indicating medium swelling severity. The Relative Free Swell Index (RFSI) follow a very similar pattern to the FSI data and range from 1.45 to 1.90, with values of less than 1.50 indicating a negligible swelling severity and within the range of 1.5 to 2.0 indicating a slight swelling severity.

4.2.9 Specific Surface Area

Total specific surface area was determined using the Ethylene Glycol Monoethyl Ether (EGME) method as specified by Cerato and Lutenegger (2002). External specific surface area was determined using the BET method using a Quantachrome MONOSORB surface area analyzer. The total specific surface area (SSA) ranges from 77.0 m^2/g to 149.3 m^2/g suggesting that the soil is composed primarily of illite.

4.2.10 One-Dimensional Consolidation (Oedometer)

One-dimensional consolidation tests were performed in general accordance with ASTM D 2435 *One-Dimensional Consolidation Properties of Soils* using a fixed ring oedometer cell and a Wykeham Farrance rear-loading dead load lever arm consolidation frame. Incremental load tests were performed on all specimens. Each specimen was obtained from a sample extruded from the Shelby tubes and directly trimmed into the 6.35 cm (2.5 inch) diameter by 1.905 cm (0.75 inch) height lightly lubricated stainless steel consolidation ring using a trimming jig.

Table 4.4 presents a summary of stress history parameters determined from one-dimensional consolidation data. The overburden effective stress, s_{vo}', at the site prior to construction is plotted with depth based upon assumed soil total unit weights of 19.5 kN/m^3 (124.2 pcf) for soil above the groundwater table (topsoil and silty sand) and 18.5 kN/m^3 (117.8 pcf) for the alternating silty and sandy soils below the groundwater table. A unit weight of 16.3 kN/m^3 (103.8 pcf) was assumed for the clay layer based upon the average of values obtained from consolidation specimens. The preconsolidation stress, σ'_p, was determined based upon Casagrande construction (Casagrande 1936) using the stress and strain data obtained from one-dimensional consolidation data. Plots of stress versus strain for each specimen are provided in Appendix A. The compression index, C_c, was determined as the slope of the virgin compression portion of the curve plotted based upon stress versus void ratio. The recompression index, C_r, was determined as the slope of the recompression portion of the stress versus void ratio curve.

The overconsolidation ratio (OCR) was determined as the ratio of the preconsolidation stress to the effective overburden stress at sample depth.

Table 4.4 Summary of One Dimensional Consolidation Tests.

Depth (m)	Depth (ft)	σ (kPa)	u (kPa)	σ_{vo}' (kPa)	σ_p' (kPa)	C_c	C_r	OCR
15.5	51.0	288.4	128.8	159.6	150	1.241	0.082	0.9
17.1	56.0	313.3	143.8	169.5	160	1.230	0.091	0.9
18.9	62.0	340.6	160.2	180.4	160	0.997	0.085	0.9
20.4	67.0	365.4	175.1	190.3	135	0.769	0.086	0.7
21.9	72.0	390.3	190.1	200.2	160	0.852	0.107	0.8
23.5	77.0	415.1	205.0	210.1	125	0.628	0.088	0.6
24.7	81.0	437.5	218.4	219.0	100	0.244	0.025	0.5
26.2	86.0	464.8	234.9	229.9	200	0.704	0.033	0.9
27.7	91.0	487.2	248.3	238.9	200	0.676	0.040	0.8
29.6	97.0	514.5	264.7	249.8	210	0.854	0.050	0.8

Table 4.5 Summary of Interpreted Undisturbed Sample Quality.

Depth (m)	Depth (ft)	e_0	Δe	$\Delta e/e_0$	NGI Sample Quality
15.5	51.0	2.11	0.12	0.06	Good to Fair
17.1	56.0	2.11	0.19	0.09	Poor
18.9	62.0	1.97	0.20	0.10	Poor
20.4	67.0	1.71	0.26	0.15	Very Poor
21.9	72.0	1.86	0.20	0.11	Poor
23.5	77.0	1.56	0.24	0.16	Very Poor
24.7	81.0	0.96	0.19	0.20	Very Poor
26.2	86.0	1.38	0.16	0.13	Poor
27.7	91.0	1.25	0.18	0.14	Poor
29.6	97.0	1.42	0.20	0.14	Poor

Based on the geology of the site and the relationship between Atterberg limits and in situ water content, the soil is expected to be normally or slightly overconsolidated (OCR of approximately 1.0). The results of one-dimensional consolidation tests show that the OCR ranges from 0.5 to 0.9, indicating possible severe sample disturbance. In order to determine the sample quality, the Norwegian Geotechnical Institute method was used based upon change in void ratio (Δe) from initial value prior to testing (e_0) to the value corresponding to the in situ overburden pressure. Figure 4.4 shows the variation in stress history with depth. The plots of OCR and void ratio change are inversely related, as sample disturbance causes a reduction in preconsolidation stress and therefore a reduction in overconsolidation ratio. According to the NGI system the samples would generally be considered of poor to very poor quality, with one sample being of good to fair quality at a depth of 15.5 m (51.0 ft). A possible explanation is disturbance due to drilling and sampling operations (incorrect drilling mud unit weight, rebound due to unloading, etc.) or disturbance during transport, storage and handling or extrusion. All of these operations may induce some sample disturbance to very soft fine-grained soils.

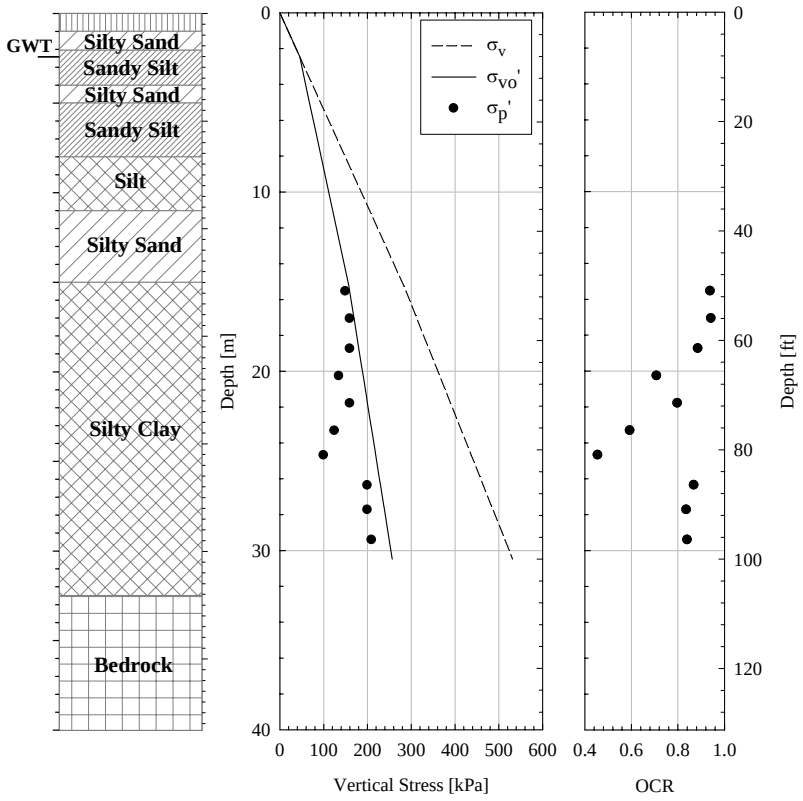

Figure 4.4 Stress History Profile for Leicester, VT Bridge Site.

4.2.11 Undrained Shear Strength

The undrained shear strength of the soil was determined using a lab vane in accordance with ASTM D 4648 *Standard Test Method for Laboratory Miniature Vane Shear Test for Fine-Grained Clayey Soils*. In addition, Torvane and Pocket Penetrometer tests were conducted in approximately the same locations as the lab vane tests. A 2:1 (H:D) vane with a diameter of 19.1 (0.75 in) and height of 38.1 mm (1.5 in) was used for all tests. Shearing of the specimen was conducted at a vane rotation rate of 90°/min. After obtaining the peak strength the soil was remolded using the vane rotating at a rate of 2700°/min for seven rotations backward and forward. Within one minute, the test was repeated at a rotation rate of 90°/min, once again allowing the vane to rotate 180° (or two minutes of rotation). Table 4.5 presents the results of miniature laboratory vane tests conducted to determine the undrained shear strength of specimens obtained from the tube samples. Also included are results of pocket penetrometer and torvane tests. Plots of undrained shear stress versus vane rotation for each specimen are provided in the Appendix B.

The peak (s_{upeak}), post-peak ($s_{upost\text{-}peak}$), and remolded ($s_{uremolded}$) undrained shear strength values obtained for each specimen are plotted versus depth in Figure 4.5. Peak and remolded undrained shear strength values obtained from field vane tests performed in Borehole B-201 are also plotted. The laboratory vane test data show a range of peak undrained shear strength ranging from 4.3 kPa to 52.1 kPa. The peak undrained shear strength values obtained from in situ vane tests tend to be less scattered, plotting within the range of values obtained through

Table 4.5 Summary of Undrained Shear Strength Measurements.

Depth (m)	Depth (ft)	w_n (%)	P.P. (kPa)	Torvane (kPa)	Lab Vane s_{upeak} (kPa)	Lab Vane $s_{upost-peak}$ (kPa)	$s_{upeak}/s_{upost-peak}$	Lab Vane $s_{uremolded}$ (kPa)	Lab Vane Sens.
15.5	51.0	80.0	27.0	29.4	41.8	13.2	3.2	9.5	4.4
15.8	52.0	80.0	12.3	19.6	52.1	13.9	3.7	7.6	6.9
17.1	56.0	57.0	24.5	29.4	30.2	14.1	2.1	10.3	2.9
17.4	57.0	73.3	19.6	36.8	34.1	13.9	2.5	6.3	5.4
18.6	61.0	59.9	12.3	19.6	47.2	13.2	3.6	3.5	13.5
18.9	62.0	51.7	12.3	19.6	28.9	10.2	2.8	5.3	5.5
20.1	66.0	75.2	28.2	19.6	42.1	11.8	3.6	10.6	4.0
20.4	67.0	72.4	14.7	24.5	51.6	15.0	3.4	7.4	7.0
21.6	71.0	56.4	24.5	19.6	14.3	5.2	2.7	8.5	1.7
21.9	72.0	61.3	24.5	31.9	50.8	15.0	3.4	7.2	7.1
23.2	76.0	68.4	24.5	19.6	18.4	12.7	1.4	6.6	2.8
23.5	77.0	58.9	24.5	24.5	44.4	12.8	3.5	10.9	4.1
24.7	81.0	50.0	14.7	19.6	11.4	0.9	12.7	0.9	12.7
25.0	82.0	58.6	14.7	24.5	30.0	11.2	2.7	5.8	5.2
26.2	86.0	55.8	12.3	14.7	30.2	11.9	2.5	6.0	5.1
26.5	87.0	70.8	40.5	44.1	33.2	11.4	2.9	5.9	5.6
27.7	91.0	45.1	14.7	19.6	41.9	15.7	2.7	5.5	7.6
28.0	92.0	39.5	17.2	24.5	27.2	9.7	2.8	5.0	5.4
29.3	96.0	89.7	< 4.9	< 9.8	4.3	0.9	5.1	-	-
29.6	97.0	40.9	19.6	29.4	36.3	12.6	2.9	7.7	4.7

laboratory tests, and show an overall trend of a slight reduction in shear strength with depth. The remolded undrained shear strength values obtained from laboratory vane tests range from 0.9 kPa to 10.9 kPa. The results obtained from the field vane tests are consistently lower. This may be due to a number of variations between the laboratory and field procedures such as the number of turns of the vane during remolding and the time lapse between remolding and retesting of the soil. The range of sensitivity values based on laboratory vane tests is 1.7 to 13.5, with a majority of the data within a range of 2 to 8. Given the lower values of remolded undrained shear strength obtained from the field vane tests, the corresponding sensitivities obtained from the field vane data tend to be significantly higher than those determined based upon laboratory data.

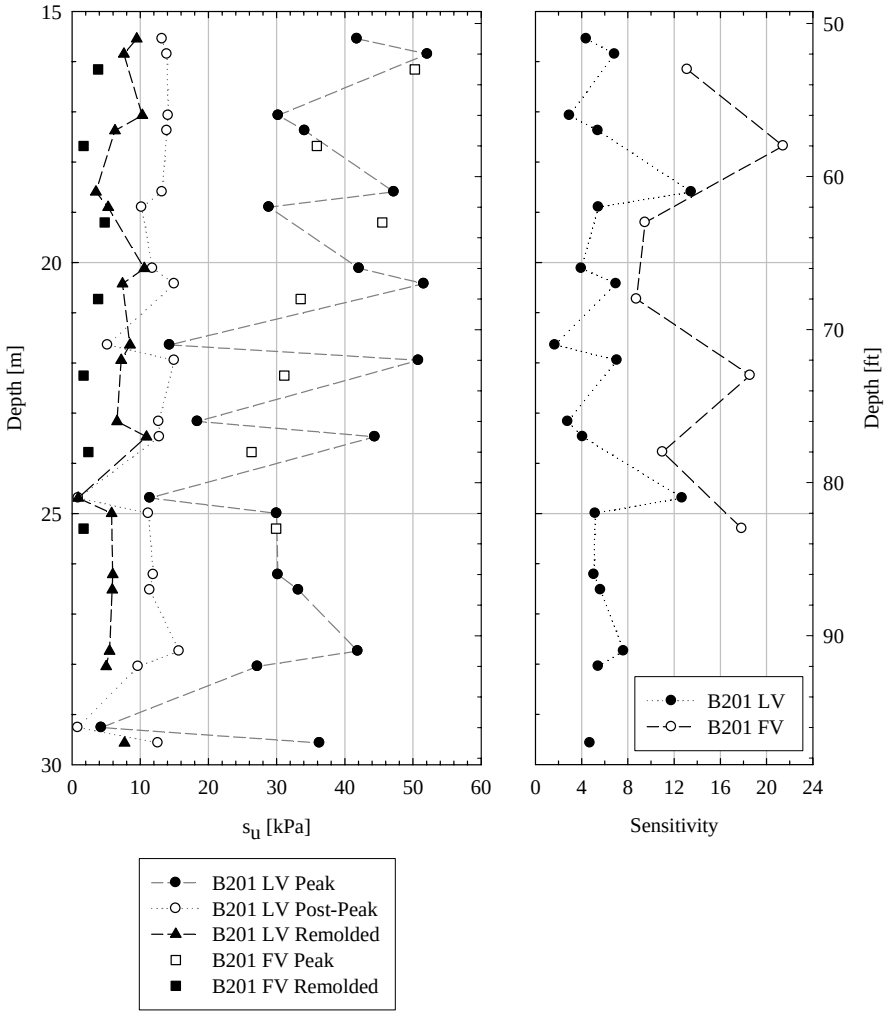

Figure 4.5 Variation in Undrained Shear Strength with Depth.

CHAPTER 5. FIELD INSTRUMENTATION

5.1 Introduction

A field instrumentation program was implemented in this project in order to measure horizontal pressures on the rear wall of the abutment as well as vertical pressures within the GeoFoam backfill. Instrumentation was installed during construction of the bridge and data were recorded periodically throughout the remainder of construction and following the opening of the bridge to vehicular traffic.

5.2 Total Earth Pressure Cells

Hydraulic contact earth pressure cells consisting of two flat plates welded together at their periphery with a hydraulic fluid filling the gap between the plates and with vibrating wire transducers were selected for instrumentation. Pressure acting upon the cell causes the plates to squeeze together resulting in a buildup of pressure inside the fluid. A hydraulic pressure transducer converts the fluid pressure to an electrical signal which is transmitted to a readout location via cable. Geokon Model 4800 Vibrating Wire Total Earth Pressure Cells were used, as shown in Figure 5.1. The plate diameter is 230 mm (9 in.) and cell thickness is 6 mm (0.24 in.) with one thin plate designed to react to soil pressure and one thick plate designed to bear against the external surface of a structure to prevent flexure of the cell. The range of operating temperatures for the cells is -20 °C to +80° C. Four tabs are welded onto the rigid plate for mounting. A thermistor within the transducer housing records temperature. Data are transmitted through a 4 conductor 22 AWG cable. Each cell has a pressure range of 70 kPa (10 psi).

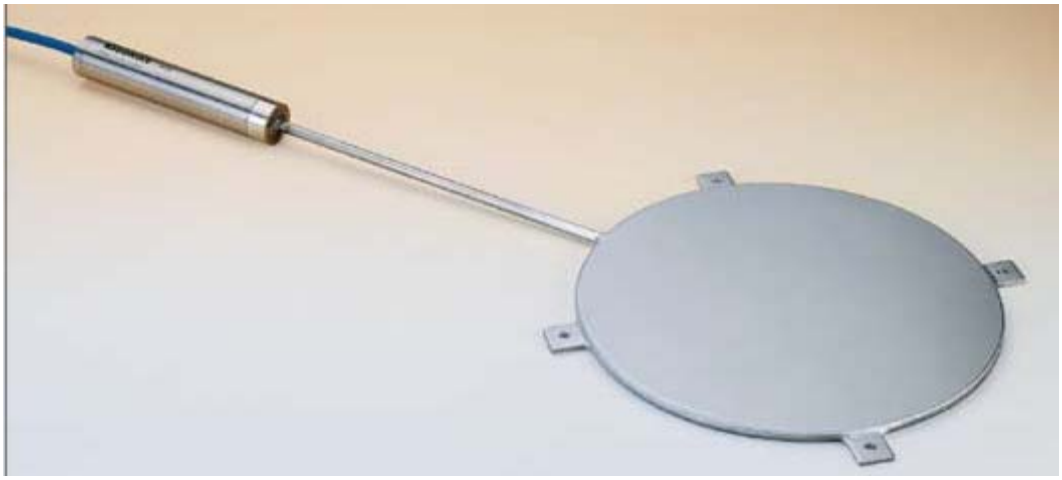

Figure 5.1 Geokon Model 4800 Total Earth Pressure Cell.

A total of 12 earth pressure cells were installed at the site during construction, with 6 cells on each side of the bridge. Prior to installation each cell was tested and the digit reading and temperature recorded upon removal from the factory packaging. Table 5.1 summarizes the pressure cells names and locations. Each cell was referenced using a 3 character symbol consisting of the abutment number (1 or 2) followed by the letter “A” and a number corresponding to the mounting configuration.

Table 5.1 Total Earth Pressure Cell Symbols and Locations.

Symbol	Serial #	Orientation	Location
1A1	06-4230	Horizontal	Base of GeoFoam Blocks
1A2	06-4231	Vertical	Lower Abutment Wall Face
1A3	06-4232	Vertical	Upper Abutment Wall Face
1A4	06-4233	Horizontal	Top of GeoFoam Blocks, Centerline
1A5	06-4234	Horizontal	Top of GeoFoam Blocks, Offset North
1A6	06-4235	Horizontal	Top of GeoFoam Blocks, Offset South
2A1	06-4236	Horizontal	Base of GeoFoam Blocks
2A2	06-4237	Vertical	Lower Abutment Wall Face
2A3	06-4238	Vertical	Upper Abutment Wall Face
2A4	06-4239	Horizontal	Top of GeoFoam Blocks, Centerline
2A5	06-4240	Horizontal	Top of GeoFoam Blocks, Offset South
2A6	06-4241	Horizontal	Top of GeoFoam Blocks, Offset North

An elevation view of the earth pressure cell locations is shown in Figure 5.2. Cell A1 was placed within the sand leveling course prior to installation of the first lift of GeoFoam blocks, as shown in Figure 5.3. The flexible plate of the cell was oriented upward, with the contact plane flush with the sand. Blocks were placed directly over the cell with care taken to avoid any block to block joints crossing the contact area. Cells A2 and A3 were mounted vertically in the abutment walls in recessed spaces formed into the concrete. A layer of plaster was applied to each recessed space and the cells were pressed into the plaster with the flexible contact plate facing outward flush with the face of the wall as shown in Figure 5.4. Additional plaster was spread over the mounting tabs to further secure the cells in place.

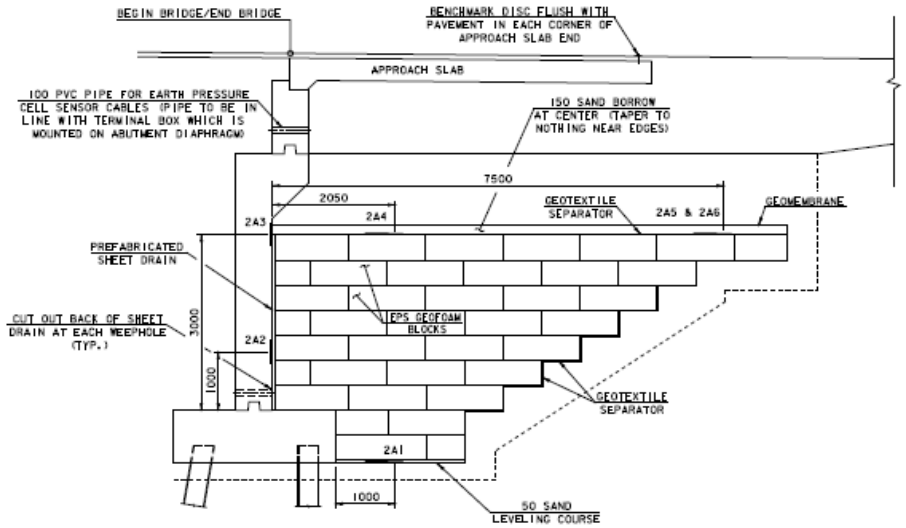

Figure 5.2 Earth Pressure Cell Locations (Abutment 2 Shown).

Figure 5.3. Location and Orientation of Earth Pressure Cells 1A1 and 2A1.

The sheet drain placed between the GeoFoam blocks and the back face of the abutment was in direct contact with the cells. Cells A4, A5, and A6 were placed horizontally onto the geotextile separator on top of the GeoFoam blocks as shown in Figure 5.5. Cell A4 was placed on the centerline of the roadway approximately 2.0 m (6.6 ft) from the abutment face. Cells A5 and A6 were placed approximately 7.5 m (24.6 ft) from the abutment face and were offset 1.0 m (3.3 ft) from the roadway centerline. V-shaped notches were cut out of the blocks in order to recess the transducer housing, allowing the cells to be placed flat. The contact plates faced upward with the sand course laid directly over the cells. A zero reading was recorded for each cell with zero load placed over the contact area. The cables for all of the pressure cells were run through a conduit to the front side of the abutment.

Figure 5.4. Installation of Earth Pressure Cells 1A2, 1A3, 2A2, and 2A3.

A Geokon GK-403 Vibrating Wire Readout Box was used for all data collection for the project. Data acquisition commenced with the installation of the first instrumentation at Abutment 1 on 25 August 2006. Instrumentation installation at Abutment 1 was completed on 6 September 2006. Instrumentation installation at Abutment 2 began on 14 September 2006 and concluded on 19 September 2006. Readings were taken during construction activities such as backfilling and compaction of the approach fills in order to verify that the pressure cells were properly registering stress changes with increased loading. The first reading with the bridge approaches complete was recorded on 16 November 2006. On 14 December 2006 the data transmission cables were wired into breaker boxes located on the front side of each abutment as shown in Figure 5.6.

Figure 5.5. Installation of Earth Pressure Cells 1A4, 1A5, 1A6, 2A4, 2A5, 2A6.

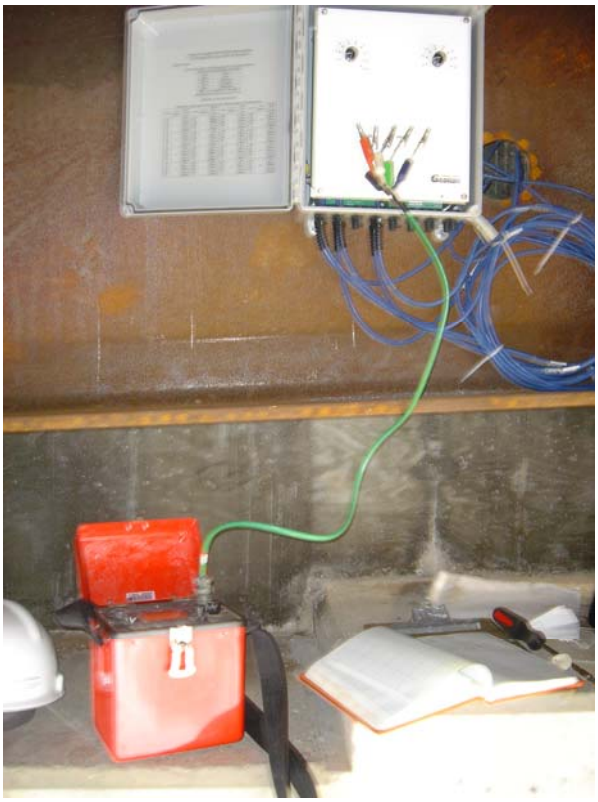

Figure 5.6. Central Breaker Box and Geokon GK-403 Vibrating Wire Readout Box.

CHAPTER 6. RESULTS AND INTERPRETATION OF INSTRUMENTATION

The installation of field instrumentation during construction of the bridge permitted measurement and monitoring of earth pressure stresses during construction operations as well as post-construction. In order to assess the performance of the GeoFoam blocks in reducing earth pressures, estimates of the lateral and vertical earth pressures using conventional backfill will be compared to actual measured pressures. The measured pressures are also compared to estimates of the lateral and vertical earth pressures using GeoFoam blocks with material properties reported in previous field studies. The at-rest coefficient of lateral earth pressure (K_0) for the GeoFoam blocks is also determined based upon measured pressures and further interpretation of the data.

6.1 Earth Pressure Measurements

The digit and temperature readings recorded for each earth pressure cell were converted to pressure values using the equation:

$$P_{corrected} = \left((R_0 - R_1)\times C\right) + \left((T_1 - T_0)\times K\right) \qquad [6.1]$$

where:

C = pressure linear gage factor, kPa/digit
K = thermal factor, kPa/°C
$P_{corrected}$ = pressure measurement corrected for temperature, kPa
R_0 = in place initial digit reading at time of installation, “digits”
R_1 = recorded digit value, “digits”
T_0 = in place initial temperature reading at time of installation, °C
T_1 = recorded temperature, °C

Digit values and temperature measurements are given in Appendix C for each earth pressure cell.

Earth pressure measurements at each transducer location for both abutments are plotted versus time in Figures 6.1 through 6.6. The end of construction operations is shown in each figure in order to identify construction related increase in pressure (paving, backfilling, etc.). There is a considerable gap in data from January 2007 to May 2007, as environmental conditions prevented access to the data acquisition boxes.

The vertical earth pressures measured at the base of the GeoFoam fill (Transducers 1A1 and 2A1, Figure 6.1) display similar behavioral patterns, however the magnitudes of the pressures in Abutment 2 are considerably larger. Initial measured pressures were approximately equal on both sides of the bridge, however between September 2006 and October 2006 a significant increase in pressure of approximately 53 kPa was recorded by Transducer 2A1. An increase in pressure over the same period was also recorded by Transducer 1A1, however the actual magnitude of the increase was approximately 12 kPa. Between October 2006 and November 2006 the pressure increased to the end of construction levels, with the magnitude of the pressure measured by Transducer 2A1 being considerably larger than the pressure measured

by Transducer 1A1. Following the end of construction operations, measured pressures at both abutments fluctuate but return to approximately the end of construction levels. The pressures measured by Transducer 1A1 increase between the end of construction and the reading recorded in January 2007, then gradually decrease to the final measured value. The behavior of the pressures measured by Transducer 2A1 is essentially the opposite; the stresses decrease from the end of construction operations to the reading recorded in May 2007, then increase to the final measured value. The pressures at both abutments appear to become constant between July 2007 and August 2007.

The lateral earth pressures measured at approximately the mid-depth of the GeoFoam blocks (Transducers 1A2 and 2A2, Figure 6.2) also display significant differences in magnitudes. Between September 2006 and October 2006, Transducer 1A2 measured a pressure increase of significantly greater magnitude than the increase measured by Transducer 2A2. The pressure increase to the end of construction level between October 2006 and November 2006 was also significantly greater at Abutment 1 than Abutment 2, with a value of 12 kPa measured at Abutment 2 and a value of 82 kPa measured at Abutment 1. The overall behavior over the course of the monitoring period is markedly different between the two abutments. The pressures at Abutment 1 remain approximately constant following an initial decrease after the end of construction, then sharply increase to a level exceeding the end of construction pressure. The pressures at Abutment 2 increase to a level exceeding the end of construction pressure, then gradually decrease to a negligible pressure level at the end of the monitoring period.

The lateral earth pressures measured at the top surface of the GeoFoam blocks (Transducers 1A3 and 2A3, Figure 6.3) are approximately the same at both abutments. The end of construction pressures were too low to register for both abutments, with negligible pressures measured throughout the remainder of the monitoring period. The pressures measured at Abutment 1 display a slight increase over time, however the overall increase of approximately 4 kPa is within an acceptable range of fluctuation for the instrumentation.

The vertical pressures measured at the top of the GeoFoam blocks at each abutment centerline (Transducers 1A4 and 2A4, Figure 6.4) display parallel behavior throughout the monitoring period. The end of construction pressure of approximately 70 kPa at Abutment 1 is slightly larger than the end of construction pressure of approximately 55 kPa. The pressure measured at the end of the monitoring period is slightly greater than the end of construction pressure at both abutments.

The vertical pressures measured at the top of the GeoFoam blocks offset left of each abutment centerline (Transducers 1A5 and 2A5, Figure 6.5) also display parallel behavior, however in this case the end of construction pressure of 55 kPa at Abutment 1 is less than the end of construction pressure of 79 kPa at Abutment 2. Both transducers registered an initial decrease in pressure following the end of construction operations followed by an increase in pressure to a final value exceeding the end of construction pressure.

The vertical pressures measured at the top of the GeoFoam blocks offset right of each abutment centerline (Transducers 1A6 and 2A6, Figure 6.6) follow a similar pattern to those measured left of the centerline, however the difference between pressures measured at Abutment

1 and those measured at Abutment 2 is slightly smaller. The end of construction pressure measured at Abutment 1 is approximately 53 kPa, while the end of construction pressure measured at Abutment 2 is approximately 65 kPa. Both transducers registered an initial decrease in pressure following the end of construction operations followed by gradual increase in pressure to values exceeding the end of construction pressure.

Vertical pressures measured at both abutments are plotted together versus time in Figure 6.7. The pressures measured at the top of the GeoFoam blocks at both abutments were of similar magnitude during construction operations with the exception of those measured by Transducer 2A5, which measured significantly larger increases in pressure between September 2006 and November 2006. As the changes in pressure measured by Transducer 2A5 are approximately parallel to those measured by the other transducers, it appears that Transducer 2A5 is functioning correctly. The larger measured pressures during construction operations may be due to the use of heavy machinery directly over the location of the transducer, which could have cause compaction of the overlying soil or damage to the transducer.

The pressures measured at the base of the GeoFoam blocks display different behavior both between the two abutments as well as between transducer locations. Transducer 1A1 measured the lowest vertical pressures during the entire monitoring period, whereas the pressures measured by Transducer 2A1 were the highest from October 2006 (during construction) until May 2007, at which point the pressures are equal to those measured by Transducer 2A5. The pressures measured by Transducer 1A1 remained approximately constant following completion of construction operations, whereas Transducer 2A1 measured pressures up to 20 kPa lower than the end of construction level before increasing to the final measured value. It is interesting to note that the pressures measured by Transducers 2A1 and 2A5 eventually converge and thus are approximately equal at the end of the monitoring period.

When comparing the behavior of the vertical pressures measured at the base of the GeoFoam blocks with those measured at the top of the GeoFoam blocks it is clear that there is a significantly different response at the base of the blocks to pressure changes at the top of the blocks at each abutment. The pressures measured by Transducer 1A1 appear to be independent of changes in the pressures acting at the top of the blocks, as measured pressures at the base of the blocks steadily decrease while pressures on the top of the blocks increase. This might indicate that the use of the GeoFoam blocks reduces vertical pressures due to both lower unit weight as well as by reducing the magnitude of stresses that are transferred through the blocks. The pressures measured by Transducer 2A1 also show a degree of independence during a portion of the monitoring period, however towards the end of the monitoring period there was a simultaneous increase in measured vertical pressures at both the top and the base of the blocks. Given the magnitude of the pressures measured by Transducer 2A1 in relation to the other vertical pressures, further analysis is required to verify that the transducer is functioning properly.

The lateral pressures measured at both abutments are plotted versus time in Figure 6.8. Comparing the measured lateral pressures at the top of the blocks with those at the mid-depth of the blocks, it appears that at both abutments the expected triangular earth pressure behavior is being exhibited; the lateral earth pressures increase with depth. In the case of Abutment 1, the

final measured lateral pressure at the top of the GeoFoam blocks was approximately 4 kPa with a final measured lateral pressure at the mid-depth of the blocks of approximately 101 kPa. The magnitudes of the pressures measured at Abutment 2 are drastically less; the final measured value of the lateral pressure at the top of the blocks was of negligible magnitude and the lateral pressure at the mid-depth of the blocks was approximately 1 kPa. Given the similarities of the approach fills at both sides of the bridge, the pressures at the mid-depths should be comparable. As no settlement surveys were conducted to indicate movement of the abutment and given the assumption that the approaches are in the at-rest condition, the probable cause for such significant differences in pressures is instrumentation malfunction. In order to confirm this, further analysis based upon estimates of the working range of lateral pressures will subsequently be discussed.

Overall, the parallel pressure behavior and relatively small difference in pressure magnitudes displayed by the vertically and horizontally positioned transducers located at the top of the GeoFoam blocks confirm that at the top of the GeoFoam blocks the vertical and lateral pressures on both sides of the bridge are very similar. The differences between the measured lateral pressures at the mid-depth and vertical pressures at the base of the GeoFoam blocks between the two abutments requires that measured values be compared with realistic estimates of the stresses in order to determine the reason for the dissimilar behavior and identify equipment malfunctions.

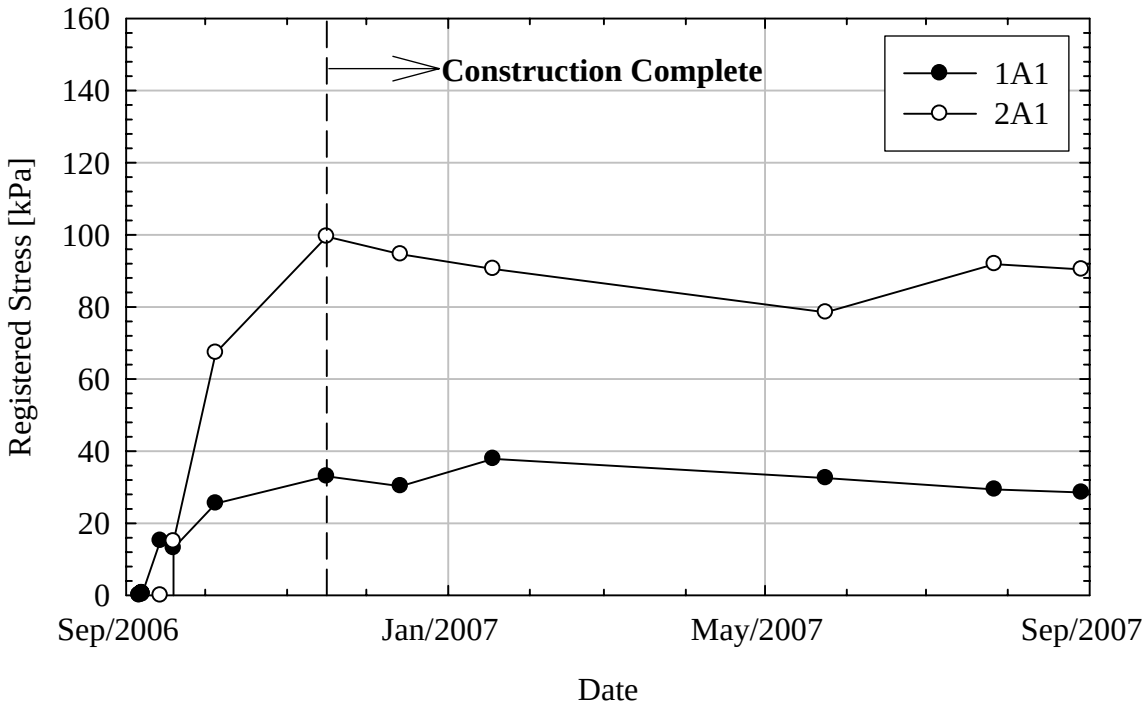

Figure 6.1 Measured Vertical Earth Pressures versus Time for Transducers 1A1 and 2A1 (Base of GeoFoam Blocks, Centerline of Abutments).

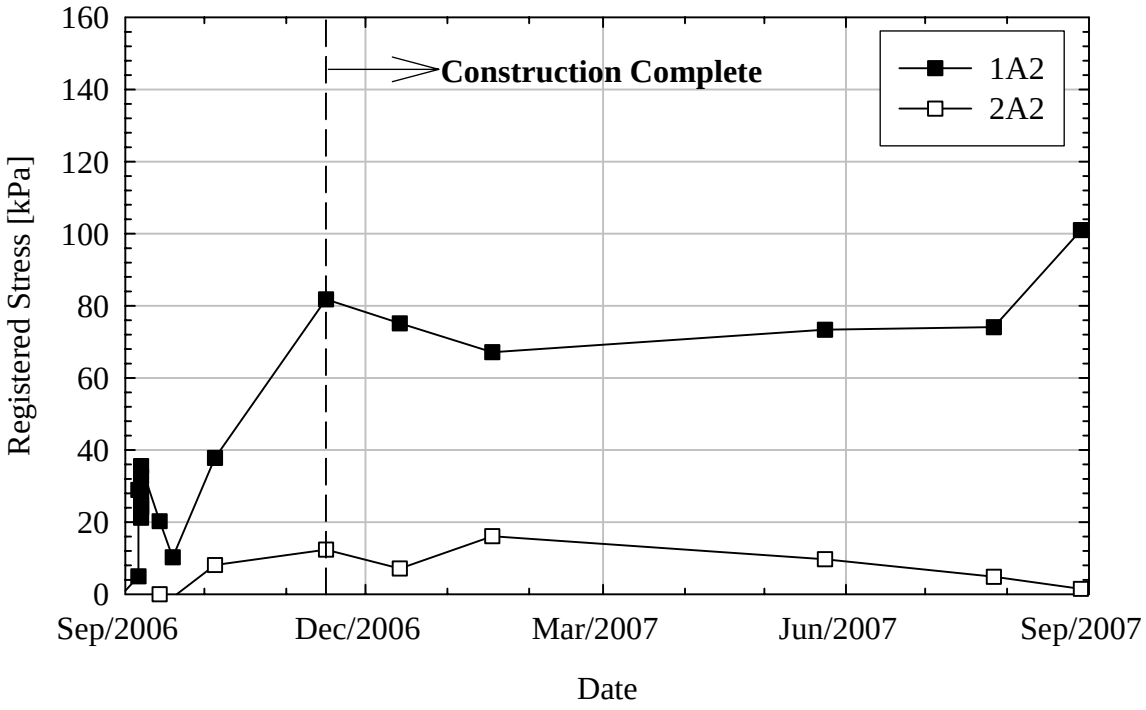

Figure 6.2 Measured Lateral Earth Pressures versus Time for Transducers 1A2 and 2A2 (Lower Back Wall, Centerline of Abutments).

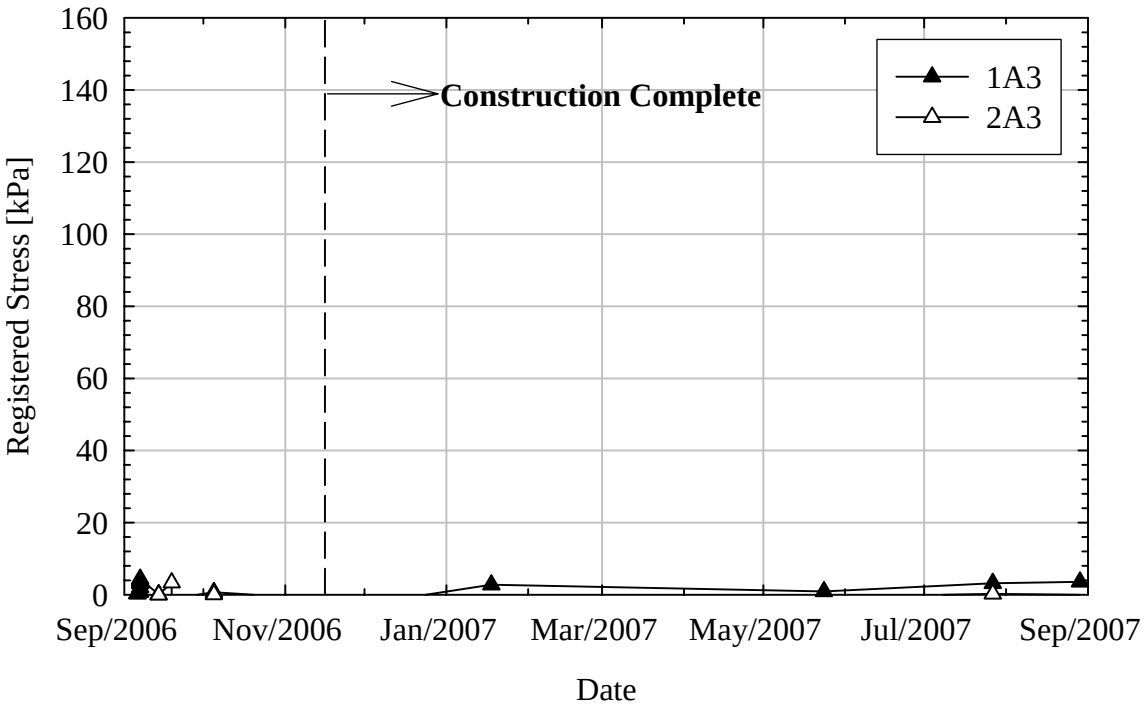

Figure 6.3 Measured Lateral Earth Pressures versus Time for Transducers 1A3 and 2A3 (Upper Back Wall, Centerline of Abutments).

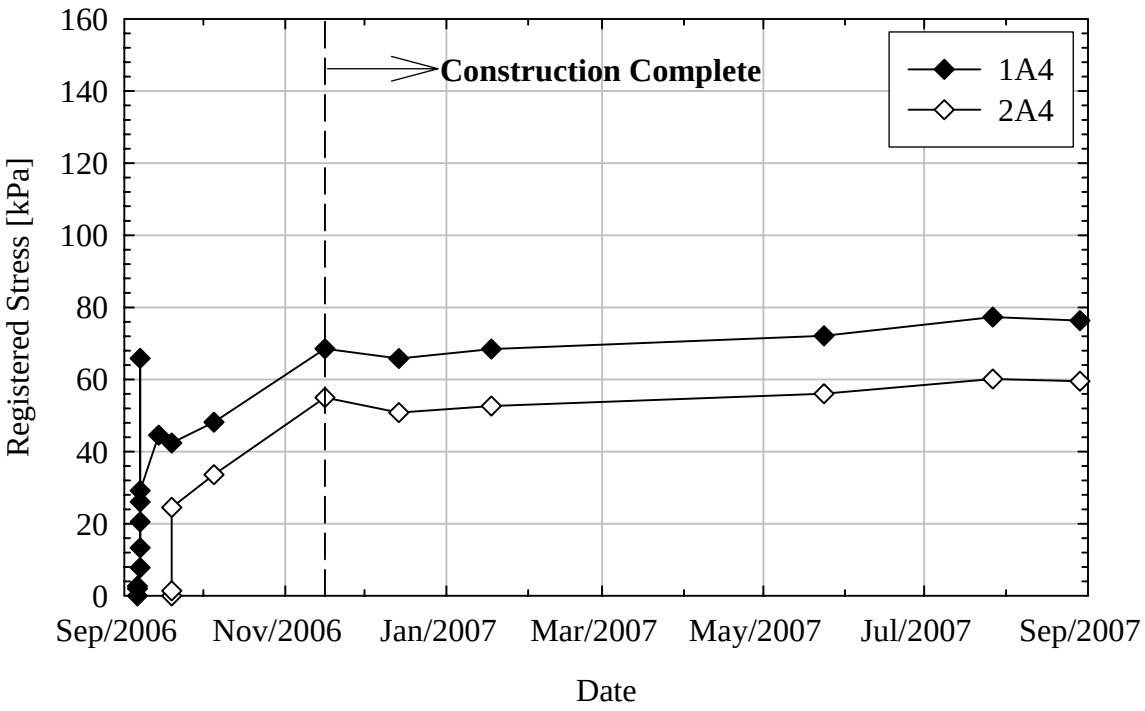

Figure 6.4 Measured Vertical Earth Pressures versus Time for Transducers 1A4 and 2A4 (Top of GeoFoam Blocks, Centerline of Abutments).

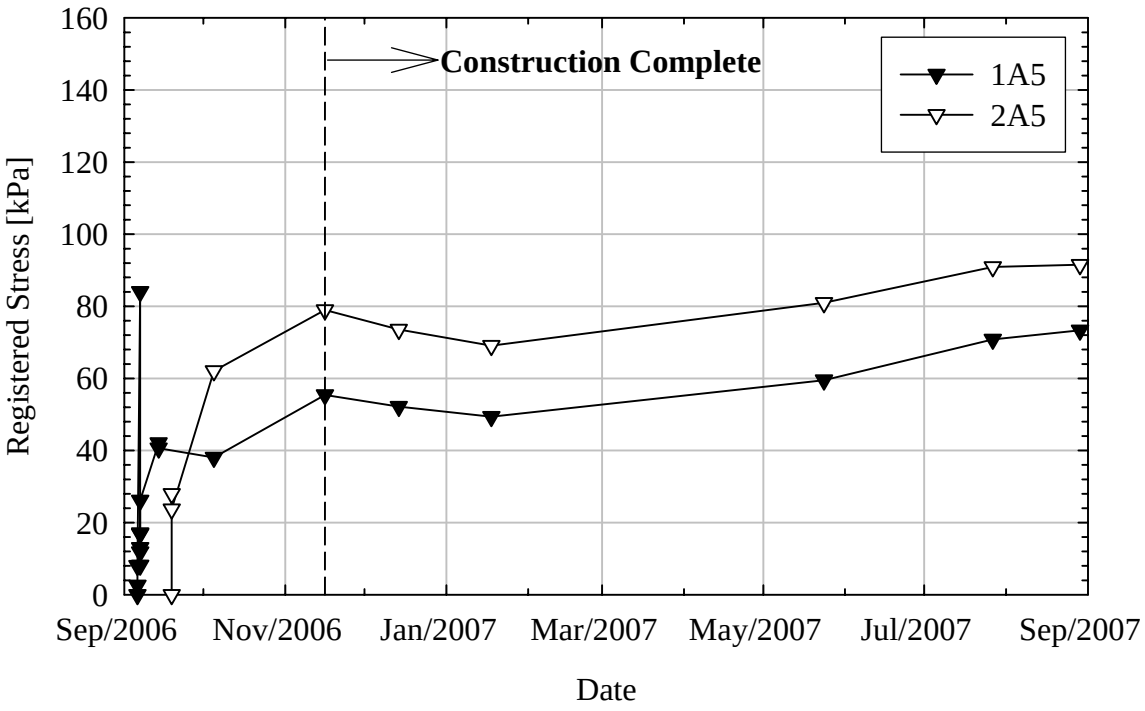

Figure 6.5 Measured Vertical Earth Pressures versus Time for Transducers 1A5 and 2A5 (Top of GeoFoam Blocks, Offset Left of Centerline of Abutments).

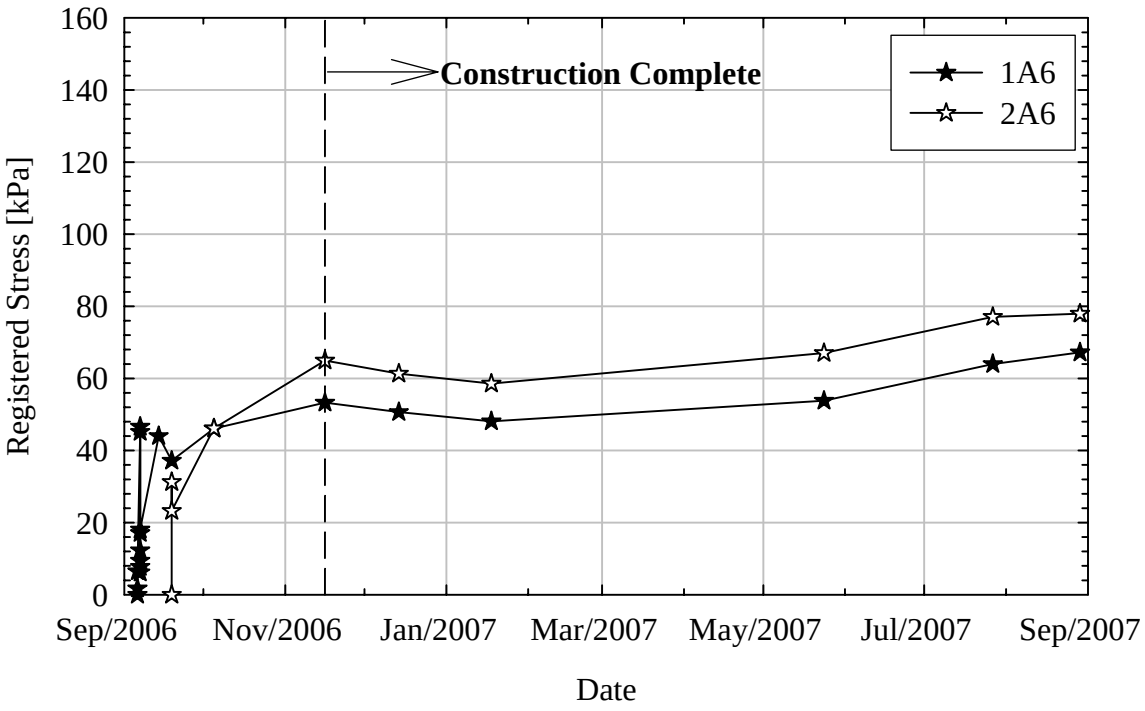

Figure 6.6 Measured Vertical Earth Pressures versus Time for Transducers 1A6 and 2A6 (Top of GeoFoam Blocks, Offset Right of Centerline of Abutments).

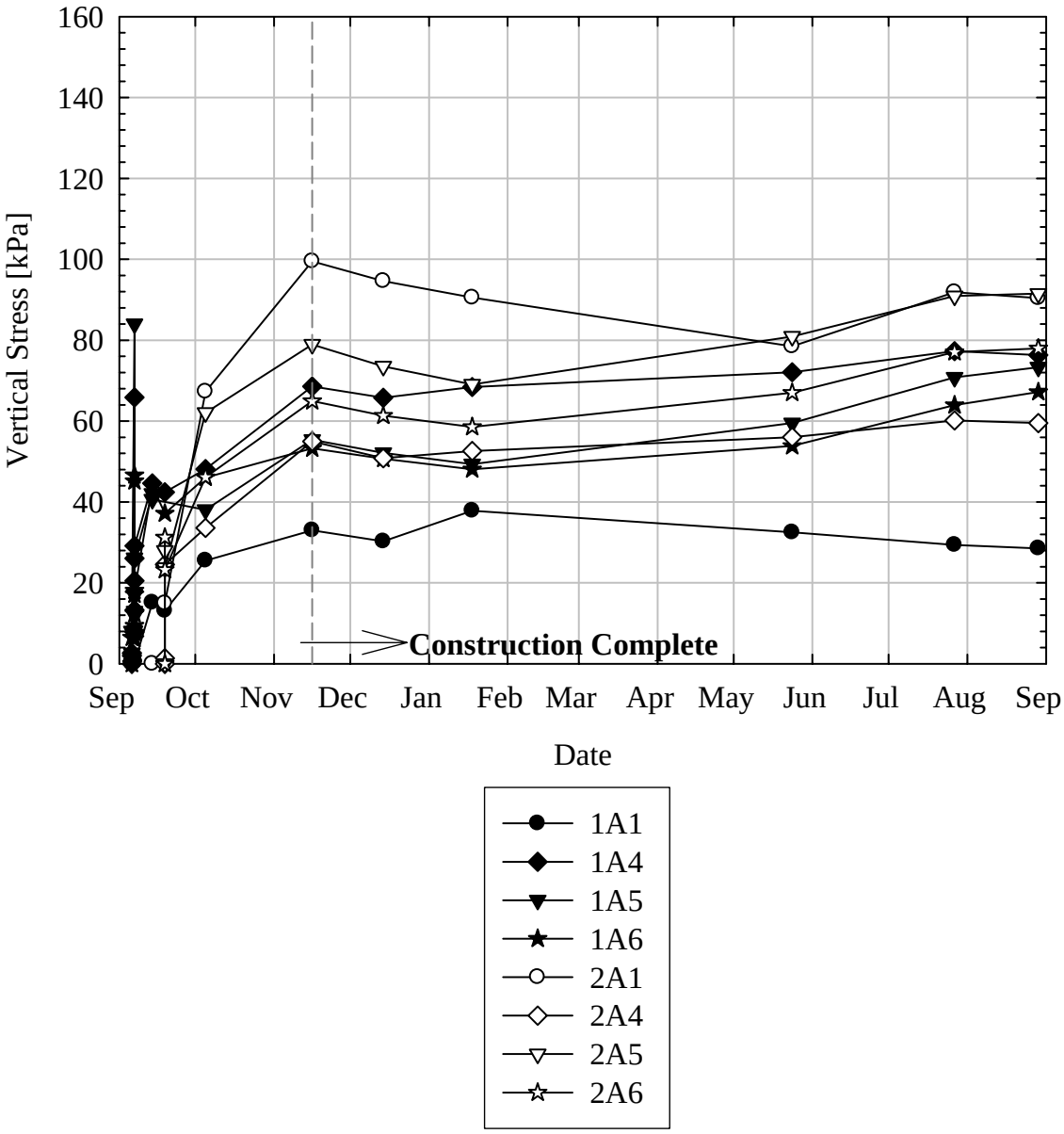

Figure 6.7 Vertical Pressures Measured at Abutments 1 and 2 versus Time.

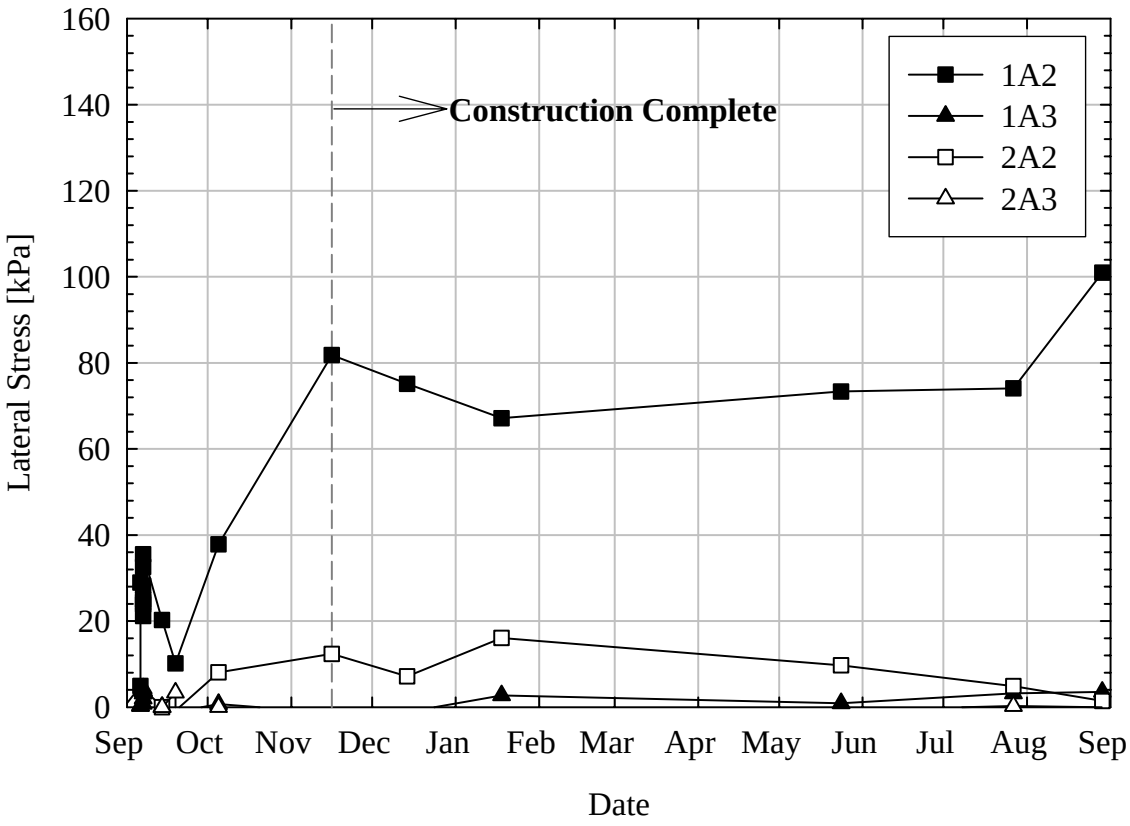

Figure 6.8 Lateral Pressures Measured at Abutments 1 and 2 versus Time.

6.2 Comparison of Measured Earth Pressures with Estimated Values

In this section, four cases of loading were considered in estimating vertical and lateral pressures behind the abutments in order to quantify reductions in pressure due to the use of GeoFoam. The estimated pressure levels were also useful in verifying proper function of the total earth pressure cells.

Case I consisted of estimated lateral and vertical pressures due to the use of conventional granular backfill rather than the lightweight GeoFoam blocks. Case II consisted of estimated vertical pressure levels at both the top and the base of the GeoFoam blocks as well as estimated lateral pressures acting upon the abutment wall. Case III consisted of estimated vertical pressure levels at the base of the GeoFoam blocks based upon the measured vertical pressure level at the top of the blocks as well as estimated lateral pressures acting upon the abutment wall. Case IV consisted of estimated lateral pressures acting upon the abutment wall based upon the measured vertical pressures at the top and base of the GeoFoam blocks. In all cases at-rest conditions were assumed, therefore lateral pressures were estimated based upon expected ranges of values of K_0 for each material. Vertical pressures were assumed to be transferred one-dimensionally, therefore pressure reduction with depth due to material elasticity is ignored. This is important to note when considering the vertical pressure levels at the base of the GeoFoam blocks, as previous studies have reported a decrease in pressure levels between the top surface and base of the blocks. Interactions between the GeoFoam blocks and the geocomposite sheet drain such as interface friction and compressibility of the sheet drain are also ignored.

Case I: Conventional Backfill Soil

Vertical pressures were determined for Case I loading based upon a single profile representing both approach fills. The profile layers consisted of a 0.08 m (0.30 ft) thick layer of asphalt pavement, a 0.38 m (1.25 ft) thick reinforced concrete approach slab, a 1.25 m (4.10 ft) thick layer of densely graded crushed stone subbase, and a 5.3 m (17.39) thick layer of compacted granular backfill. The thin layers of sand serving as leveling and drainage layers at the base and top of the GeoFoam blocks are ignored. The unit weights of both the asphalt pavement and reinforced concrete approach slab were assumed to be 23.6 kN/m^3 (150 lb/ft^3). The unit weights of both the subbase and granular backfill were assumed to be 21.6 kN/m^3 (135 lb/ft^3) based upon density and water content data obtained using a nuclear density gage during backfilling. Lateral pressures were determined based upon a range of K_0 values of 0.45 to 0.60 as recommended by Coduto (2000) for compacted backfill soils. A summary of the material properties is found in Table 6.1. A profile of the estimated pressures is shown in Figure 6.9. Individual symbols represent the most recent measured pressure for each earth pressure cell. The horizontal hatched lines represent the depths of the pressure cells located at the top of the GeoFoam blocks and at a depth of 2.0 m (6.6 ft) below the top of the GeoFoam blocks.

Table 6.1 Material Properties for Case I.

Material	Layer Thickness (m)	Depth to Base (m)	γ (kN/m^3)	σ_v (kPa)	σ_h (kPa)	
					K_0 = 0.45	K_0 = 0.60
Surface	0.00	0.00	0.0	0.0	0.0	0.0
Asphalt Roadway	0.08	0.08	23.6	1.9	0.9	1.1
RC Approach Slab	0.38	0.46	23.6	10.9	4.9	6.5
Stone Subbase	1.25	1.71	21.3	37.4	16.8	22.5
Granular Backfill	1.40	3.11	21.3	67.2	30.2	40.3
Granular Backfill	2.00	5.11	21.3	109.7	49.4	65.8
Granular Backfill	1.90	7.01	21.3	150.1	67.5	90.1

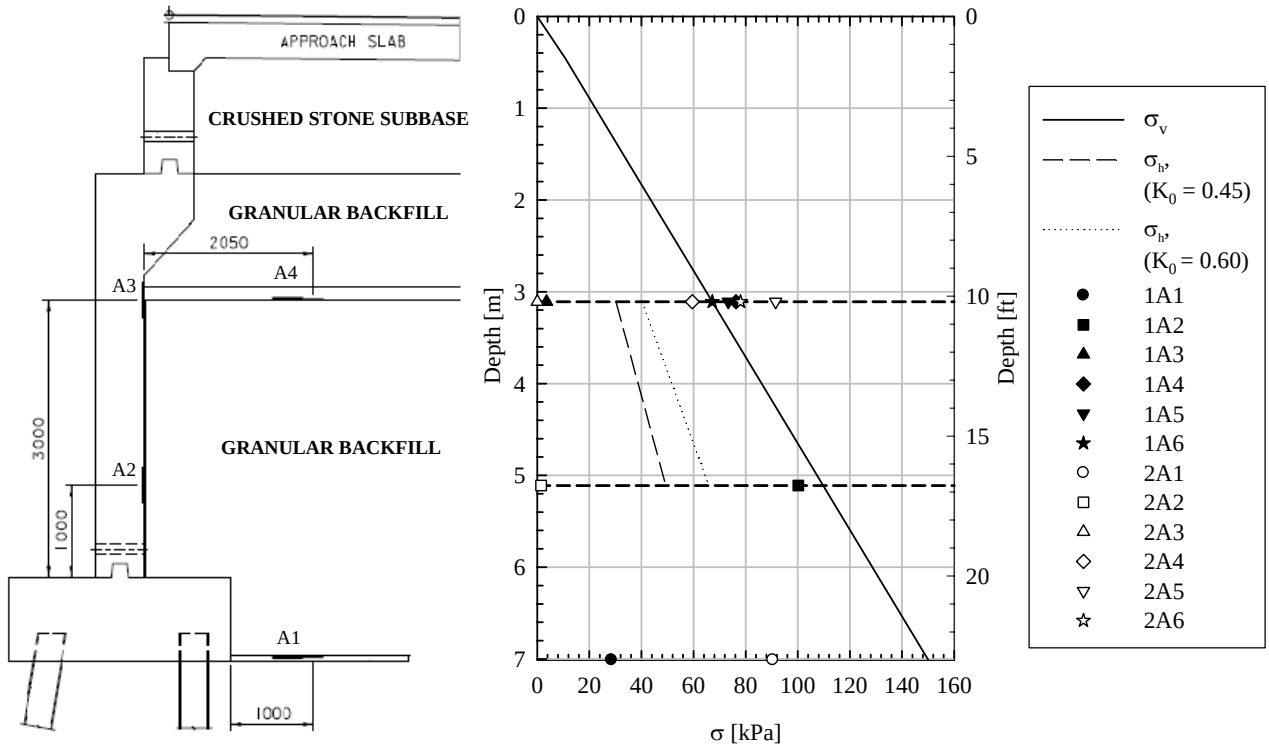

Figure 6.9 Estimated and Measured Vertical and Lateral Pressures at Abutments 1 and 2 for Case I Loading.

Vertical Pressures

A summary of the estimated vertical pressures and final measured vertical pressures is presented in Table 6.2. The measured vertical pressures are plotted versus time in Figure 6.10, with horizontal lines representing the estimated values.

At the end of construction operations the measured vertical stresses at Transducers 1A4 and 2A6 were approximately equal to the estimated value and the measured vertical stresses at Transducers 1A5, 1A6, and 2A4 were all approximately 12 kPa lower than the estimated value. Following the slight increase in measured stresses over the course of the monitoring period, the final measured values are within a range of approximately +/- 16 percent of the estimated value. The assumed unit weight of the granular backfill was the average value of the data obtained using the nuclear density gauge, therefore the distribution of the measured pressures above and below the estimated value indicates that the estimated value is reasonable. As the larger vertical pressures measured by Transducer 2A5 are considered to be a result of construction operations, the more significant difference between the estimated pressure level and the measured pressures is expected. The final measured vertical pressure at Transducer 2A5 is approximately 36 percent greater than the estimated value.

The pressures measured at the base of the GeoFoam blocks are considerably less than the estimated value using conventional backfill. The pressure measured by Transducer 1A1 indicates a reduction in pressure due to the use of GeoFoam of approximately 81 percent and the pressure measured by Transducer 2A1 indicates a reduction of approximately 40 percent. As the estimated pressure value is larger than both of the measured values, it appears that the use of GeoFoam as a backfill material resulted in reduced vertical pressures.

Table 6.2 Summary of Measured and Estimated Vertical Stresses at Abutments 1 and 2 for Case I Loading.

Transducer ID	$\sigma_{v\text{-}Meas}$ (kPa)	$\sigma_{v\text{-}Est}$ (kPa)	$\sigma_{v\text{-}Est} - \sigma_{v\text{-}Meas}$ (kPa)*	$\sigma_{v\text{-}Est} - \sigma_{v\text{-}Meas}$ (%)*
1A1	28.5	150.1	121.6	81.0
1A4	76.3	67.2	-9.1	-13.5
1A5	73.3	67.2	-6.1	-9.1
1A6	67.2	67.2	0.0	0.0
2A1	90.4	150.1	59.7	39.8
2A4	59.5	67.2	7.7	11.5
2A5	91.5	67.2	-24.3	-36.2
2A6	78.0	67.2	-10.8	-16.1

*Note: Positive values indicate that the estimated pressure exceeds the measured pressure. Negative values indicate that the measured pressure exceeds the estimated pressure.

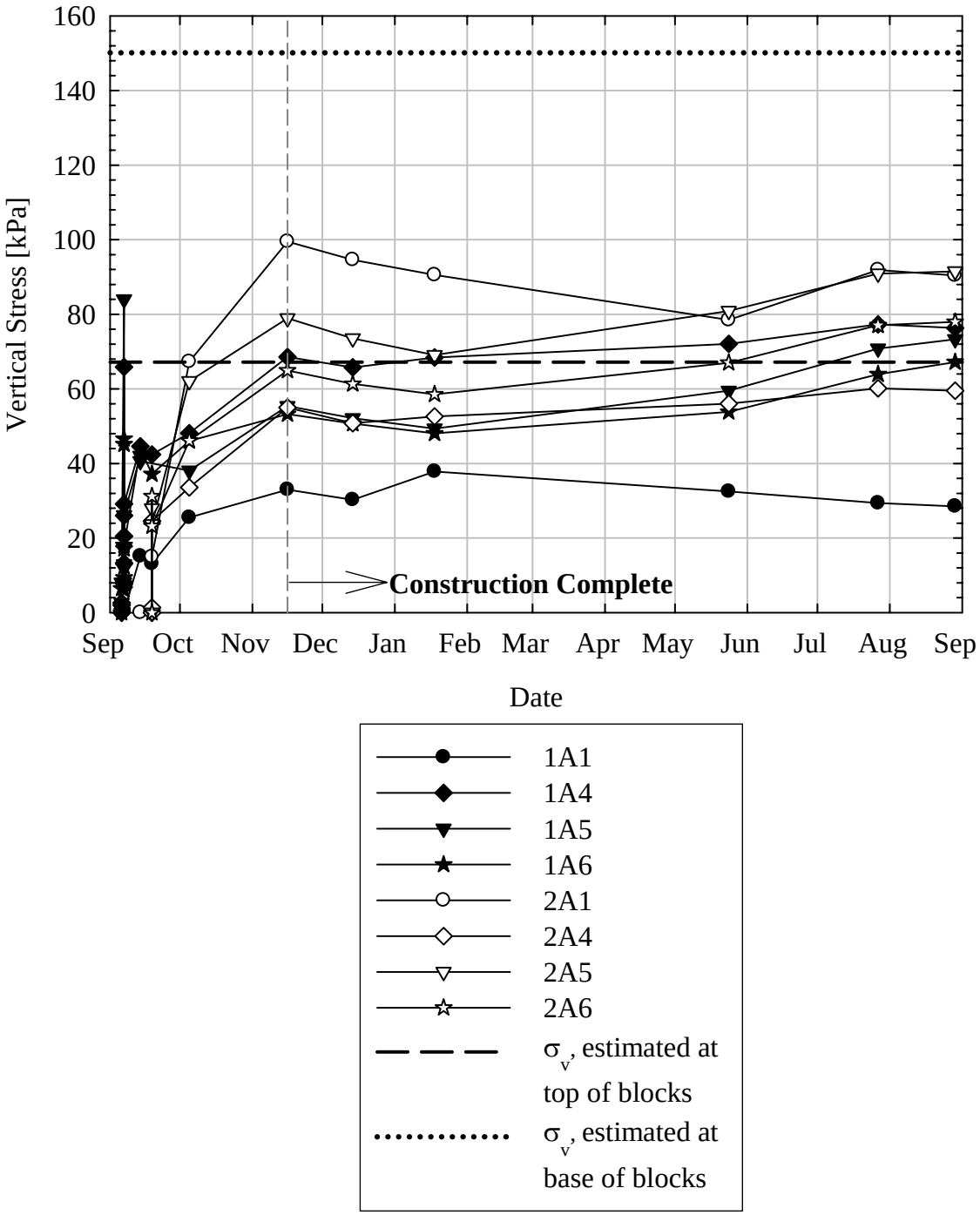

Figure 6.10 Estimated and Measured Vertical Pressures at Abutments 1 and 2 versus Time for Case I Loading.

Lateral Pressures

A summary of the estimated lateral pressures and final measured lateral pressures for Case I is presented in Table 6.3. The measured lateral pressures are plotted versus time in Figure 6.11, with horizontal lines representing the estimated values.

The use of the GeoFoam blocks as a substitute for conventional soil backfill material resulted in a reduction in lateral pressures of between 88 and 100% based upon the estimated lateral stress levels and the negligible final measured pressures at Transducers 1A3, 2A2, and 2A3. As the final measured lateral pressure at Transducer 1A2 exceeded both the upper bound estimated lateral stress level (corresponding to $K_0 = 0.6$) by approximately 52 percent as well as the estimated vertical stress at the same depth (corresponding to a K_0 value of greater than 1.0), it is likely that the transducer is not functioning incorrectly or was damaged during construction operations.

Table 6.3 Summary of Measured and Estimated Lateral Stresses at Abutments 1 and 2 for Case I Loading.

Transducer ID	$\sigma_{h\text{-}Meas}$ (kPa)	$\sigma_{h\text{-}Est}$, $K_0 = 0.45$ (kPa)	$\sigma_{h\text{-}Est}$, $K_0 = 0.60$ (kPa)	$\sigma_{h\text{-}Est} - \sigma_{h\text{-}Meas}$, $K_0 = 0.45$ (kPa)*	$\sigma_{h\text{-}Est} - \sigma_{h\text{-}Meas}$, $K_0 = 0.60$ (kPa)*	$\sigma_{h\text{-}Est} - \sigma_{h\text{-}Meas}$, $K_0 = 0.45$ (%)*	$\sigma_{h\text{-}Est} - \sigma_{h\text{-}Meas}$, $K_0 = 0.60$ (%)*
1A2	100.2	49.4	65.8	-50.8	-34.4	-102.8	-52.3
1A3	3.6	30.2	40.3	26.6	36.7	88.1	91.1
2A2	1.5	49.4	65.8	48.0	64.4	97.1	97.8
2A3	0.0	30.2	40.3	30.2	40.3	100.0	100.0

*Note: Positive values indicate that the estimated pressure exceeds the measured pressure. Negative values indicate that the measured pressure exceeds the estimated pressure.

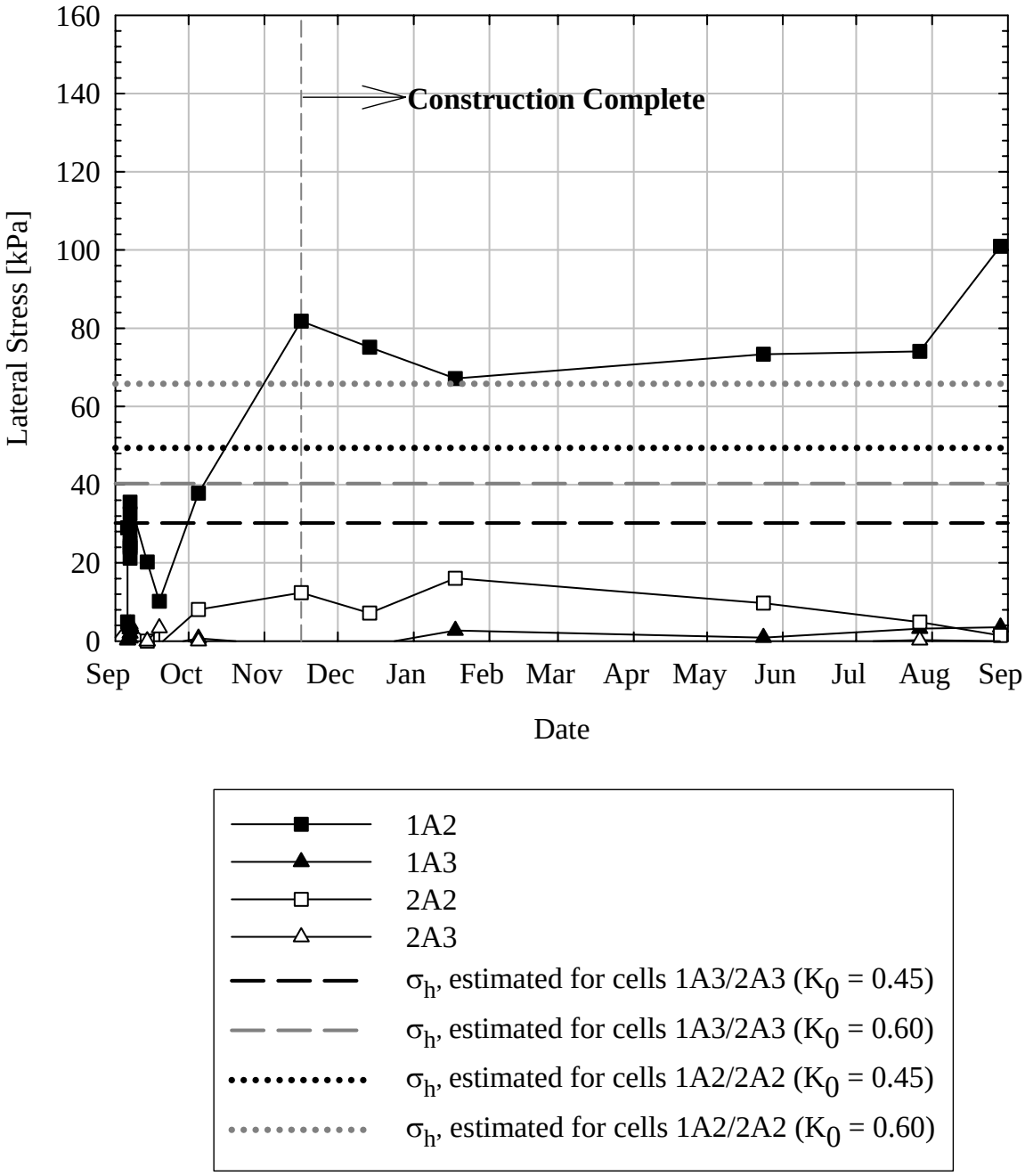

Figure 6.11 Estimated and Measured Lateral Pressures at Abutments 1 and 2 versus Time for Case I Loading.

Case II: GeoFoam Backfill

Vertical pressures were determined for Case I loading based upon a single profile representing both approach fills. The profile layers consisted of a 0.08 m (0.30 ft) thick layer of asphalt pavement, a 0.38 m (1.25 ft) thick reinforced concrete approach slab, a 1.25 m (4.10 ft) thick layer of densely graded crushed stone subbase, a 1.4 m (4.59 ft) thick layer of compacted granular backfill, and a 3.90 m (12.80 ft) thick layer of EPS GeoFoam blocks with a unit weight of 0.3 kN/m^3 (2 lb/ft^3). The unit weights of the other materials are identical to those used in the Case I analysis. Lateral pressures were determined based on a range of K_0 values of 0.1 to 0.5, representing the minimum and maximum values reported in the literature for the working range of vertical pressures. A summary of the material properties is found in Table 6.4. A profile of the estimated pressures is shown in Figure 6.12. Individual symbols represent the most recent measured pressure for each earth pressure cell. The horizontal hatched lines represent the depths of the pressure cells located at the top of the GeoFoam blocks and at a depth of 2.0 m (6.6 ft) below the top of the GeoFoam blocks.

Table 6.4 Material Properties for Case II.

Material	**Layer Thickness (m)**	**Depth to Base (m)**	**γ (kN/m^3)**	**σ_v (kPa)**	**σ_h (kPa)**	
					K_0 = 0.1	**K_0 = 0.5**
	0.00	0.00	0.0	0.0	0.0	0.0
Asphalt Pavement	0.08	0.08	23.6	1.9	0.9	1.1
RC Approach Slab	0.38	0.46	23.6	10.9	4.9	6.5
Stone Subbase	1.25	1.71	21.3	37.4	16.8	22.5
Granular Backfill	1.40	3.11	21.3	67.2	6.7	33.6
GeoFoam	2.00	5.11	0.3	67.8	6.8	33.9
GeoFoam	1.90	7.01	0.3	68.4	6.8	34.2

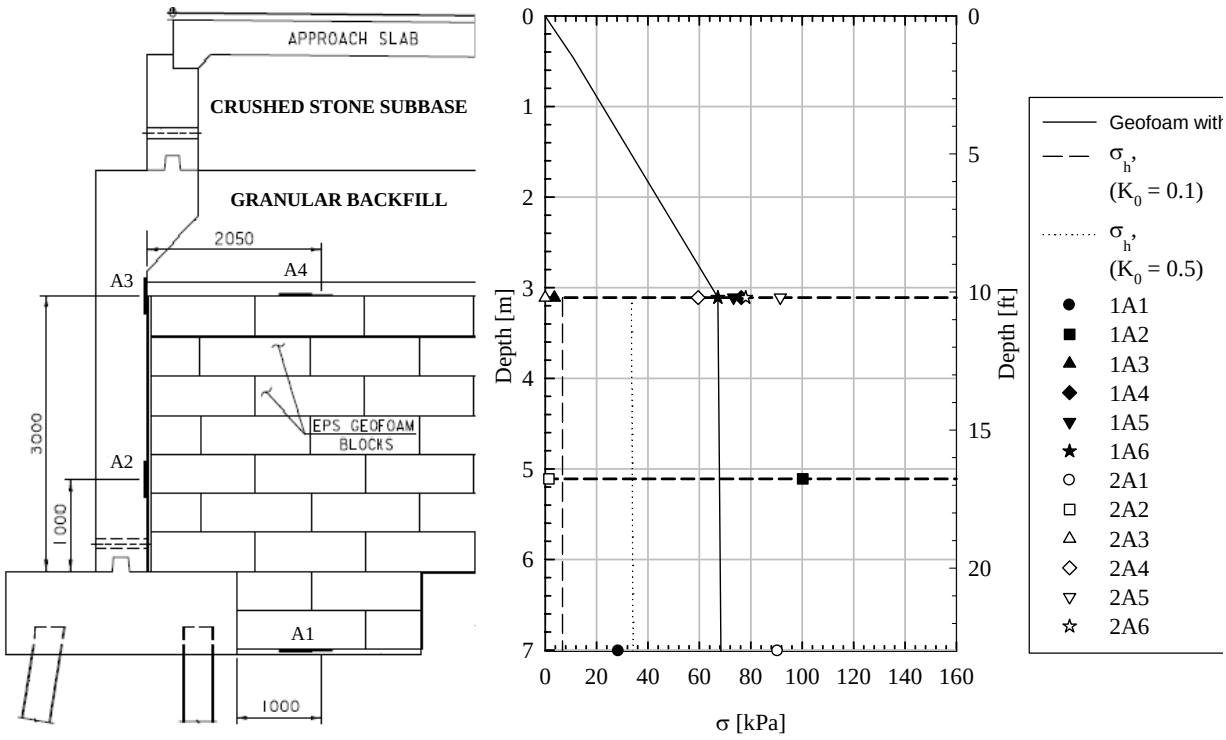

Figure 6.12 Estimated and Measured Vertical and Lateral Pressures at Abutments 1 and 2 for Case II Loading.

Vertical Pressures

A summary of the estimated vertical pressures and final measured vertical pressures is presented in Table 6.5. The measured vertical pressures are plotted versus time in Figure 6.13, with horizontal lines representing the estimated values.

As the estimated vertical pressure level at the top of the GeoFoam blocks is identical to the level in Case I, the focus of Case II is the difference between the estimated and measured vertical pressures at the base of the GeoFoam blocks. The stress reduction behavior observed in previous studies has not been considered in the estimated pressures, therefore the estimated vertical pressures at the base of the GeoFoam blocks in this case simply represent the sum of the estimated pressures at the top of the blocks and the additional vertical pressures due to the weight of the GeoFoam. Given the low unit weight of GeoFoam, the estimated vertical pressures at the base of the blocks are only slightly larger than those at the top of the blocks.

The vertical pressures measured at Transducer 1A1 were consistently lower than the estimated vertical pressure level, with the final measured pressure approximately 58 percent less than estimated. The vertical pressures measured at Transducer 2A1 were higher than the estimated pressure level from the end of construction operations until the final measurement. The final measured vertical pressure at Transducer 2A1 was approximately 32 percent higher than the estimated pressure level.

In the case of the approach fill at Abutment 1, the bridging effect described in previous studies may be occurring in which the GeoFoam blocks distribute the vertical pressures in a manner similar to a slab foundation. This monolithic behavior can result in the lower pressures at the base of the GeoFoam blocks than at the top of the blocks. The pressures measured by Transducer 2A1 are larger than both the estimated pressure level at the base of the blocks and pressures measured at the top of the blocks, which may indicate that the instrument is malfunctioning. This will be further analyzed in Case III.

Table 6.5 Summary of Measured and Estimated Vertical Pressures at Abutments 1 and 2 for Case II Loading.

Transducer ID	$\sigma_{v\text{-}Meas}$ (kPa)	$\sigma_{v\text{-}Est}$ (kPa)	$\sigma_{v\text{-}Est} - \sigma_{v\text{-}Meas}$ (kPa)*	$\sigma_{v\text{-}Est} - \sigma_{v\text{-}Meas}$ (%)*
1A1	28.5	68.4	39.9	58.3
1A4	76.3	67.2	-9.1	-13.5
1A5	73.3	67.2	-6.1	-9.1
1A6	67.2	67.2	0.0	0.0
2A1	90.4	68.4	-22.0	-32.2
2A4	59.5	67.2	7.7	11.5
2A5	91.5	67.2	-24.3	-36.2
2A6	78.0	67.2	-10.8	-16.1

Note: Positive values indicate that the estimated pressure exceeds the measured pressure. Negative values indicate that the measured pressure exceeds the estimated pressure.

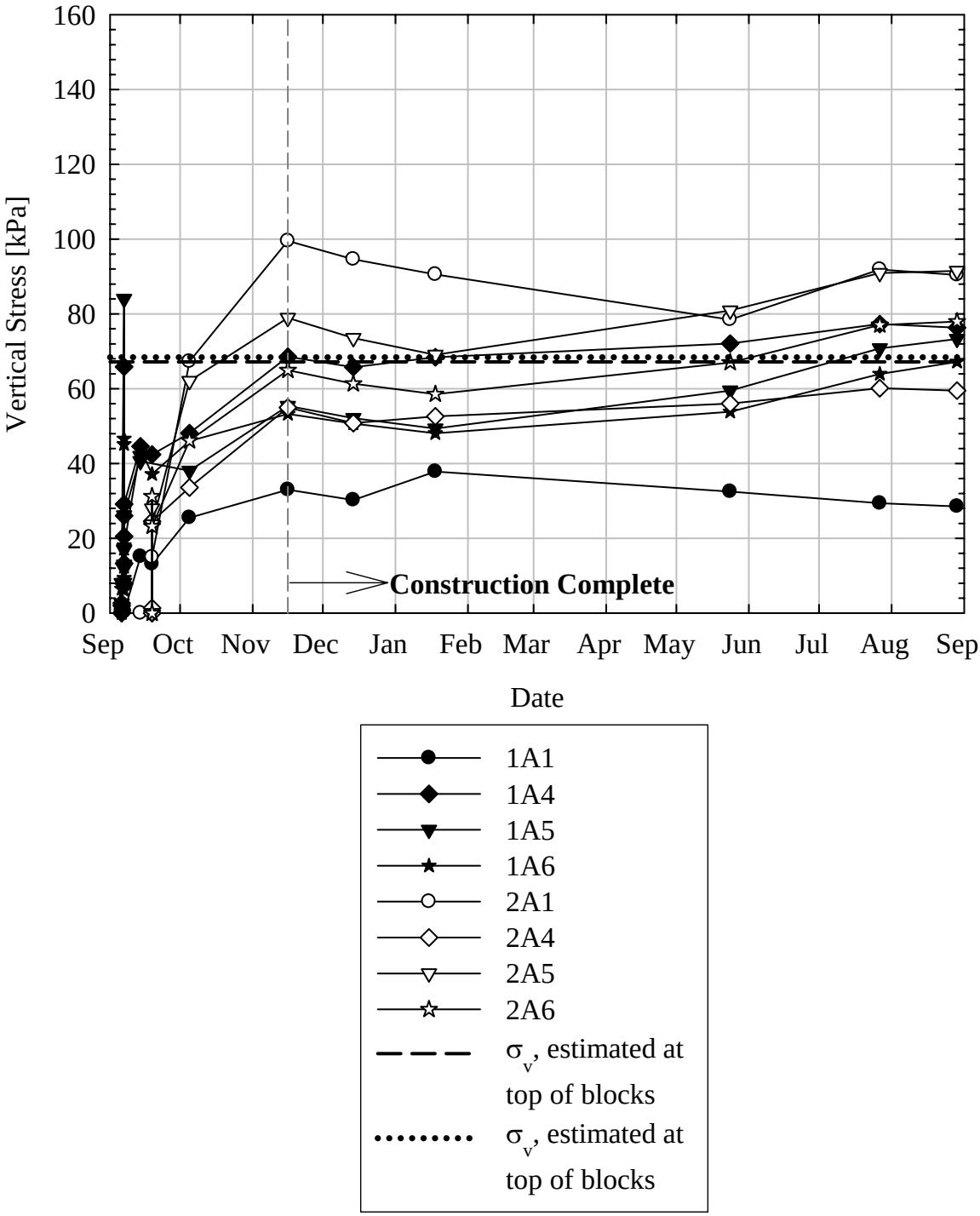

Figure 6.13 Estimated and Measured Vertical Pressures at Abutments 1 and 2 versus Time for Case II Loading.

Lateral Pressures

A summary of the estimated lateral pressures and final measured lateral pressures is presented in Table 6.6. The measured lateral pressures are plotted versus time in Figure 6.14, with horizontal lines representing the estimated values. It should be noted that as the difference in estimated pressures at the top and base of the blocks is so small, the corresponding difference in lateral pressures at the top and base of the blocks would be negligible. Therefore the presented estimated lateral pressures levels are based solely on the chosen K_0 values and not depth into the GeoFoam blocks.

It is clear that the upper bound estimate of the lateral pressure based on K_0 equal to 0.5 is significantly higher than the measured lateral pressures, with the exception of the malfunctioning Transducer 1A2. The lower bound estimate of the lateral pressure based on K_0 equal to 0.1 is in better agreement with the measured stresses, however the final measured pressures are all lower than the estimated pressure level. The pressures measured by Transducers 1A3 and 2A3 were consistently less than the estimated pressure level, with the final measured lateral pressure at Transducer 1A3 approximately 46 percent less than the already low estimated value. The final measurement at Transducer 2A3 was 100% percent less than the estimated value, as the final measured lateral pressure was negative and thus assumed to be zero.

The measured pressures at Transducer 2A2 were higher than the estimated pressure level throughout most of the monitoring period until the pressures decreased to a final value approximately 79 percent lower than the estimated level. As both the actual measured lateral pressures and measured pressures are of similarly low magnitude, even slight variations of the estimated value (such as due to the change in the unit weight of the backfill) could drastically affect the percent difference between measured and estimated values. Therefore the estimated lateral stress level based upon K_0 equal to 0.1 seems to be quite realistic although slightly conservative. Further analysis considering the actual measured pressures should yield different results, as the actual measured vertical pressures at the base of the GeoFoam blocks varied significantly from the estimated values used to predict the lateral pressure level.

Table 6.6 Summary of Measured and Estimated Lateral Pressures at Abutments 1 and 2 for Case II Loading.

Transducer ID	$\sigma_{h\text{-}Meas}$ (kPa)	$\sigma_{h\text{-}Est}$, K_0 = 0.10 (kPa)	$\sigma_{h\text{-}Est}$, K_0 = 0.50 (kPa)	$\sigma_{h\text{-}Est} - \sigma S_{h\text{-}Meas}$, K_0 = 0.1 (kPa)	$\sigma_{h\text{-}Est} - \sigma S_{h\text{-}Meas}$, K_0 = 0.5 (kPa)	$\sigma_{h\text{-}Est} - \sigma_{h\text{-}Meas}$, K_0 = 0.1 (%)	$\sigma_{h\text{-}Est} - \sigma_{h\text{-}Meas}$, K_0 = 0.5 (%)
1A2	100.2	6.8	33.9	-93.4	-66.3	-1373.5	-195.6
1A3	3.6	6.7	33.6	3.1	30.0	46.3	89.3
2A2	1.5	6.8	33.9	5.4	32.5	78.7	95.7
2A3	0.0	6.7	33.6	6.7	33.6	100.0	100.0

*Note: Positive values indicate that the estimated pressure exceeds the measured pressure. Negative values indicate that the measured pressure exceeds the estimated pressure.

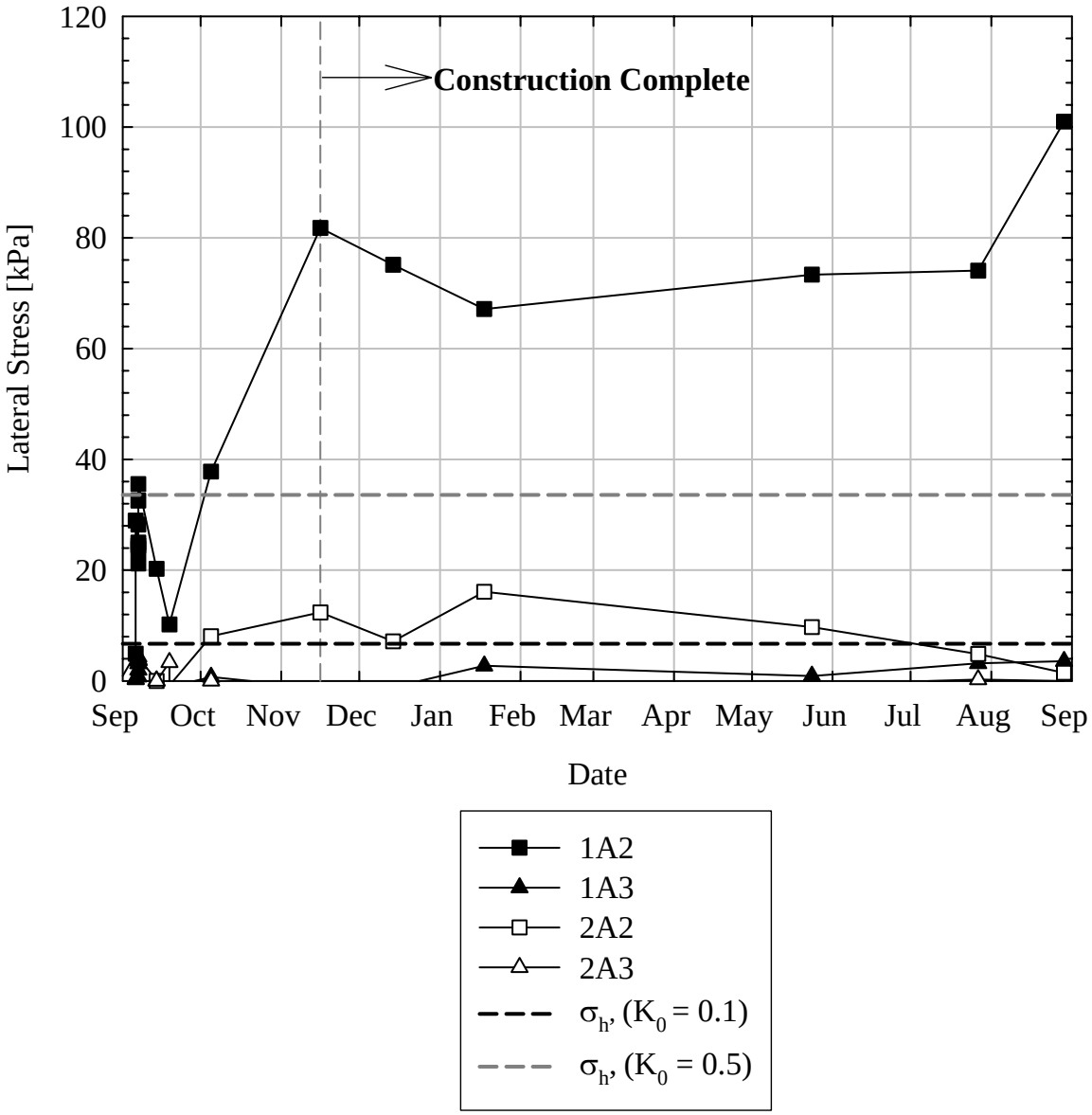

Figure 6.14 Estimated and Measured Lateral Pressures at Abutments 1 and 2 versus Time for Case II Loading.

Case III: Estimated Lateral and Basal Pressures

Vertical pressures were determined independently for each abutment for Case III loading. The vertical pressure profiles from the surface to the top of the GeoFoam blocks were determined based upon the actual measured pressures at the top of the blocks. The pressure profiles from the top of the blocks to base of the blocks were then determined based upon the unit weight of the GeoFoam blocks in order to quantify any pressure reduction behavior through the blocks. Lateral pressures were determined based upon a range of K_0 values from 0.1 to 0.5, as in Case III. A summary of the estimated pressures is found in Table 6.7. Profiles of the estimated pressures at Abutments 1 and 2 are shown in Figures 6.15 and 6.16, respectively. Individual symbols represent the most recent measured pressure for each earth pressure cell. The horizontal hatched lines represent the depths of the pressure cells located at the top of the GeoFoam blocks and at a depth of 2.0 m (6.6 ft) below the top of the GeoFoam blocks.

Table 6.7 Summary of Case III Estimated Pressures.

Depth (m)	Abutment 1			Abutment 2		
	σ_v (kPa)	σ_h (kPa)		σ_v (kPa)	σ_h (kPa)	
		$K_0 = 0.1$	$K_0 = 0.5$		$K_0 = 0.1$	$K_0 = 0.5$
0.0	0.0	0.0	0.0	0.0	0.0	0.0
3.1	76.3	7.6	38.2	59.4	5.9	29.7
5.1	77.0	7.7	38.5	60.0	6.0	30.0
7.0	77.5	7.7	38.7	60.6	6.1	30.3

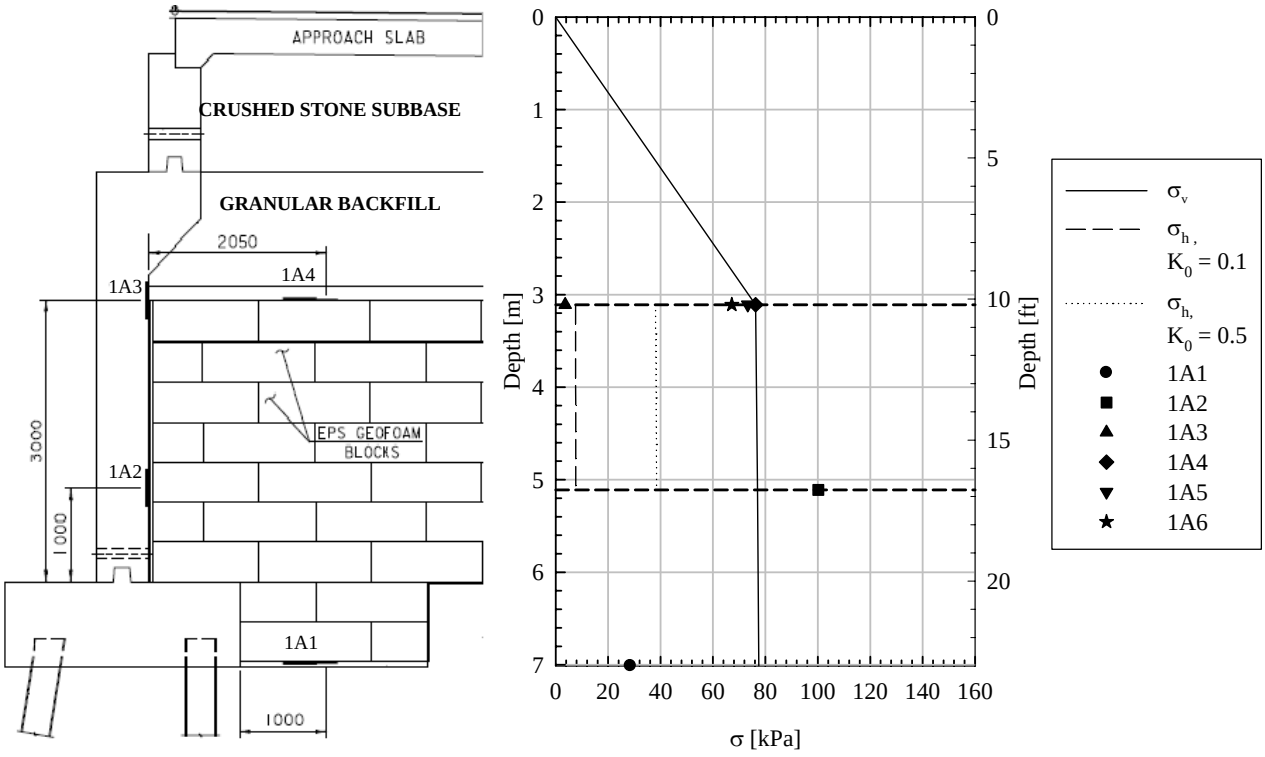

Figure 6.15 Estimated and Measured Vertical and Lateral Pressures at Abutment 1 for Case III Loading.

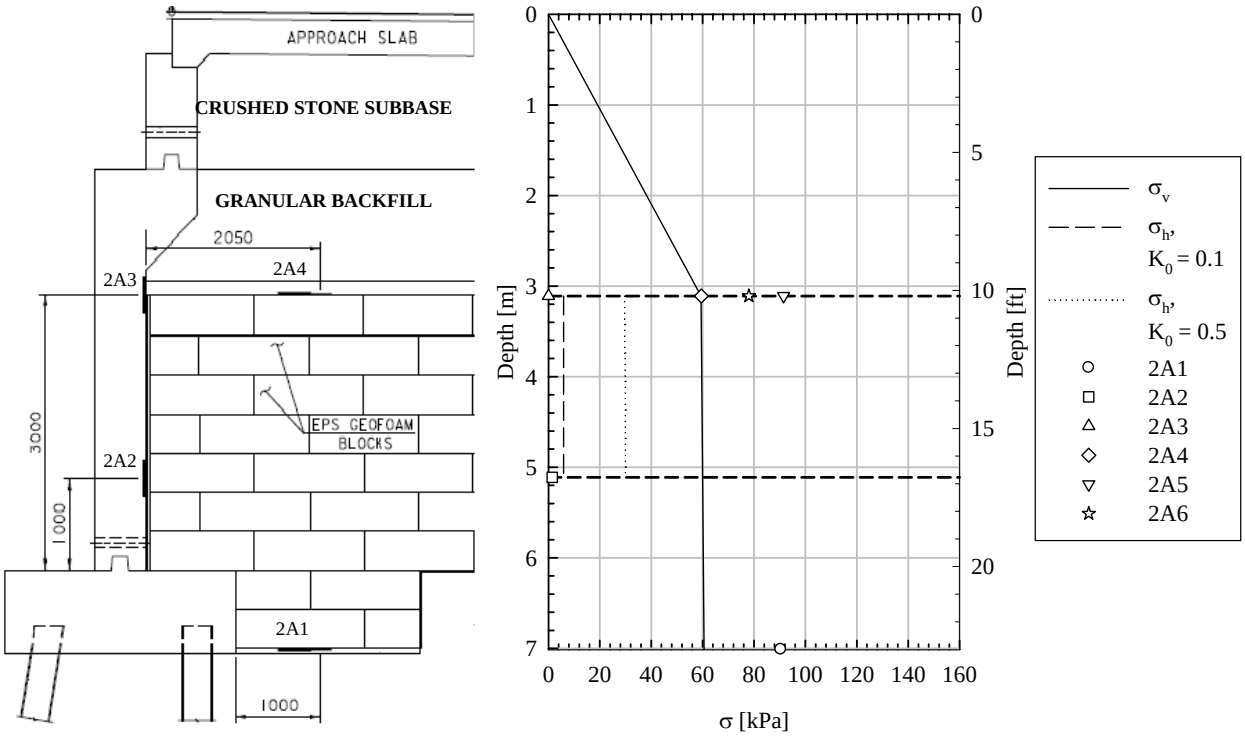

Figure 6.16 Estimated and Measured Vertical and Lateral Pressures at Abutment 2 for Case III Loading.

Vertical Pressures

A summary of the estimated vertical pressures and final measured vertical pressures is presented in Table 6.8. The measured vertical pressures are plotted versus time in Figures 6.17 and 6.18, with horizontal lines representing the estimated values.

The estimated vertical pressures at the top of the blocks were assumed to be equal to the values measured by Transducers 1A4 and 2A4, and therefore the estimated vertical pressure values at the base of the GeoFoam blocks approximate the maximum vertical pressures that should be measured by Transducers 1A1 and 2A1. A measured value less than an estimated value will indicate stress reduction properties of the GeoFoam blocks.

Vertical pressures measured by Transducer 1A1 were consistently lower than the estimated pressure level at the base of the blocks. The final measured vertical stress was approximately 63% less than the estimated value, indicating that the GeoFoam blocks are exhibiting either bridging or pressure reduction behavior at Abutment 1. The result is a reduction of pressure from the top of the blocks to the base blocks to approximately one third of the applied vertical pressure.

Vertical pressures measured by Transducer 2A1 were consistently higher than the estimated pressure level throughout the monitoring period. The final measured vertical pressure was approximately 52 percent greater than the estimated value. The final vertical pressure measured at the top of the blocks by Transducer 2A4 was estimated to be the actual pressure acting on the top of the blocks, however a comparison of the final measured vertical pressures at the locations of Transducers 2A5 and 2A6 shows that the measured vertical pressures at those transducers are larger than the measured value at Transducer 2A4.

Given the fairly wide range of vertical stress values measured by the transducers in a fairly small area, it is possible that if Transducers 2A4 and 2A1 were not placed concentrically the vertical stress acting over the target area may be significantly larger than the value measured by the transducer. If this actual vertical stress at the top of the blocks directly over the location of Transducer 2A1 were closer to the value measured by Transducer 2A5, the resulting estimate of the vertical pressure at the base of the blocks would also approximate the value measured by Transducer 2A5. The end result would be no bridging or pressure reduction through the GeoFoam blocks, however there would also be no major increase in stress as presently shown. The only other explanation for such an increase in stress is instrumentation malfunction.

Table 6.8 Summary of Measured and Estimated Vertical Pressures at Abutments 1 and 2 for Case III Loading.

Transducer ID	$S_{v\text{-}Meas}$ (kPa)	$S_{v\text{-}Est}$ (kPa)	$S_{v\text{-}Est} - S_{v\text{-}Meas}$ (kPa)*	$S_{v\text{-}Est} - S_{v\text{-}Meas}$ (%)*
1A1	28.5	77.5	49.0	63.2

2A1	90.4	59.4	-31.0	-52.2

*Note: Positive values indicate that the estimated pressure exceeds the measured pressure. Negative values indicate that the measured pressure exceeds the estimated pressure.

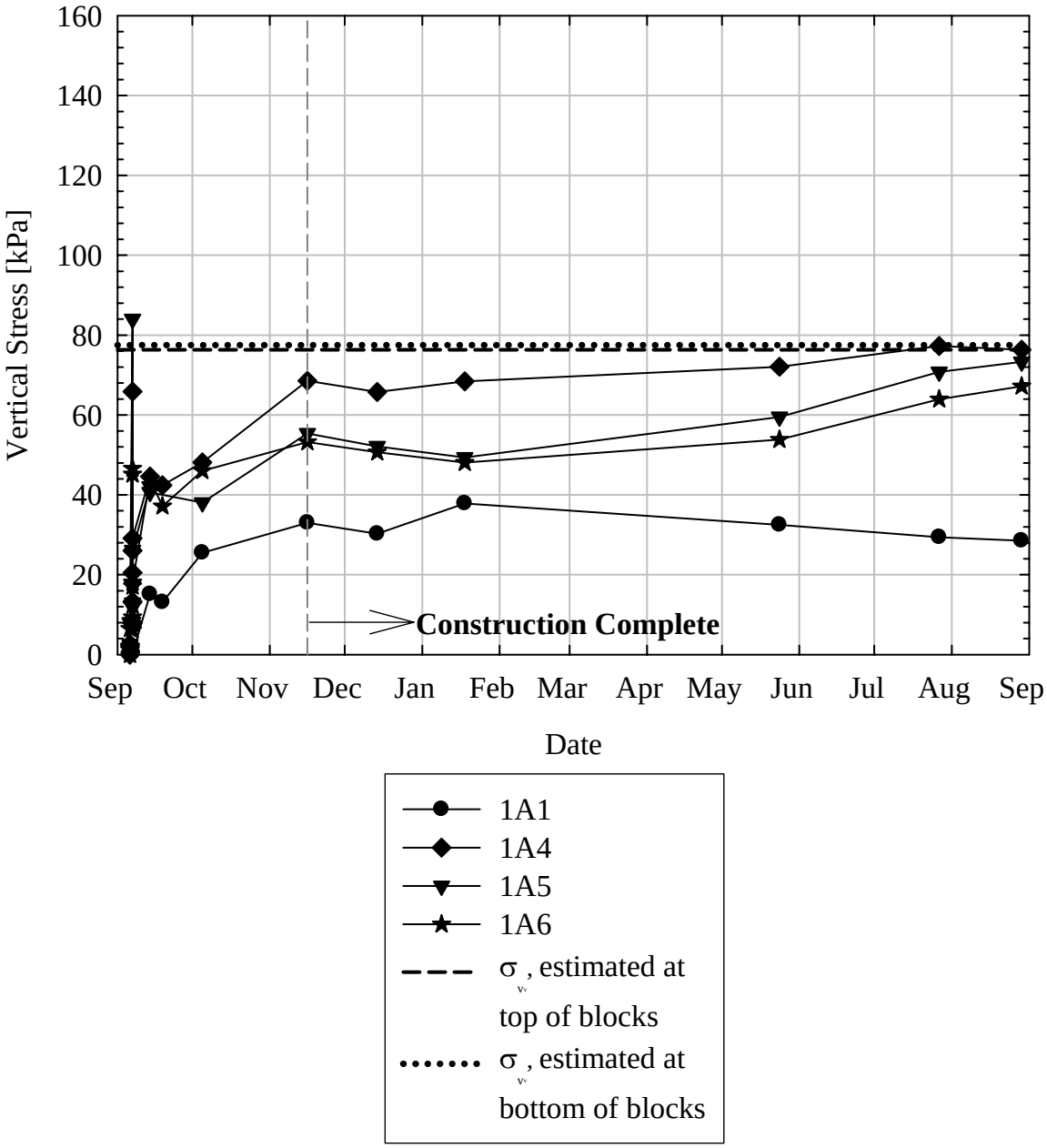

Figure 6.17 Estimated and Measured Vertical Pressures at Abutment 1 versus Time for Case III Loading.

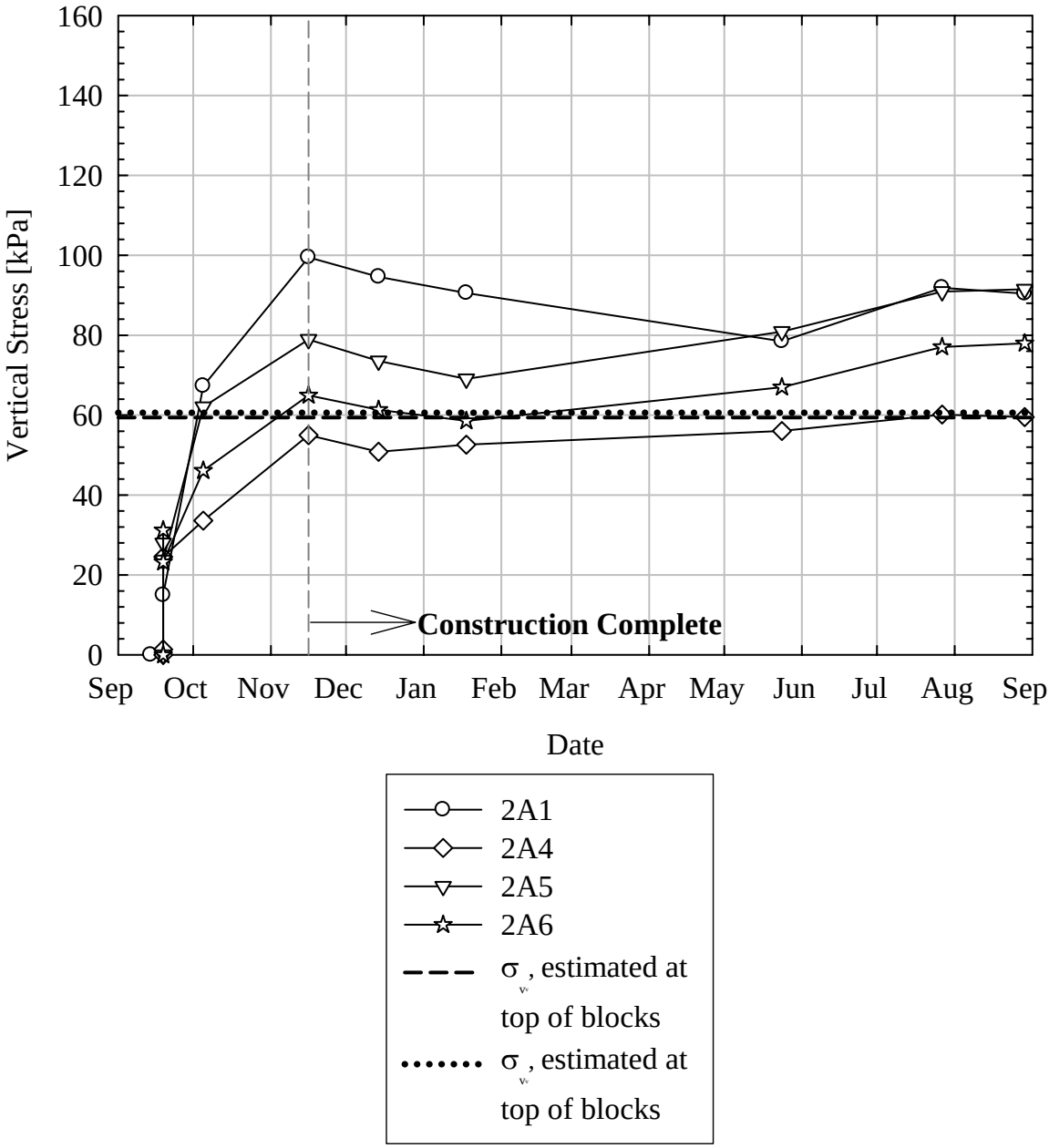

Figure 6.18 Estimated and Measured Vertical Pressures at Abutment 2 versus Time for Case III Loading.

Lateral Pressures

A summary of the estimated vertical pressures and final measured vertical pressures is presented in Table 6.9. The measured vertical pressures are plotted versus time in Figures 6.19 and 6.20, with horizontal lines representing the estimated values.

The estimated lateral pressure levels were determined from the vertical pressure profile based upon measured vertical pressure at the top of the blocks and estimated vertical pressure at

the base of the blocks. Although there is a slight difference in the measured vertical pressures acting on the top of the blocks from Abutment 1 to Abutment 2, the lateral pressures at both abutments should be comparable, as K_0 reflecting the actual stress level should not vary significantly.

Lateral pressures measured by Transducer 1A3 were consistently lower than the lower bound estimated value, with the slight increase to the final measured value representing the maximum lateral pressure during the monitoring period. The final measured lateral pressure at Transducer 1A3 was approximately 53 percent less than the estimated value.

Lateral pressures measured by Transducer 2A2 were greater than the lower bound estimated pressure level for the initial portion of the post-construction monitoring period, however the largest measured pressure during this period was still significantly less than the upper bound estimated stress level. The final measured pressure following a period of decrease was approximately 76 lower than the estimated value.

Lateral pressures measured by Transducer 2A3 were negligible throughout the post construction period and are considered to be zero. As noted previously, the actual measured stresses and estimated stresses are of such small magnitude that despite the estimated stress being significantly larger than the measured stress when expressed as a percent, the lower bound estimated pressure level still represents a realistic value for conservatively predicting lateral stresses.

Table 6.9 Summary of Measured and Estimated Lateral Pressures at Abutments 1 and 2 for Case III Loading.

Transducer ID	$\sigma_{h\text{-}Meas}$ (kPa)	$\sigma_{h\text{-}Est}$, $K_0 = 0.10$ (kPa)	$\sigma_{h\text{-}Est}$, $K_0 = 0.50$ (kPa)	$\sigma_{h\text{-}Est} - \sigma_{h\text{-}Meas}$, $K_0 = 0.1$ (kPa)*	$\sigma_{h\text{-}Est} - \sigma_{h\text{-}Meas}$, $K_0 = 0.5$ (kPa)*	$\sigma_{h\text{-}Est} - \sigma_{h\text{-}Meas}$, $K_0 = 0.1$ (%)*	$\sigma_{h\text{-}Est} - \sigma_{h\text{-}Meas}$, $K_0 = 0.5$ (%)*
1A2	100.2	7.7	38.5	-92.5	-61.7	-1201.3	-160.3
1A3	3.6	7.6	38.2	4.0	34.6	52.6	90.6
2A2	1.5	6.0	30.0	4.6	28.6	75.8	95.2
2A3	0.0	5.9	29.7	5.9	29.7	100.0	100.0

*Note: Positive values indicate that the estimated pressure exceeds the measured pressure. Negative values indicate that the measured pressure exceeds the estimated pressure.

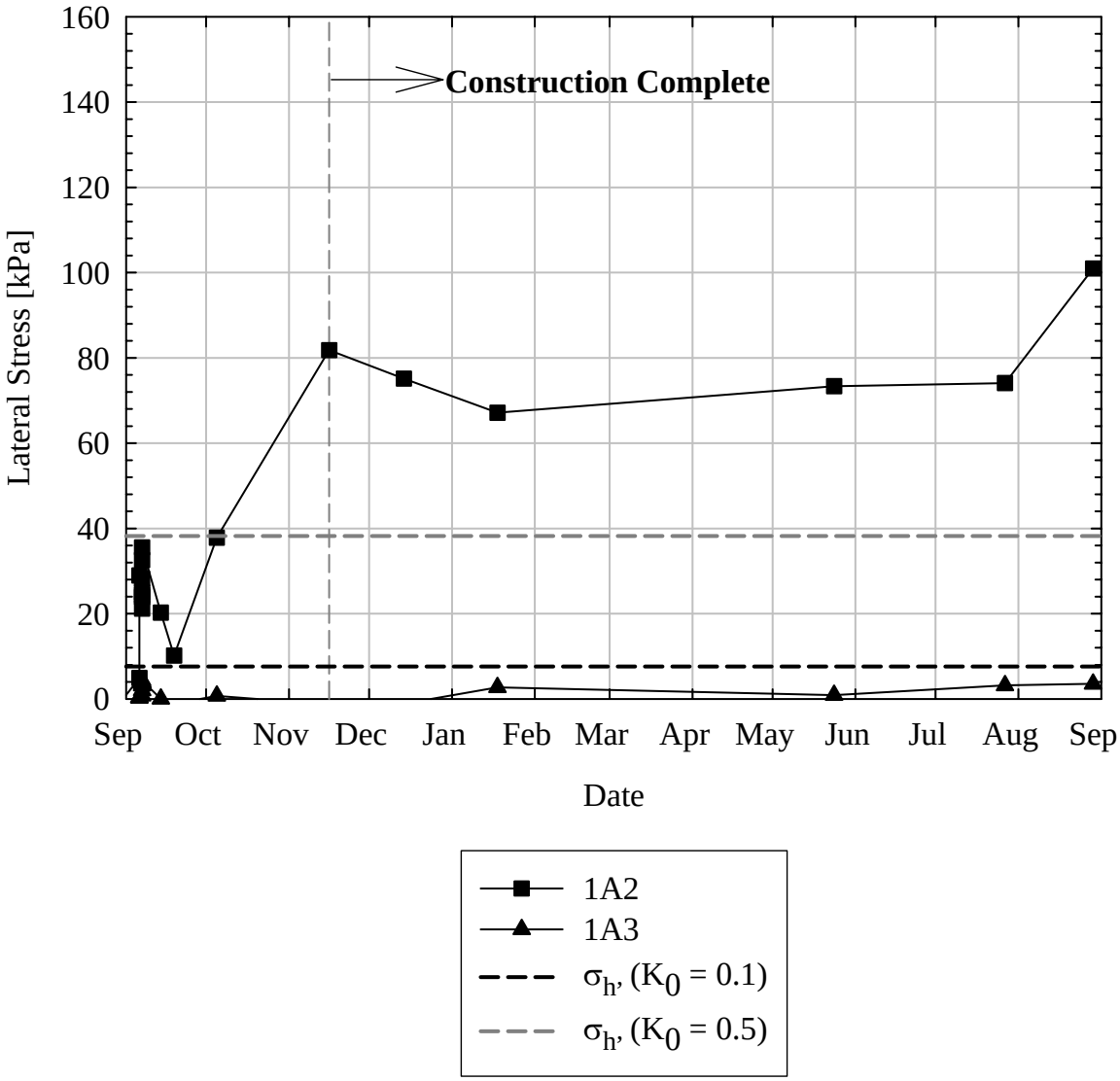

Figure 6.19 Estimated and Measured Lateral Pressures at Abutment 21 versus Time for Case III Loading.

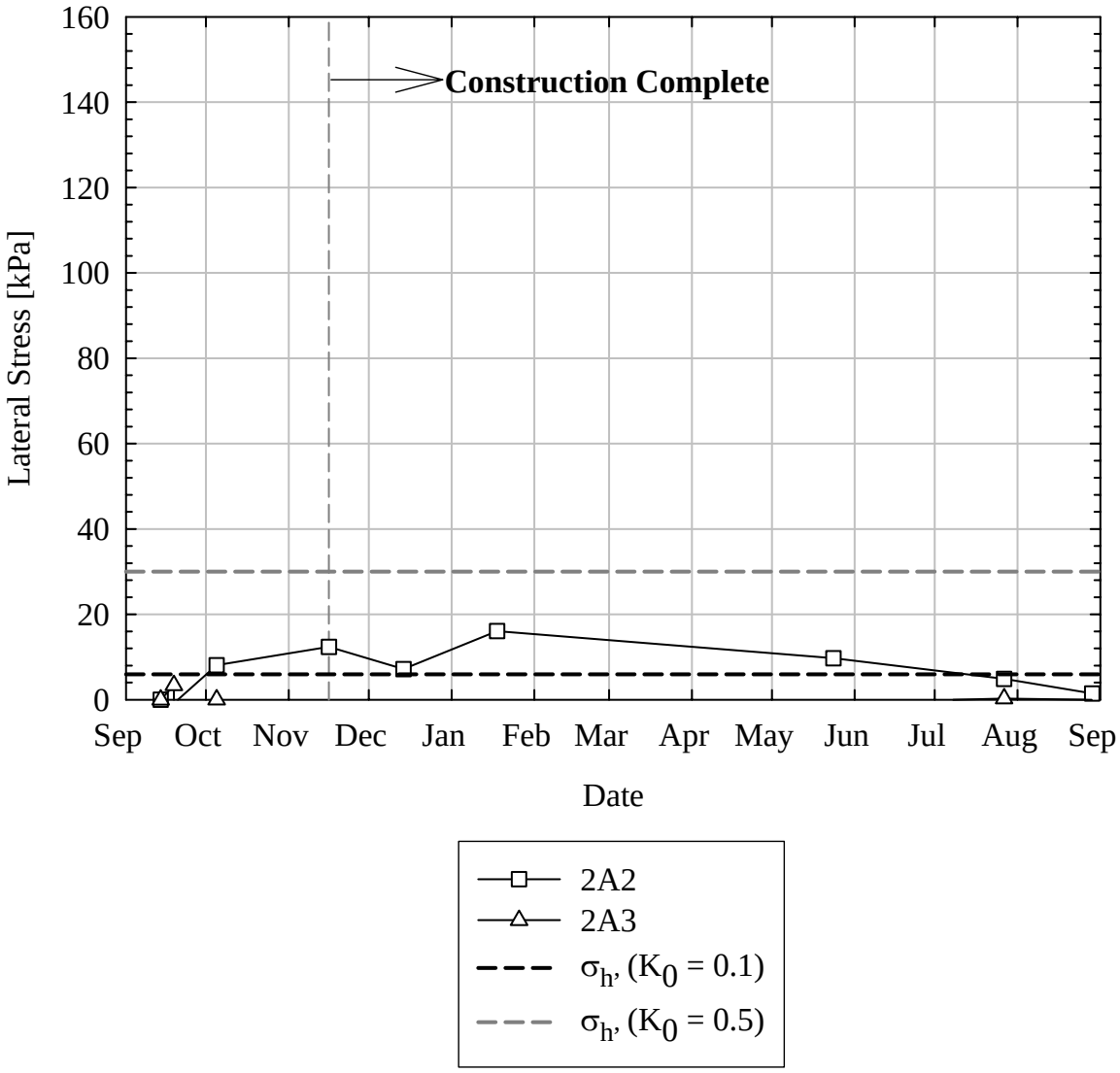

Figure 6.20 Estimated and Measured Lateral Pressures at Abutment 2 versus Time for Case III Loading.

Case IV: Estimated Lateral Pressures

The vertical pressure profile for the Case IV analysis consists of the actual final measured vertical pressures at the top and base of the GeoFoam blocks. Only the lateral pressures are estimated based upon a range of K_0 values from 0.1 to 0.5 as in the previous cases. A summary of the estimated pressures is found in Table 6.10. Profiles of the estimated pressures at Abutments 1 and 2 are shown in Figures 6.21 and 6.22, respectively. Individual symbols represent the most recent measured pressure for each earth pressure cell. The horizontal hatched lines represent the depths of the pressure cells located at the top of the GeoFoam blocks and at a depth of 2.0 m (6.6 ft) below the top of the GeoFoam blocks.

Table 6.10 Summary of Measured and Estimated Pressures for Loading Case IV.

Depth (m)	Abutment 1			Abutment 2		
	σ_v (kPa)	σ_h (kPa)		σ_v (kPa)	σ_h (kPa)	
		$K_0 = 0.1$	$K_0 = 0.5$		$K_0 = 0.1$	$K_0 = 0.5$
0.0	0.0	0.0	0.0	0.0	0.0	0.0
3.1	76.3	7.6	38.2	59.5	6.0	29.8
5.1	51.8	5.2	25.9	75.4	7.5	37.7
7.0	28.5	2.9	14.3	90.4	9.0	45.2

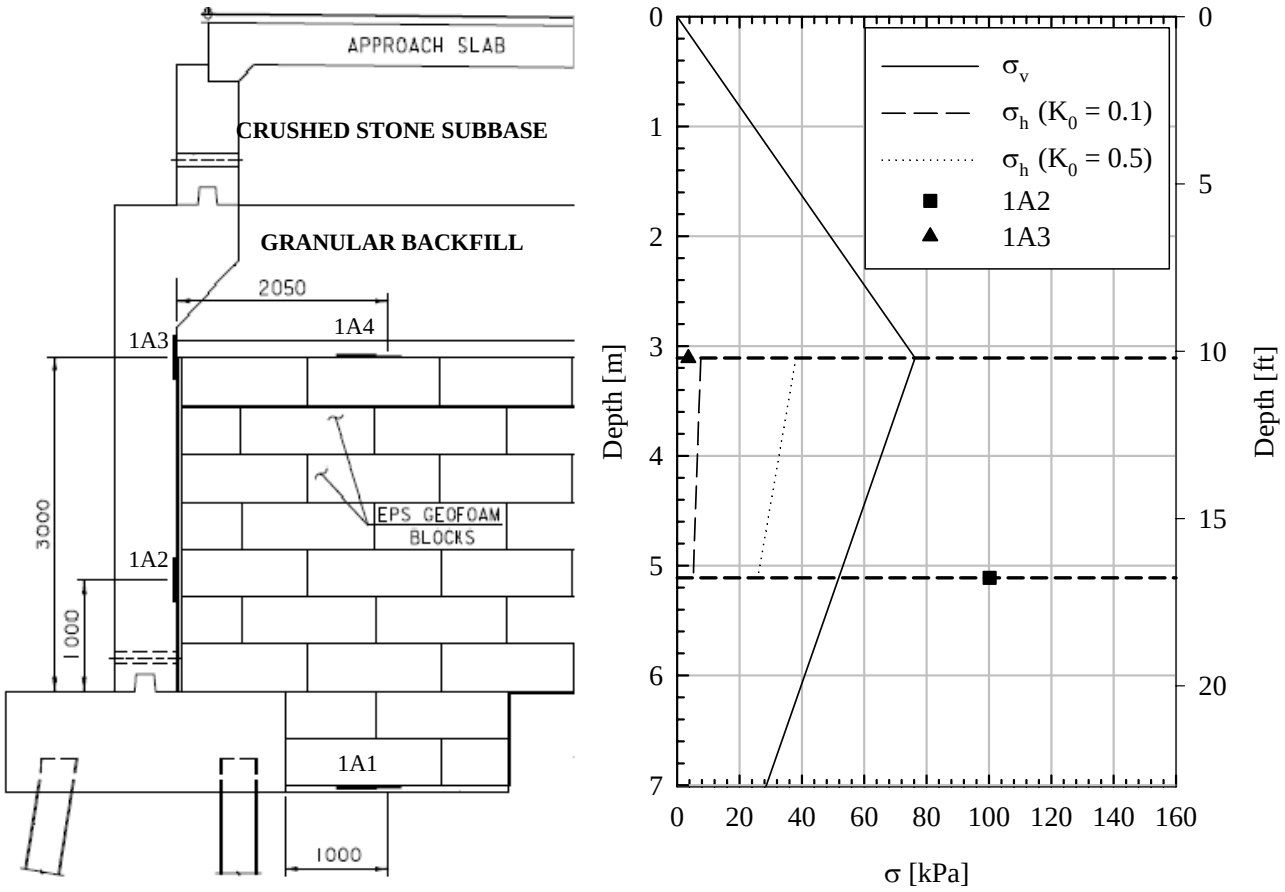

Figure 6.21 Estimated and Measured Vertical and Lateral Pressures at Abutment 1 for Case IV Loading.

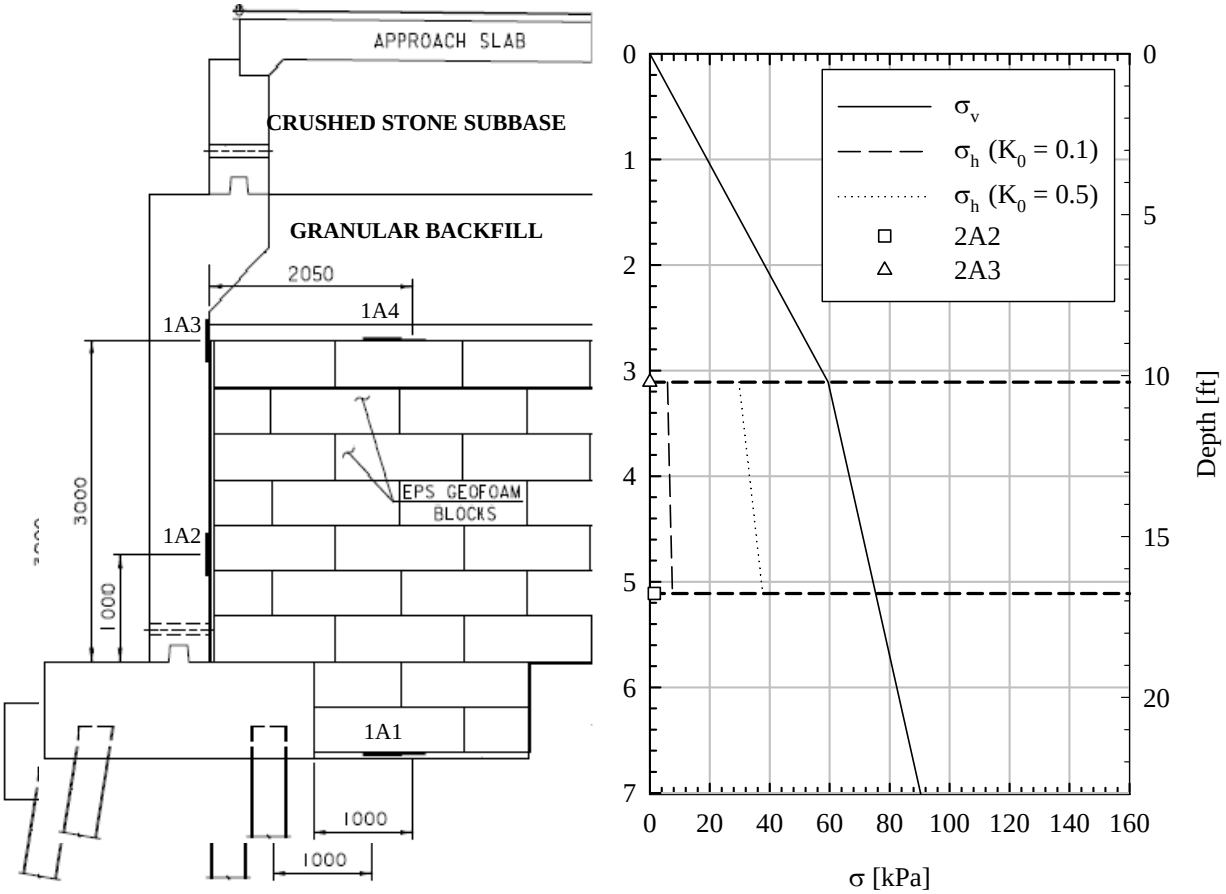

Figure 6.22 Estimated and Measured Vertical and Lateral Pressures at Abutment 2 for Case IV Loading.

Lateral Pressures

A summary of the estimated lateral pressures and final measured lateral pressures is presented in Table 6.11. The measured lateral pressures are plotted versus time in Figures 6.23 and 6.24, with horizontal lines representing the estimated values.

The estimated lateral pressures are based upon a range of values of K_0 reported in a number of previous studies and therefore should represent the upper and lower bounds of the actual measured lateral pressures. It is clear that Transducers 1A3, 2A2, and 2A3 all measured lateral pressures corresponding to values of K_0 less than the values used for the estimates, as the estimates are based upon the actual measured vertical pressures at the top and base of the GeoFoam blocks. The final lateral pressure measured by Transducer 1A3 was approximately 53 percent lower than the estimated value. The final pressure measured by Transducer 2A2 was approximately 84 percent less than the estimated value. The pressures measured by Transducer 2A3 were of negligible magnitude throughout the monitoring period. As these differences have remained fairly consistent for Cases II, III, and IV, it appears that the values of K_0 that were used were not representative of the actual measured pressures. The actual value of K_0 must be determined based upon the measured vertical and lateral pressures, as will be discussed in the next section.

Table 6.11 Summary of Measured and Estimated Lateral Pressures at Abutments 1 and 2 for Case IV Loading.

Transducer ID	$\sigma_{h\text{-}Meas}$ (kPa)	$\sigma_{h\text{-}Est}$, $K_0 = 0.10$ (kPa)	$\sigma_{h\text{-}Est}$, $K_0 = 0.50$ (kPa)	$\sigma_{h\text{-}Est} - \sigma_{h\text{-}Meas}$, $K_0 = 0.1$ (kPa)*	$\sigma_{h\text{-}Est} - \sigma_{h\text{-}Meas}$, $K_0 = 0.5$ (kPa)*	$\sigma_{h\text{-}Est} - \sigma_{h\text{-}Meas}$, $K_0 = 0.1$ (%)*	$\sigma_{h\text{-}Est} - \sigma_{h\text{-}Meas}$, $K_0 = 0.5$ (%)*
1A2	100.2	5.2	38.2	-95.0	-62.0	-1826.9	-162.3
1A3	3.6	7.6	14.3	4.0	10.7	52.6	74.8
2A2	1.5	9.0	45.2	7.6	43.8	83.9	96.8
2A3	0.0	6.0	29.8	6.0	29.8	100.0	100.0

*Note: Positive values indicate that the estimated pressure exceeds the measured pressure. Negative values indicate that the measured pressure exceeds the estimated pressure.

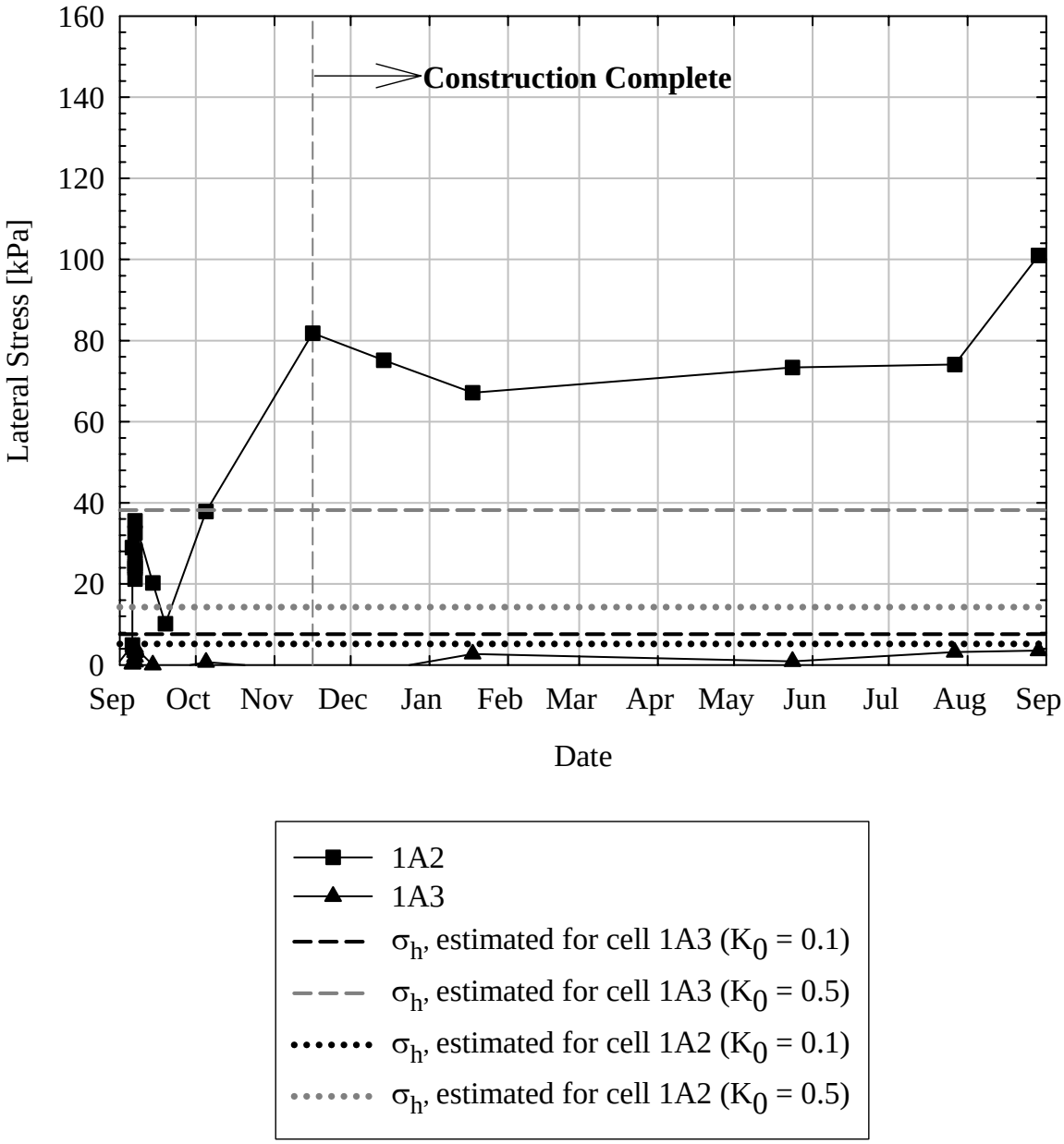

Figure 6.23 Estimated and Measured Lateral Pressures at Abutment 1 versus Time for Case IV Loading.

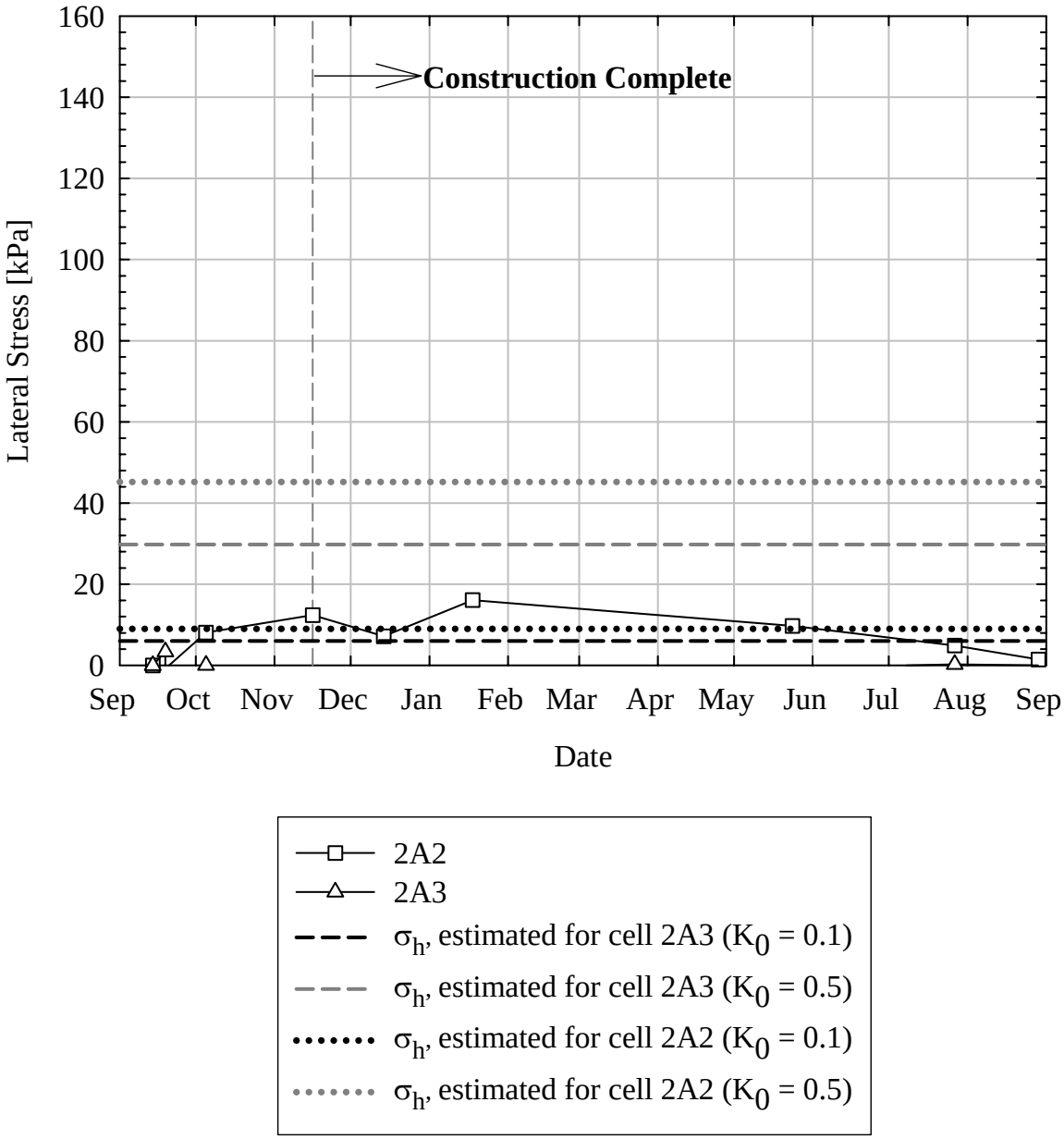

Figure 6.24 Estimated and Measured Lateral Pressures at Abutment 2 versus Time for Case IV Loading.

6.3 Determination of the At-Rest Coefficient of Lateral Earth Pressure (K_0)

Given the locations and orientations of the earth pressure transducers, K_0 was determined in two ways. The first was based purely on measured vertical and lateral earth pressures at the top of the GeoFoam blocks by Transducers 1A4/2A4 and 1A3/2A3. A summary of the calculated values of K_0 is presented in Table 6.12. K_0 and measured vertical pressure at Transducers 1A4/2A4 are plotted versus time in Figure 6.25 and 6.26. The K_0 values are reported to two decimal places due to the very low magnitudes.

The values of K_0 based upon directly measured earth pressures are much lower than the typical range reported in the literature of approximately 0.2 to 0.5. This suggests that lateral stresses are not transmitted to the wall through the blocks. The values corresponding to measurements at Abutment 1 fluctuated with changes in vertical pressure, however the normal trend observed in previous studies is a decrease in K_0 with increasing pressure. A possible reason for this is the low range of stresses over which K_0 was determined. The K_0 value corresponding to the final data measurement was approximately 0.05. The values of K_0 corresponding to Abutment 2 zero for the entire monitoring period due to the negligible magnitude of the measured stresses.

Table 6.12 Summary of K_0 Values Determined at Top of GeoFoam Blocks.

Date	Abutment 1			Abutment 2		
	$\sigma_{v\text{-}Meas}$ (kPa)	$\sigma_{h\text{-}Meas}$ (kPa)	K_0	$\sigma_{v\text{-}Meas}$ (kPa)	$\sigma_{h\text{-}Meas}$ (kPa)	K_0
11/16/2006	68.5	-1.2	0.00	55.0	0.0	0.00
12/14/2006	65.8	-1.1	0.00	50.8	0.0	0.00
1/18/2007	68.4	2.7	0.04	52.6	0.0	0.00
5/24/2007	72.1	0.9	0.01	56.0	0.0	0.00
7/27/2007	77.3	3.2	0.04	60.2	0.3	0.00
8/29/2007	76.3	3.6	0.05	59.5	0.0	0.00

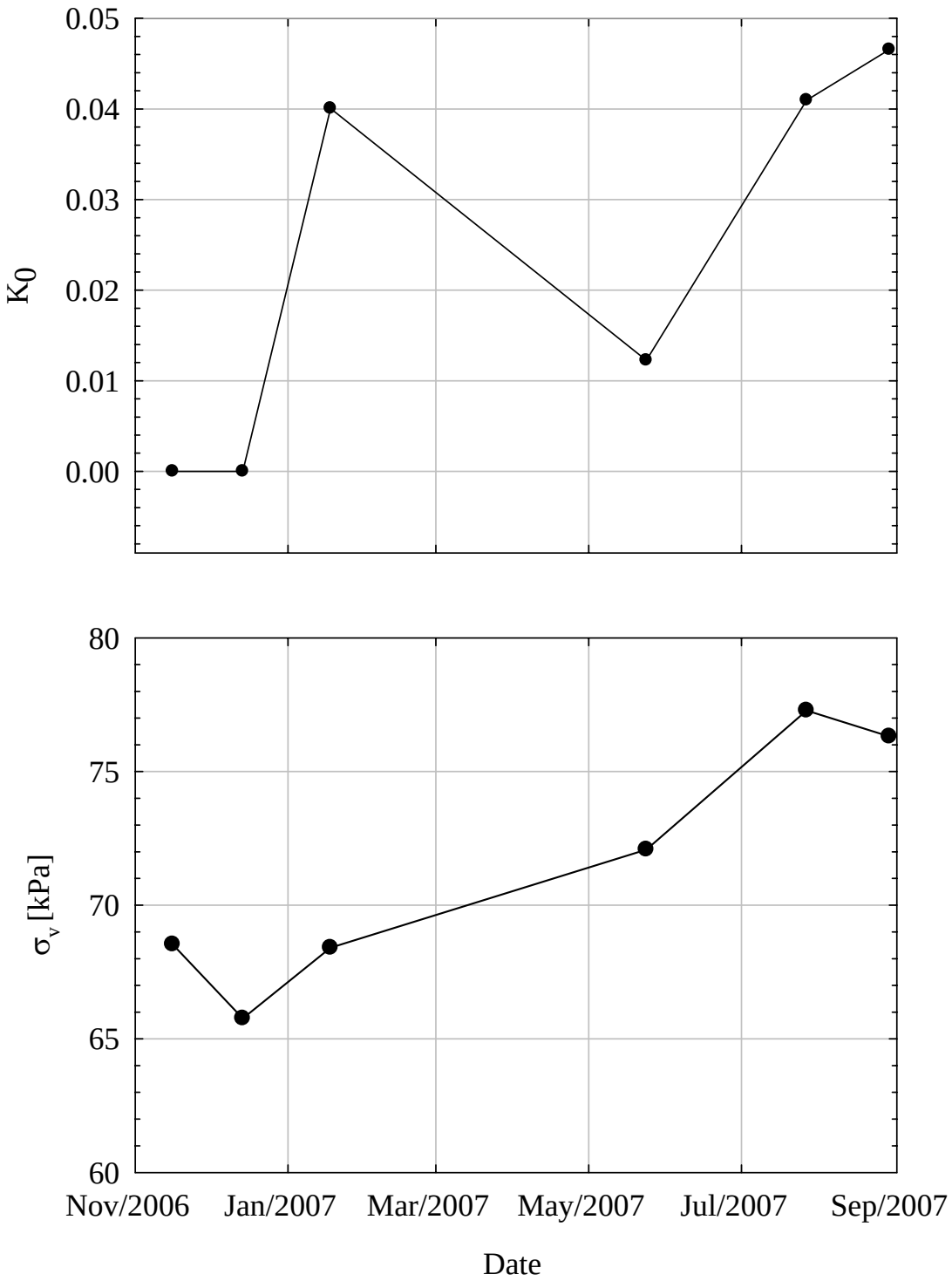

Figure 6.25 K_0 and Measured Vertical Pressure at Top of GeoFoam Blocks at Abutment 1 versus Time.

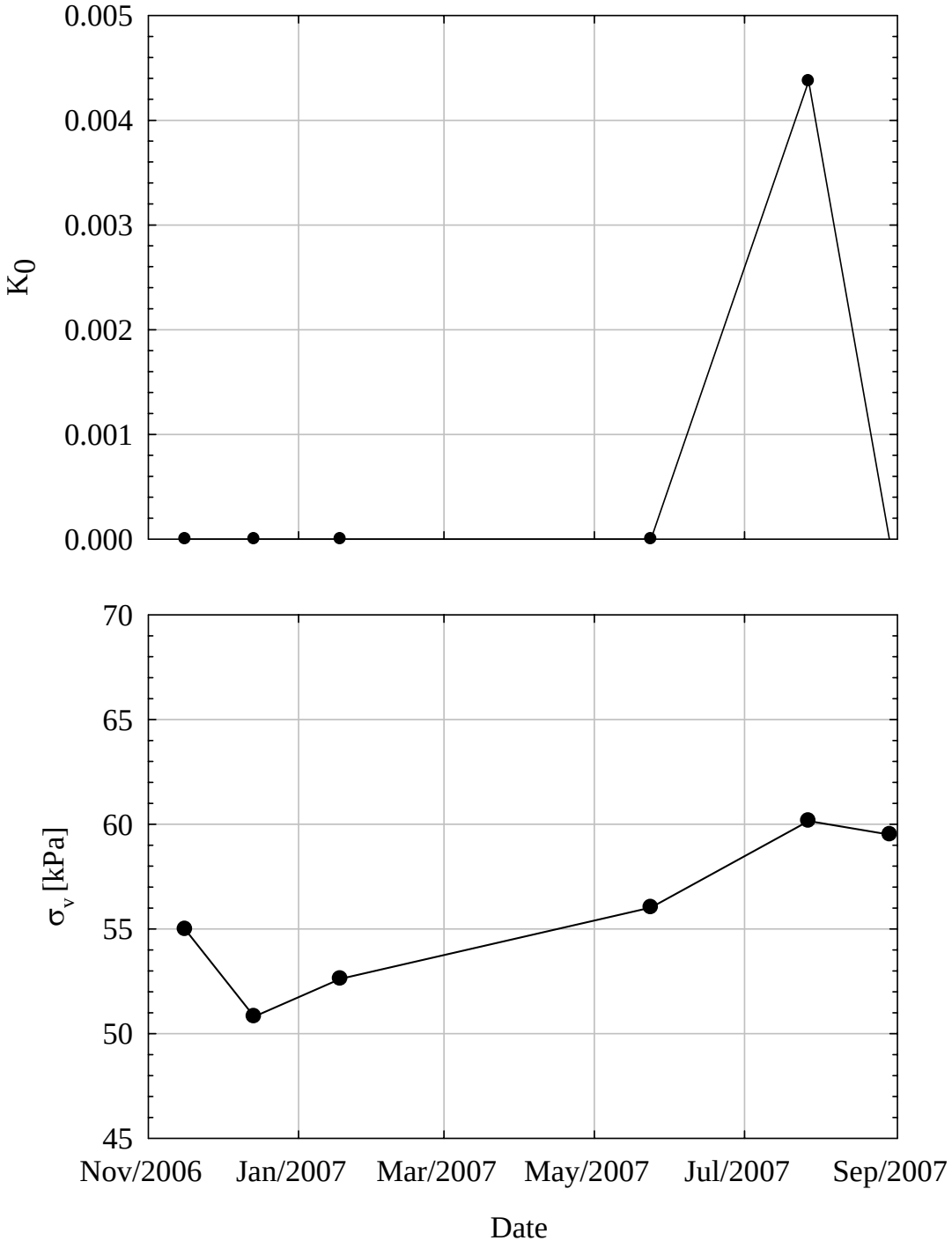

Figure 6.26 K_0 and Measured Vertical Pressure at Top of GeoFoam Blocks at Abutment 2 versus Time.

The second method of determining K_0 required that the vertical pressure 2.0 m (6.6 ft) below the top of the GeoFoam blocks be determined based upon interpolation of the profile of measured vertical pressures at the top and base of the blocks. This depth represents the location of Transducers 1A2 and 2A2, which measured the horizontal stress required to calculated values of K_0. Table 6.13 presents a summary of the values of K_0 corresponding to the monitoring period from the end of construction through the final measurement. The values of K_0 and interpreted vertical pressure are plotted versus time in Figures 6.27 and 6.28.

The K_0 values determined based upon pressure measurements from Transducer 1A2 ranged from 1.27 to 1.95, which is not considered possible in terms of stress transfer and therefore again confirms that the transducer is not functioning correctly. The K_0 values determined based upon the pressure measurements from Transducer 2A2 ranged from 0.02 to 0.22, with a final measurement of 0.02. Again, no relationship between vertical pressure and K_0 can be observed within the data. More frequent readings during the construction period and monitoring period would have measured larger stress changes, in which case the expected behavior might have been observed.

Table 6.13 Summary of K_0 Values for Depth of 2.0 m (6.6 ft) Below Top of GeoFoam Blocks, Abutments 1 and 2.

	Abutment 1			Abutment 2		
Date	$\sigma_{v\text{-}Est}$ (kPa)	$\sigma_{h\text{-}Meas}$ (kPa)	K_0	$\sigma_{v\text{-}Est}$ (kPa)	$\sigma_{h\text{-}Meas}$ (kPa)	K_0
11/16/2006	50.3	81.8	1.63	77.8	12.4	0.16
12/14/2006	47.6	75.1	1.58	73.3	7.1	0.10
1/18/2007	52.7	67.1	1.27	72.0	16.1	0.22
5/24/2007	51.8	73.4	1.42	67.5	9.7	0.14
7/27/2007	52.7	74.1	1.41	76.5	4.9	0.06
8/29/2007	51.8	101.0	1.95	75.3	1.4	0.02

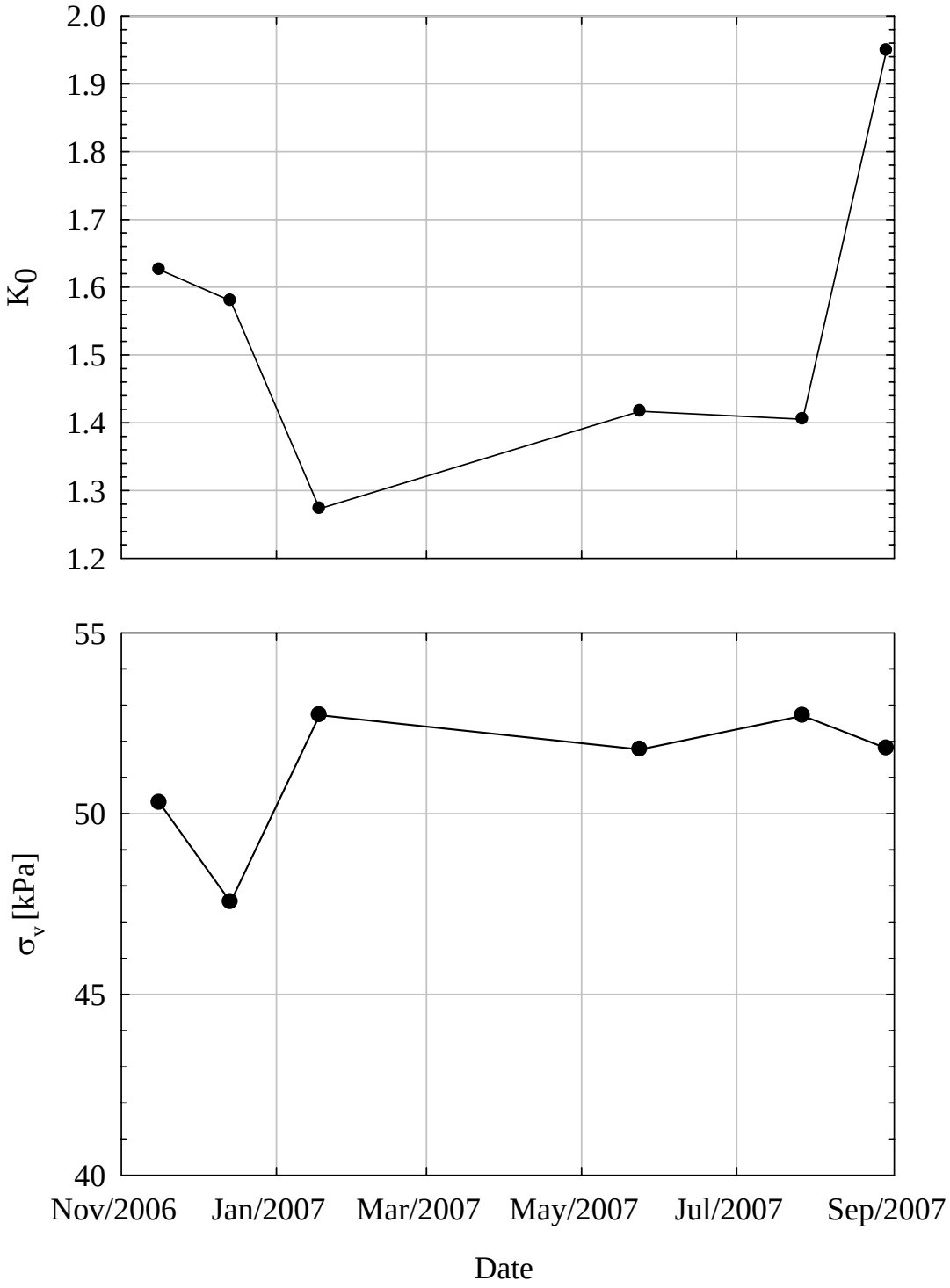

Figure 6.27 K_0 and Estimated Vertical Pressure 2.0 m (6.6 ft) Below Top of GeoFoam Blocks at Abutment 1.

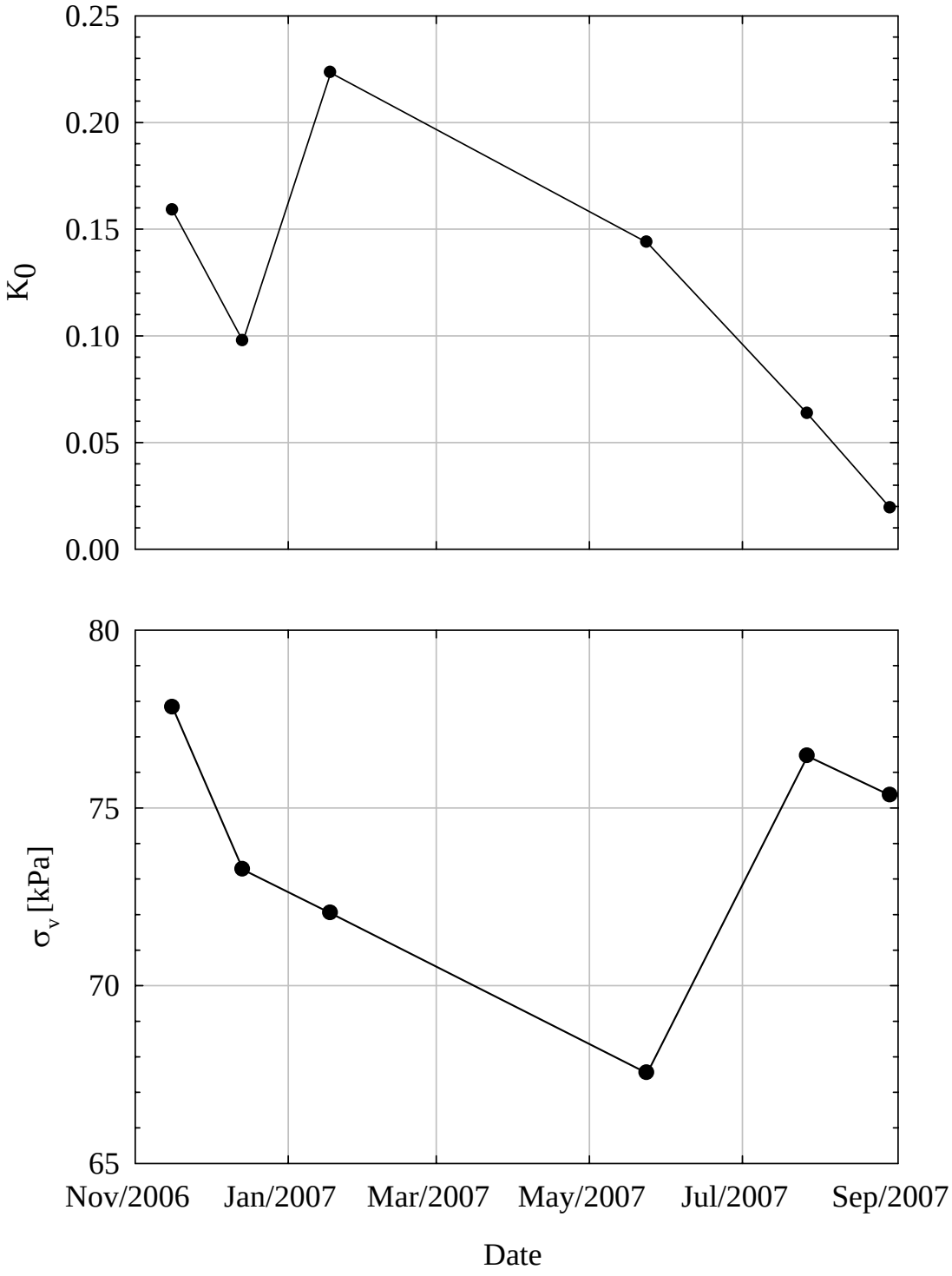

Figure 6.28 K_0 and Estimated Vertical Pressure 2.0 m (6.6 ft) Below Top of GeoFoam Blocks at Abutment 2.

CHAPTER 7. SUMMARY AND CONCLUSIONS

7.1 Conclusions

A full scale highway bridge was constructed using GeoFoam backfill. Earth pressure measurements were obtained on the back face of the concrete abutments to evaluate the lateral earth pressures resulting from the replacement of conventional backfill with the GeoFoam. Based on the results from this investigation, it was determined that the use of EPS GeoFoam as a substitute for conventional granular backfill resulted in significant reductions in both lateral and vertical earth pressures behind the bridge abutments. Lateral pressures measured at the boundary between the GeoFoam blocks and the overlying fill were of negligible magnitude (i.e., on the order of 2 to 6 kPa; except for one pressure cell which gave a reading of about 100kPa and may have been faulty). Lateral pressures measured at the mid-depth of the GeoFoam blocks were of slightly higher magnitude. Similar behavior has been reported in previous studies as discussed in the literature review and attributed to rotation of the blocks due to differential settlement of the approach fill, however this cannot be confirmed without actual settlement data.

Vertical pressures measured above and below the GeoFoam blocks indicated a pressure spreading effect; greater pressures were measured at the top of the blocks than at the base of the blocks, indicating that the GeoFoam blocks dissipate the vertical stresses. Several loading conditions based upon both measured and estimated vertical pressures were used to estimate corresponding lateral pressures based on K_0 values of 0.1 and 0.5, however under all conditions the resulting estimated lateral pressures exceeded the measured lateral pressures. Based upon the final measured vertical and lateral pressures, the resulting values of the at-rest coefficient of lateral earth pressure (K_0) were between 0.02 and 0.05.

7.2 Recommendations

7.2.1 Surveys and Modeling

One of the major assumptions in this project was that of an at-rest condition existing within the approach fill/abutment systems. Although the bridge abutments are open-seat (as opposed to integral), include supported wingwalls, and are founded on battered piles, there is still potential for movement of the abutment walls both away from (active condition) and towards (passive condition) the approach fills. The use of instrumentation such as inclinometers or conducting periodic surveys would identify any such wall movements.

An advantage to using any lightweight fill material is the potential for reduced differential settlements. In the case of this project, settlement of the abutments is assumed minimal due to deep foundations resting on bedrock, however given the geometry of the GeoFoam blocks (a wedge shape) and the soil conditions at the site there is potential for differential settlements. Such differential settlements would affect the measured pressures, especially the lateral pressures on the abutment walls. Periodic surveys of the approaches would indicate any settlements of the embankments.

In the event of abutment rotation or differential settlements being measured, it is recommended that a modeling program be used to predict the effect of movements on the measured pressures. This would aid in accounting for pressure measurements that seem to lie outside of the range of predicted at-rest pressures.

7.2.2 Data Acquisition

The length of the post-construction monitoring period for this project was 10 months, however only 6 monthly measurements could be made as weather conditions made access to the instrumentation impossible. The gap in data between January 2007 and June 2007 represents a period of significant changes in weather and temperature, the effects of which on the GeoFoam blocks would be of great interest to this study. A datalogger or data transmitter would eliminate this problem and could also be set to record pressure measurements with greater frequency than once per month.

8.0 REFERENCES

ASTM D 1623-78, "Standard Test Method for Tensile Adhesion Properties of Rigid Cellular Plastics." Vol. 08.01, American Society for Testing and Materials, West Conshohocken, PA (2001)

ASTM C 203-99, "Standard Test Methods for Breaking Load and Flexural Properties of Block-Type Thermal Insulation." Vol. 04.06, American Society for Testing and Materials, West Conshohocken, PA (1999).

ASTM D 5321-92, "Standard Test Method for Determining the Coefficient of Soil and Geosynthetic or Geosynthetic and Geosynthetic Friction by the Direct Shear Method." Vol. 04.09 (II), American Society for Testing and Materials, West Conshohocken, PA (2001).

ASTM D 2216, "Standard Test Method for Laboratory Determination of Water (Moisture) content of Soil, Rock, and Soil-Aggregate Mixtures." Vol. 04.08, American Society for Testing and Materials, West Conshohocken, PA (1996)

ASTM D 2435-04 "Standard Test Method for One-Dimensional Consolidation Properties of Soils." Vol. 04.08, American Society for Testing and Materials, Conshohocken, PA (2000)

ASTM D 4221-90. "Test Method for Dispersive Characteristics of Clay by Double Hydrometer." Vol. 04.08., American Society for Testing and Materials, West Conshohocken, PA (2005)

ASTM D 422-63. "Standard Test Method for Particle-Size Analysis of Soils." Vol. 04.08, American Society for Testing and Materials, Conshohocken, PA (2005).

ASTM D 4318-00. "Standard Test Methods for Liquid Limit, Plastic Limit, and Plasticity Index of Soils." Vol. 04.08., American Society for Testing and Materials, West Conshohocken, PA (2005).

ASTM D 4648-05. "Standard Test Method for Laboratory Miniature Vane Shear Test for Saturated Fine-Grained Clayey Soil." Vol 04.08., American Society for Testing and Materials, West Conshohocken, PA (2000).

ASTM D854-06. "Standard Test Methods for Specific Gravity of Soil Solids by Water Pycnometer." Vol 04.08., American Society for Testing and Materials, West Conshohocken, PA (2005).

Athanasopoulos, G. A., Pelekis, P. C. and Xenaki, V. C., "Dynamic Properties of EPS Geofoam: An Experimental Investigation". *Geosynthetics International*, Industrial Fabrics Association International, Roseville, Minn., U.S.A., Vol. 6, No. 3 pp. 171-194. (1999).

Briaud, J.-L., X. Zhang, and S. Moon. "Shrinkage Test – Water Content Method for Shrink and Swell Predictions", Journal of Geotechnical and Geoenvironmental Engineering ASCE, Vol. 129, No. 7, pp 590-600. (2003).

Cerato, A.B. and Lutenegger, A.J., "Recommended Method for Determining Surface Area of Fine-Grained Soils.", Geotechnical Testing Journal, ASTM. Vol. 25, #3, pp. 314-320. (2002).

Dreimanis, A., “Quantitative gasometric determination of calcite and dolomite by using Chittick apparatus”. Journal of Sedimentary Petrology, 32, 520-529. (1962).

Duškov, M., "Measurements on a Flexible Pavement Structure with an EPS Geofoam Sub-Base". *Geotextiles and Geomembranes*, Elsevier Science Ltd., London, U.K., Vol. 15, Nos. 1-3 pp. 5-27. (1997).

Head, K. H. Manual of soil laboratory testing, Vol. 1: Soil Classification and Compaction Tests, Pentech Press Limited, Plymouth, London. (1980)

Horvath, J. S., "Expanded Polystyrene (EPS) Geofoam: An Introduction to Material Behavior". *Geotextiles and Geomembranes*, Elsevier Science Ltd., London, U.K., Vol. 13, No. 4 (1994) pp. 263-280.

Horvath, J. S., "Expanded Polystyrene (EPS) Properties for Geotechnical Engineering Applications". In "Proceedings; International Geotechnical Symposium on Polystyrene Foam in Below-Grade Applications; March 30, 1994; Honolulu, Hawaii, U.S.A.", *Research Report No. CE/GE-94-1*, J. S. Horvath (ed.), Manhattan College, Bronx, N.Y., U.S.A. (1994).

Horvath, J. S.. "*Geofoam geosynthetic*", Horvath Engineering, P.C., Scarsdale, NY, U.S.A. (1995)

Horvath, J. S. "Cellular Geosynthetics in Transportation Applications", *Geotechnical Engineering for Transportation Projects*, M. K. Yegian and E. Kavazanjian (eds.), American Society of Civil Engineers, Reston, VA, U.S.A., pp. 627-636. (2004).

Horvath, J. S. "Expanding the use of expanded polystyrene (EPS) geofoam in practice." *Proc. BSCES ASCE Geo-Institute Fall 2005 Geotech. Engrg. Sem*. (2005).

Negussey, D. and Sun, M. C., “Reducing Lateral Pressure by Geofoam (EPS) Substitution”. *Proceedings of the International Symposium on EPS Construction Method (EPS Tokyo ‘96)*, EPS Construction Method Development Organization, Tokyo, Japan (1996) pp. 201-211.

Preber, T., Bang, S., Chung, Y., and Cho, Y., “Behavior of Expanded Polystyrene Blocks.” T*ransportation Research Record No. 1462*, Transportation Research Board, Washington, D.C. (1994) pp. 36-46.

Stark, T. D., Arellano, D., Horvath, J. S. and Leshchinsky, D. *Guidelines for Geofoam Applications in Embankment Projects*, Final Rpt. - Natl. Coop. Hwy. Res. Prog. Proj. 24-11. (2004).

Stuedlein, A. W., Negussey, D., and Mathioudakis, M., “A Case History of the Use of Geofoam for Bridge Approach Fills”, Proceedings of the 5th International Conference on Case Histories in Geotechnical Engineering, NY, 2004.

Yang, J.S., Huang, S.W., and Wang, M.C., “A Model Study of EPS Constructed Bridge Approach Embankment.” Journal of the Southeast Asian Geotechnical Society, Hong Kong. (2003).

APPENDIX A. Results of One-Dimensional Consolidation Tests.

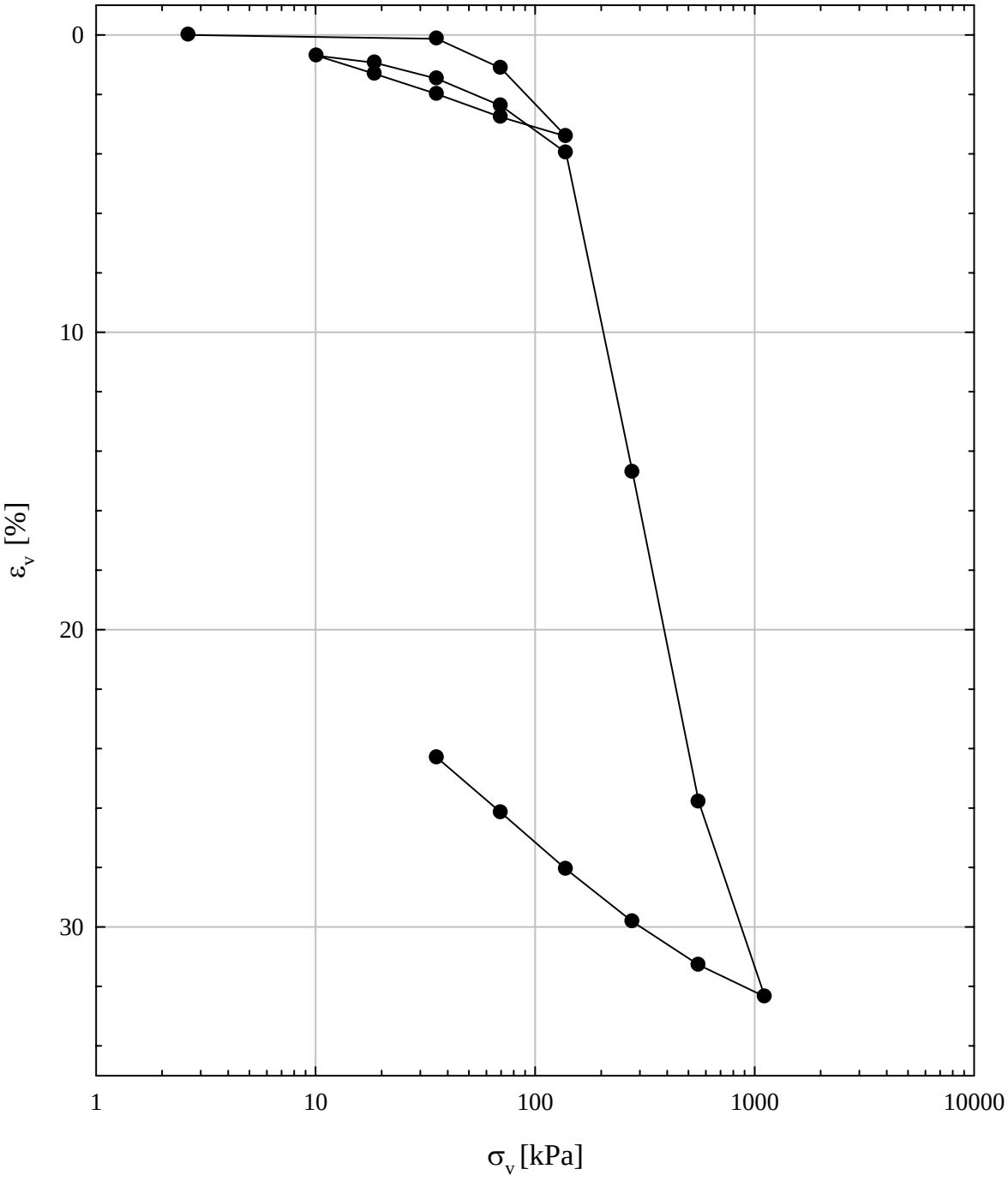

Figure A.1 Incremental Load Consolidation Test Results for Borehole B-201, 15.5 m (51.0 ft).

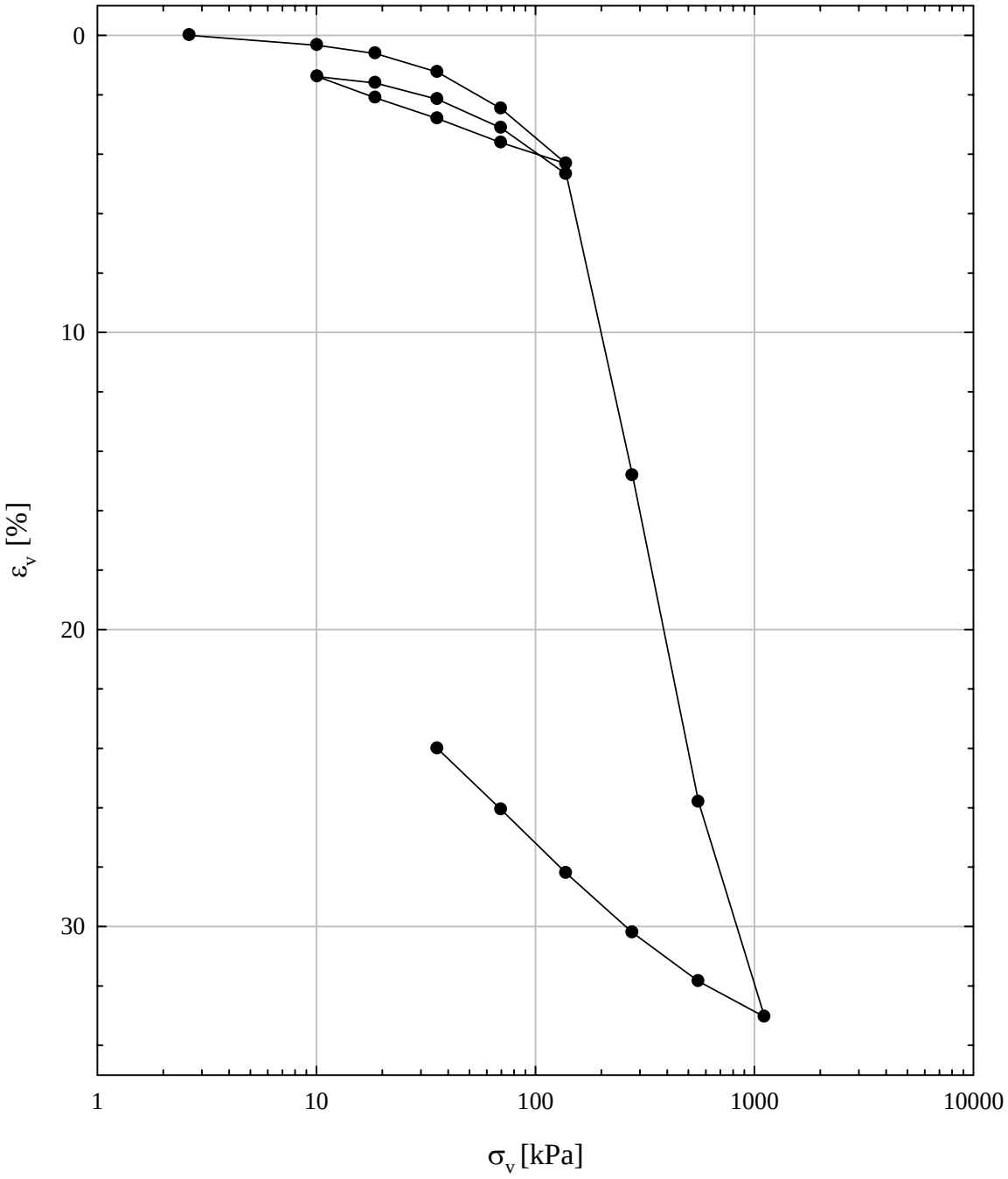

Figure A.2 Incremental Load Consolidation Test Results for Borehole B-201, 17.1 m (56.0 ft).

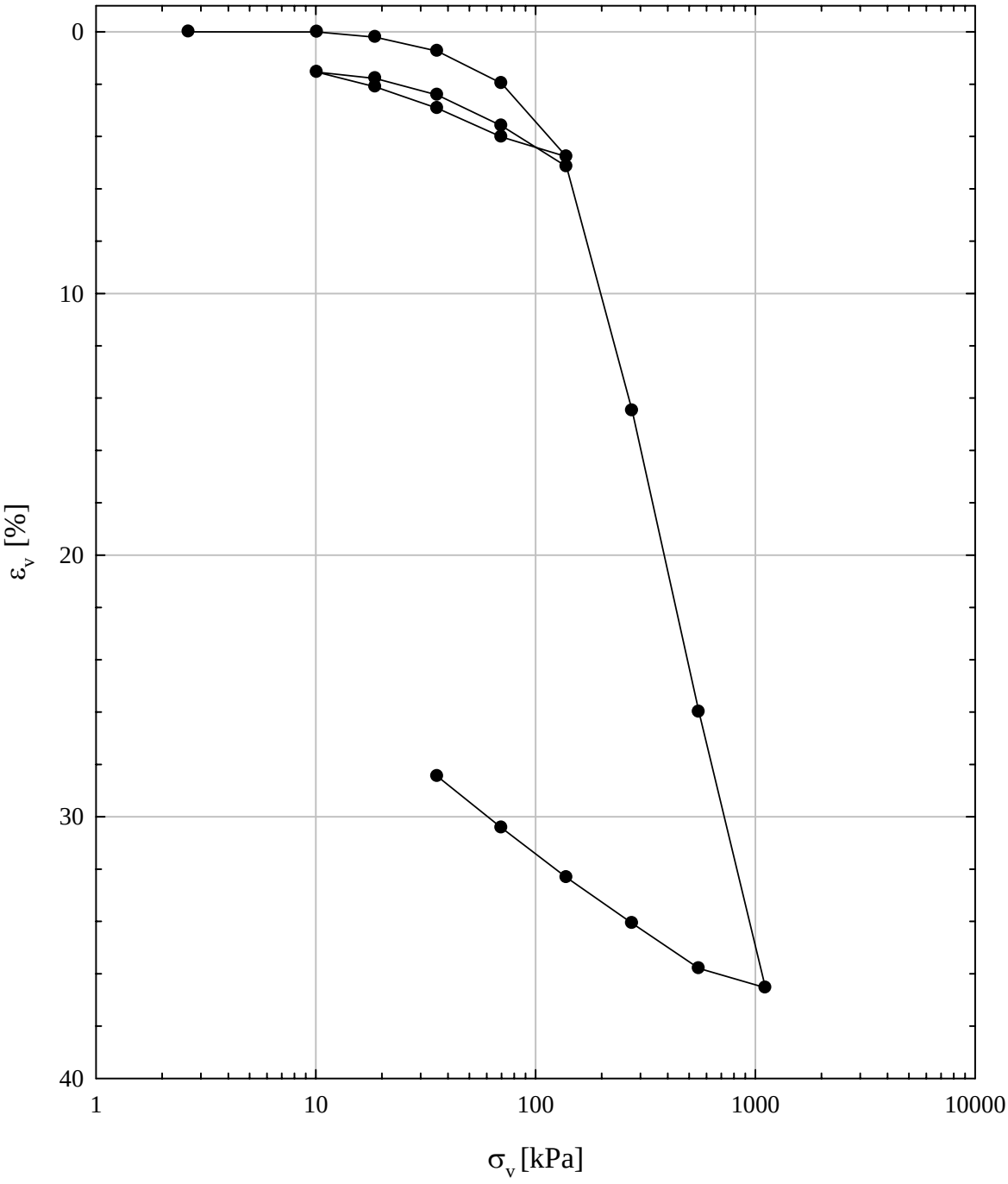

Figure A.3 Incremental Load Consolidation Test Results for Borehole B-201, 18.9 m (62.0 ft).

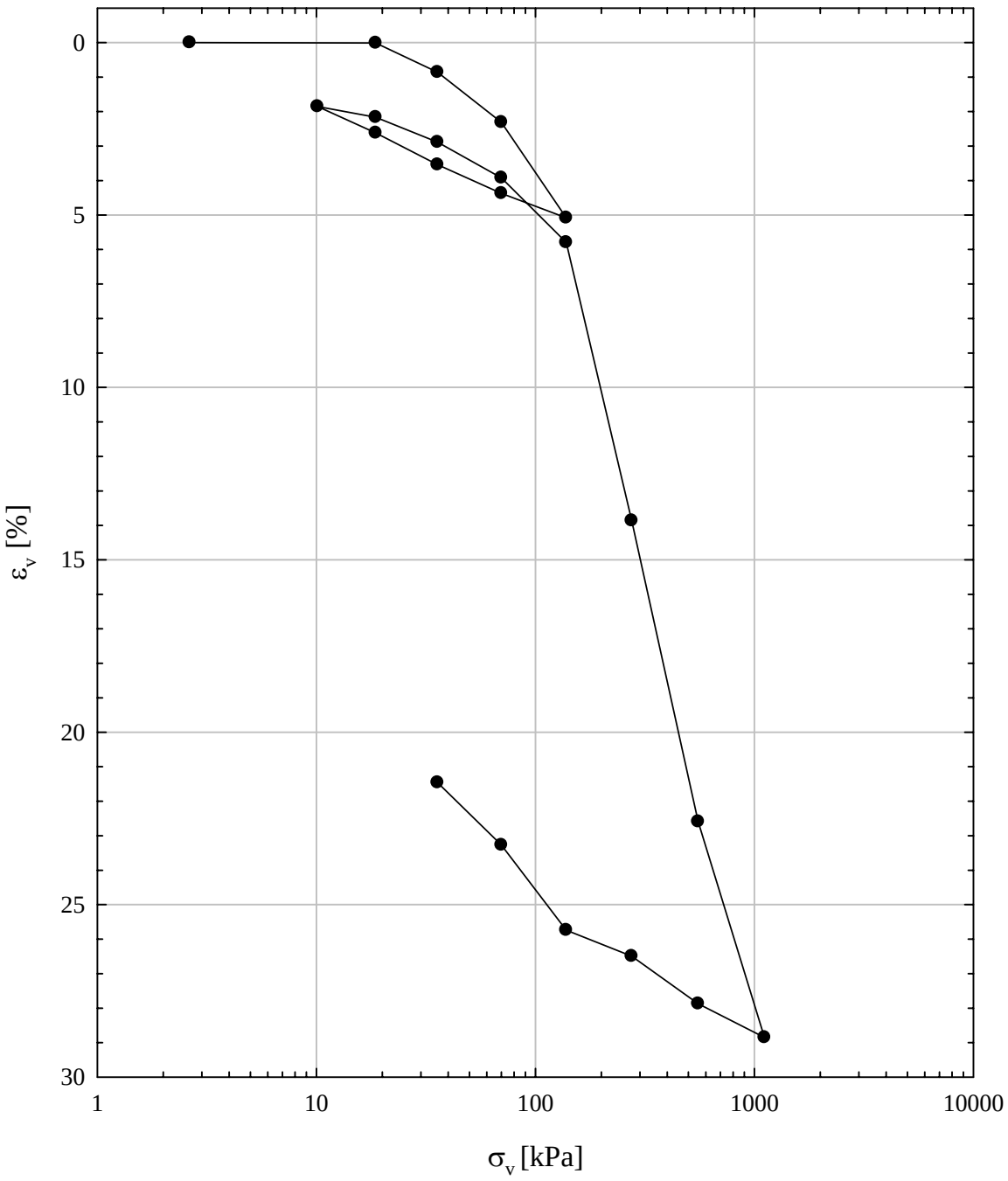

Figure A.4 Incremental Load Consolidation Test Results for Borehole B-201, 20.4 m (67.0 ft).

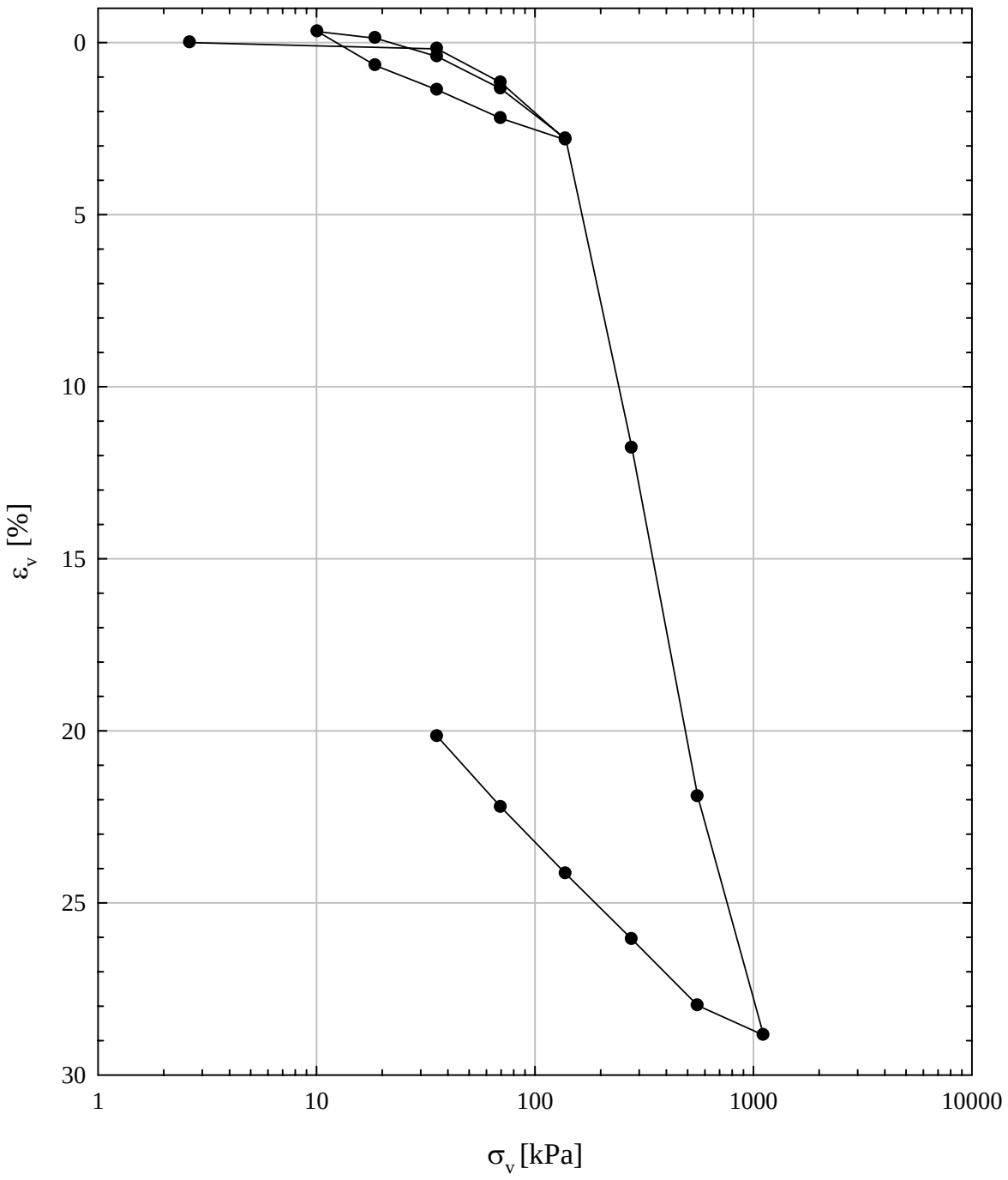

Figure A.5 Incremental Load Consolidation Test Results for Borehole B-201, 21.9 m (72.0 ft).

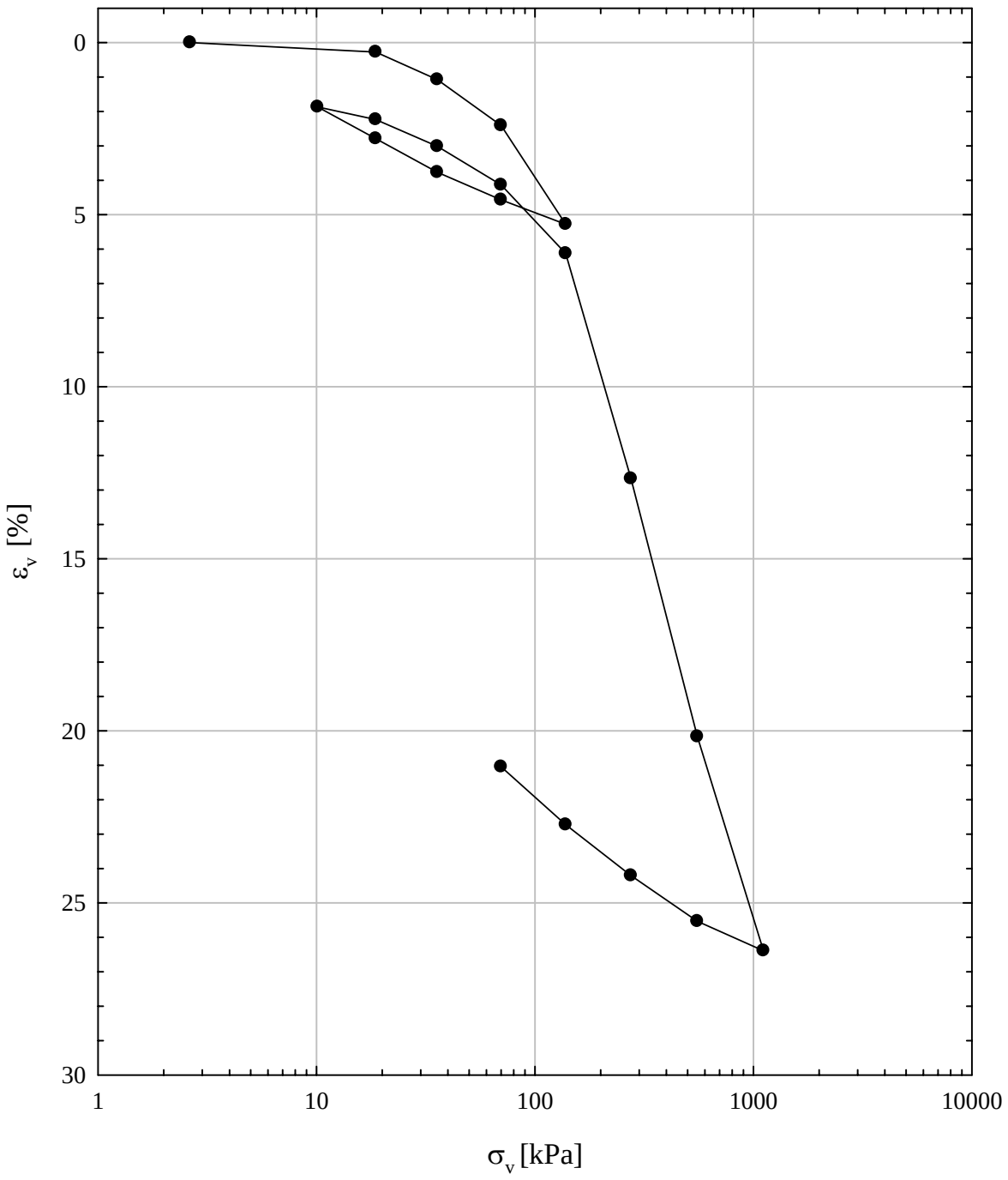

Figure A.6 Incremental Load Consolidation Test Results for Borehole B-201, 23.5 m (77.0 ft).

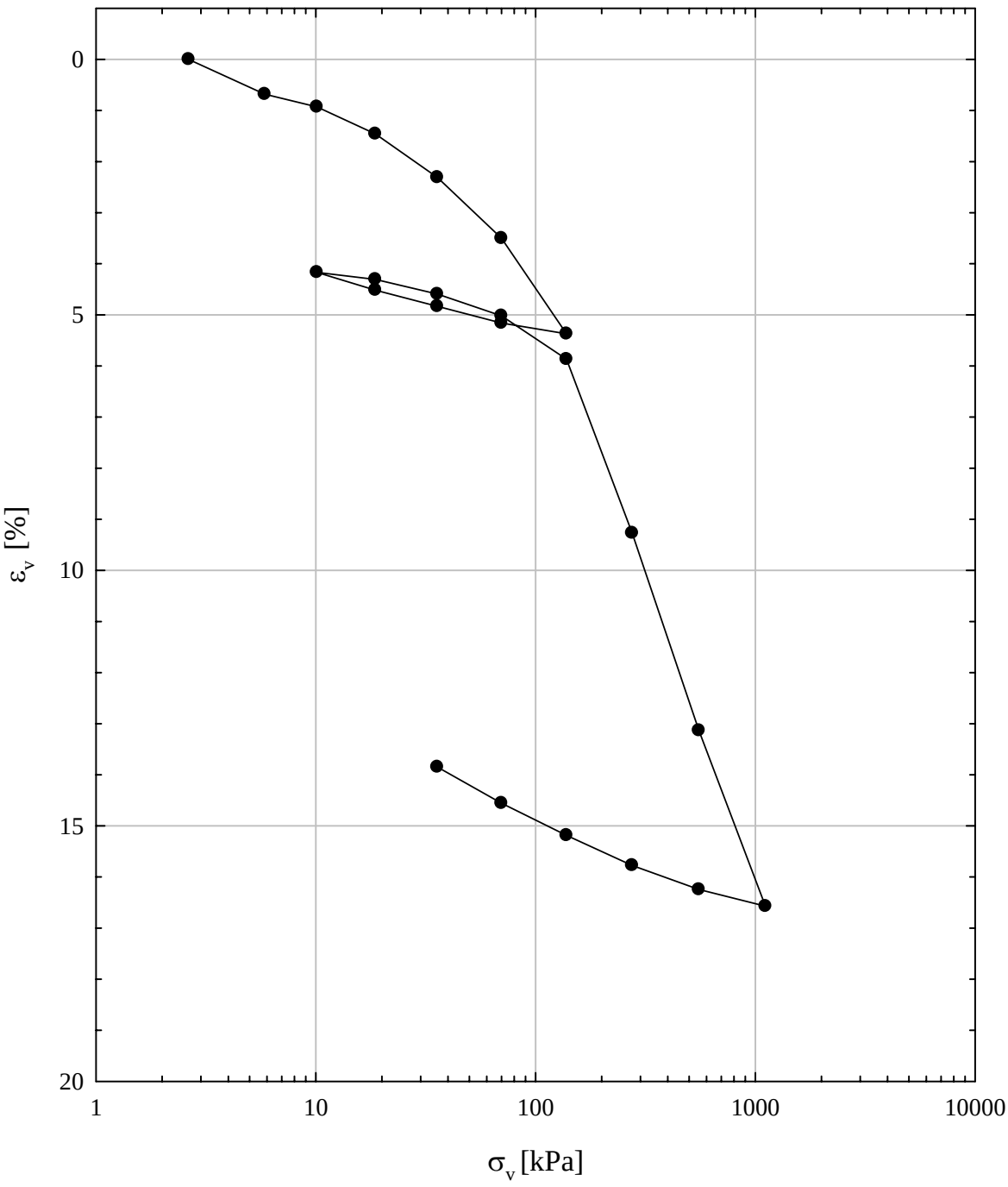

Figure A.7 Incremental Load Consolidation Test Results for Borehole B-201, 24.7 m (81.0 ft)

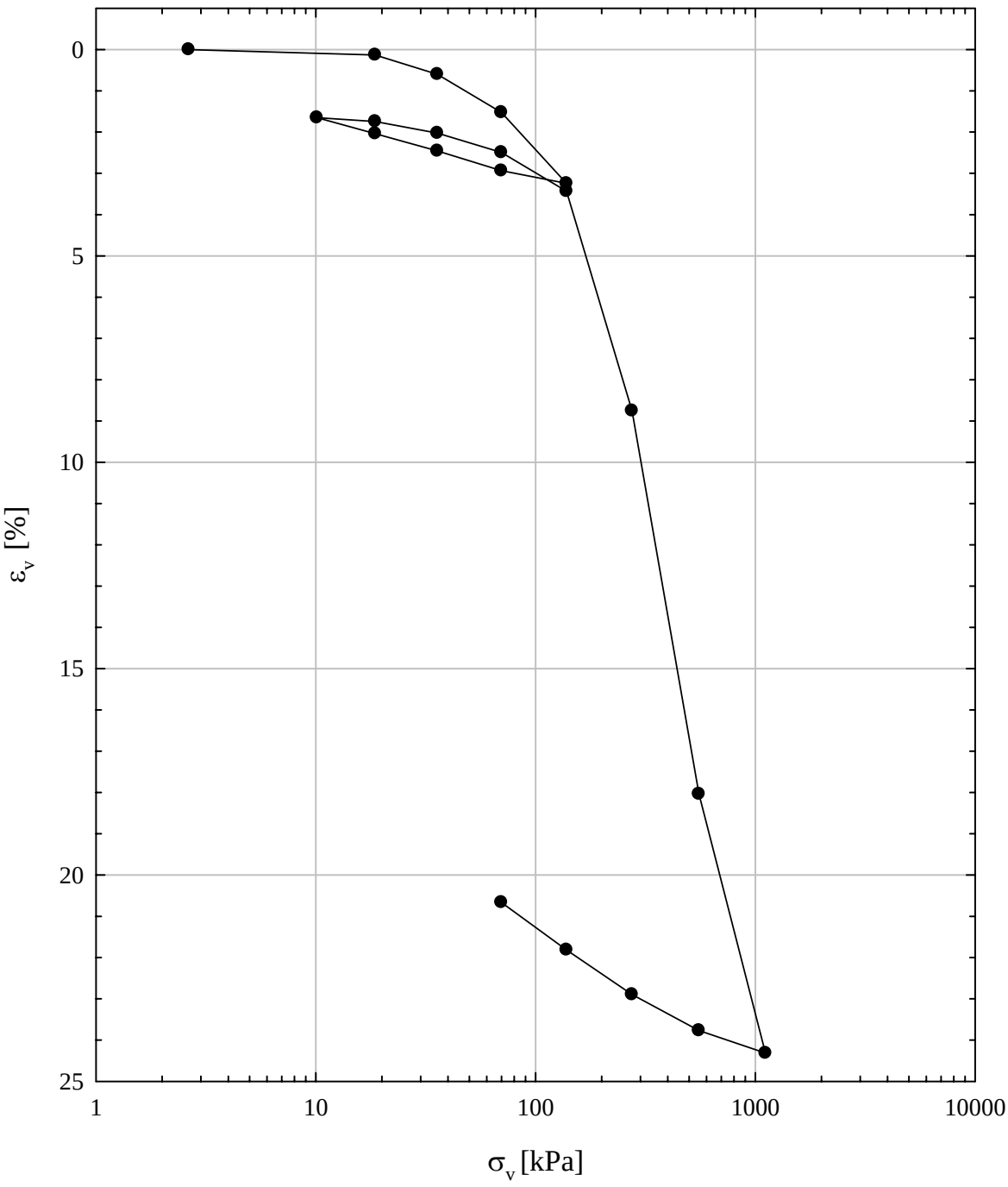

Figure A.8 Incremental Load Consolidation Test Results for Borehole B-201, 26.2 m (86.0 ft).

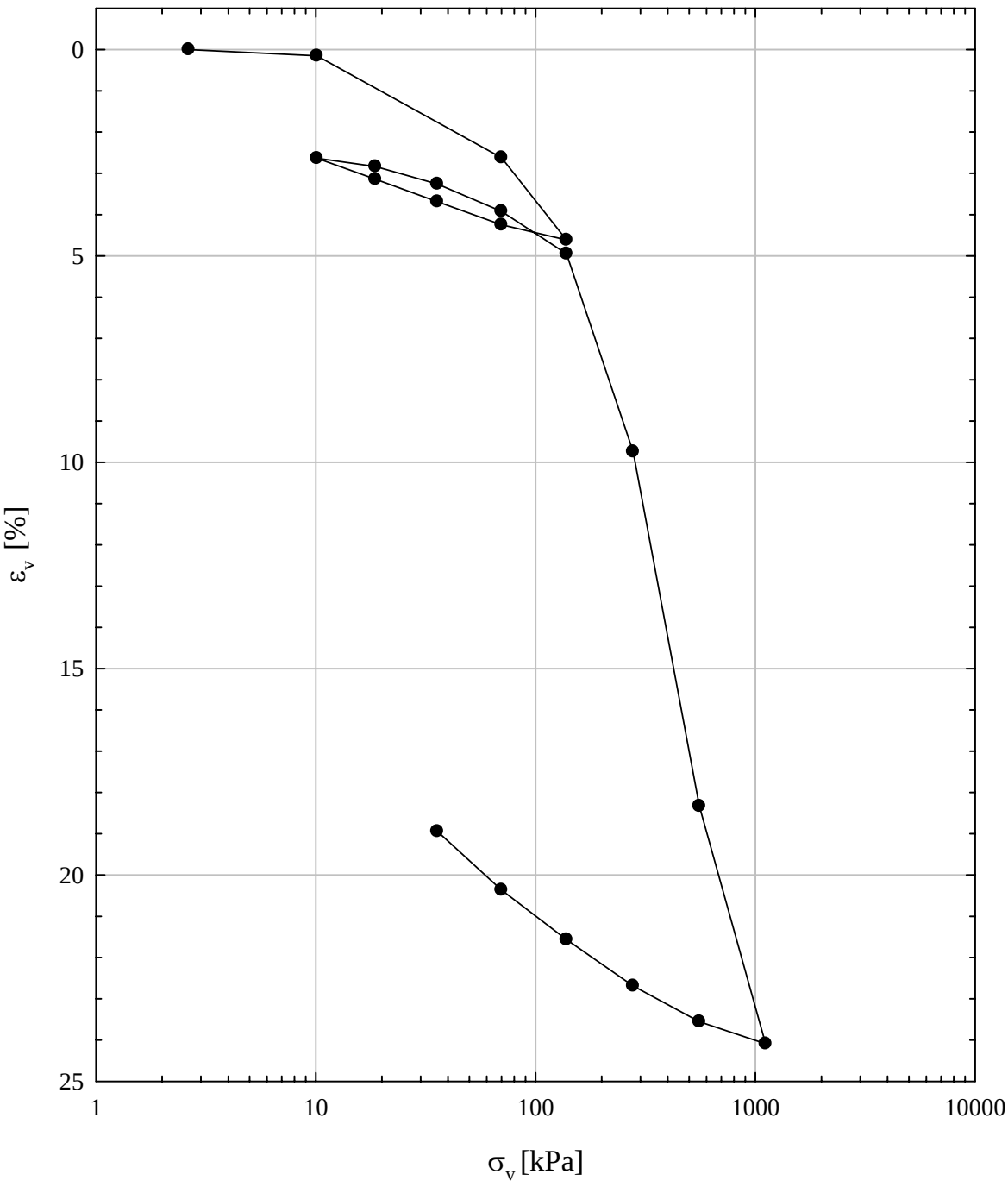

Figure A.9 Incremental Load Consolidation Test Results for Borehole B-201, 27.7 m (91.0 ft).

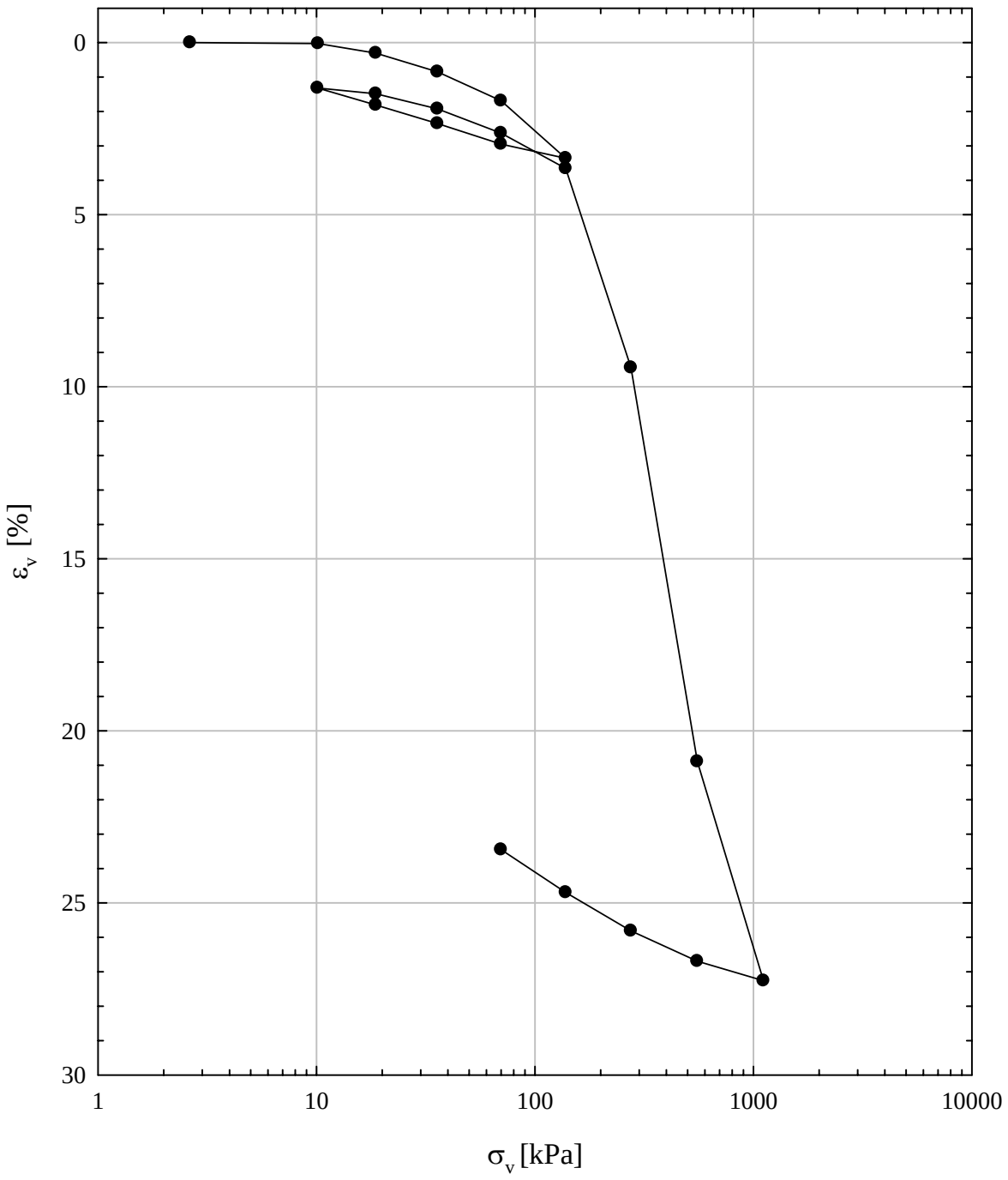

Figure A.10 Incremental Load Consolidation Test Results for Borehole B-201, 29.6 m (97.0 ft).

Appendix B. Results of Lab Vane Tests.

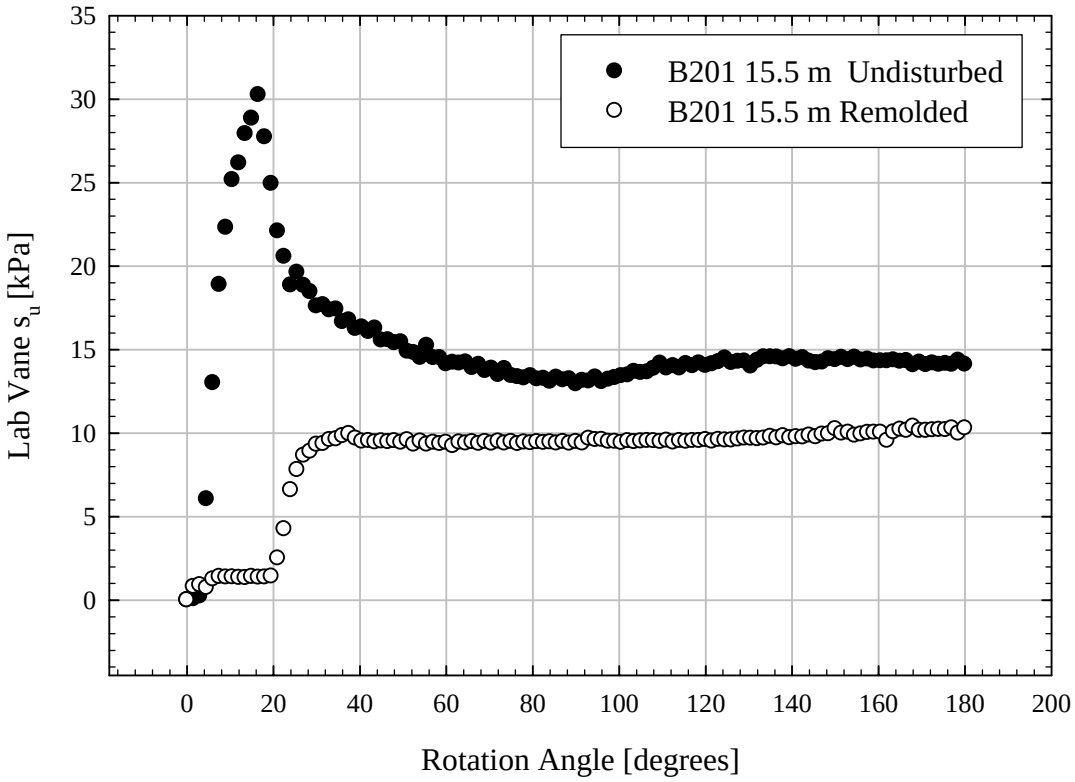
B201 15.5 m Undisturbed
B201 15.5 m Remolded
Lab Vane s_u [kPa]
Rotation Angle [degrees]
0
5
10
15
20
25
30
35
0
20
40
60
80
100
120
140
160
180
200

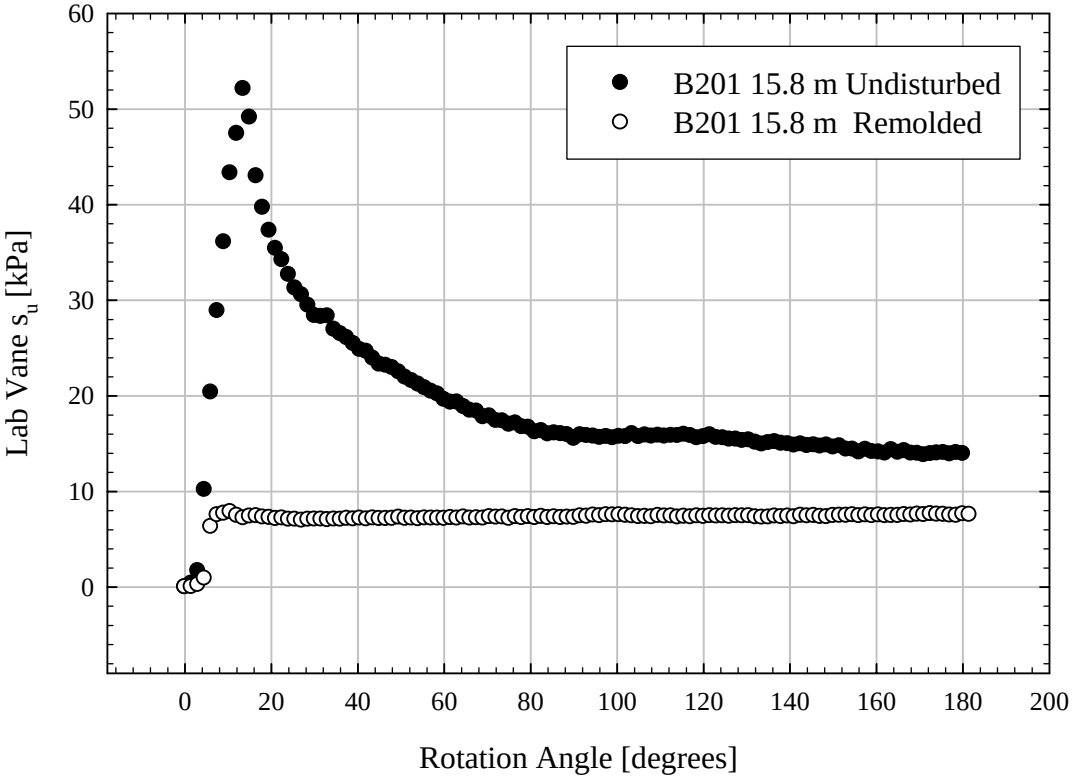
B201 15.8 m Undisturbed
B201 15.8 m Remolded
Lab Vane s_u [kPa]
Rotation Angle [degrees]
0
10
20
30
40
50
60
0
20
40
60
80
100
120
140
160
180
200

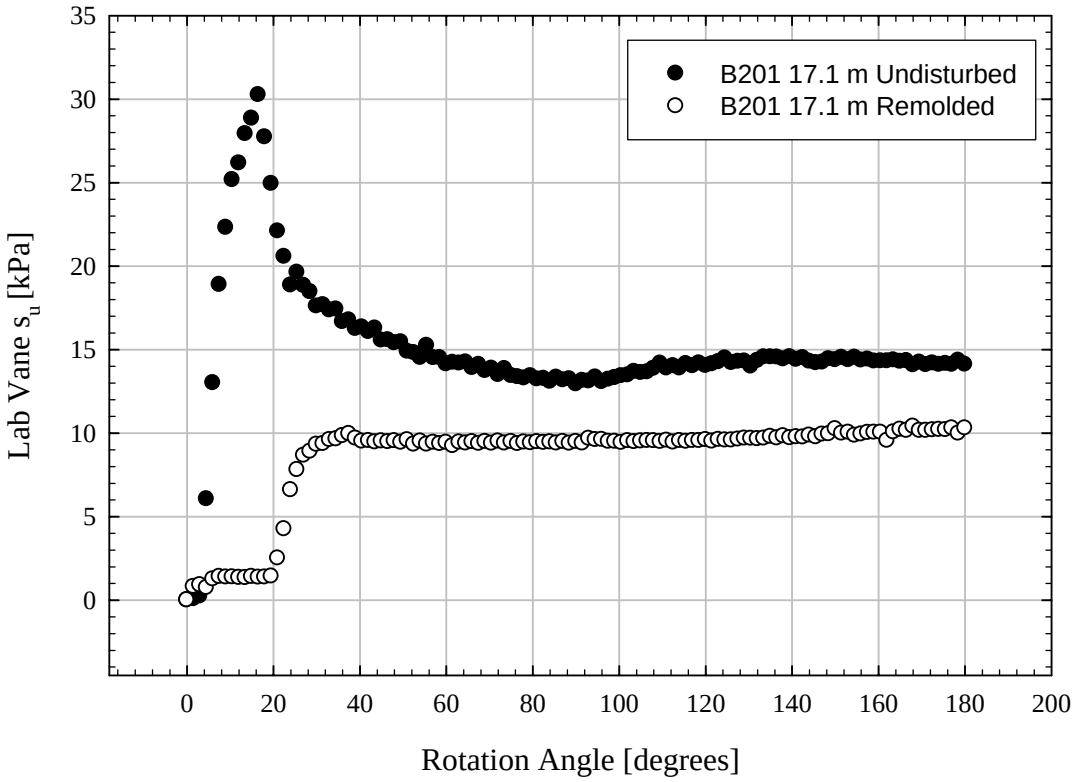
B201 17.1 m Undisturbed
B201 17.1 m Remolded
Lab Vane s_u [kPa]
Rotation Angle [degrees]
0
5
10
15
20
25
30
35
0
20
40
60
80
100
120
140
160
180
200

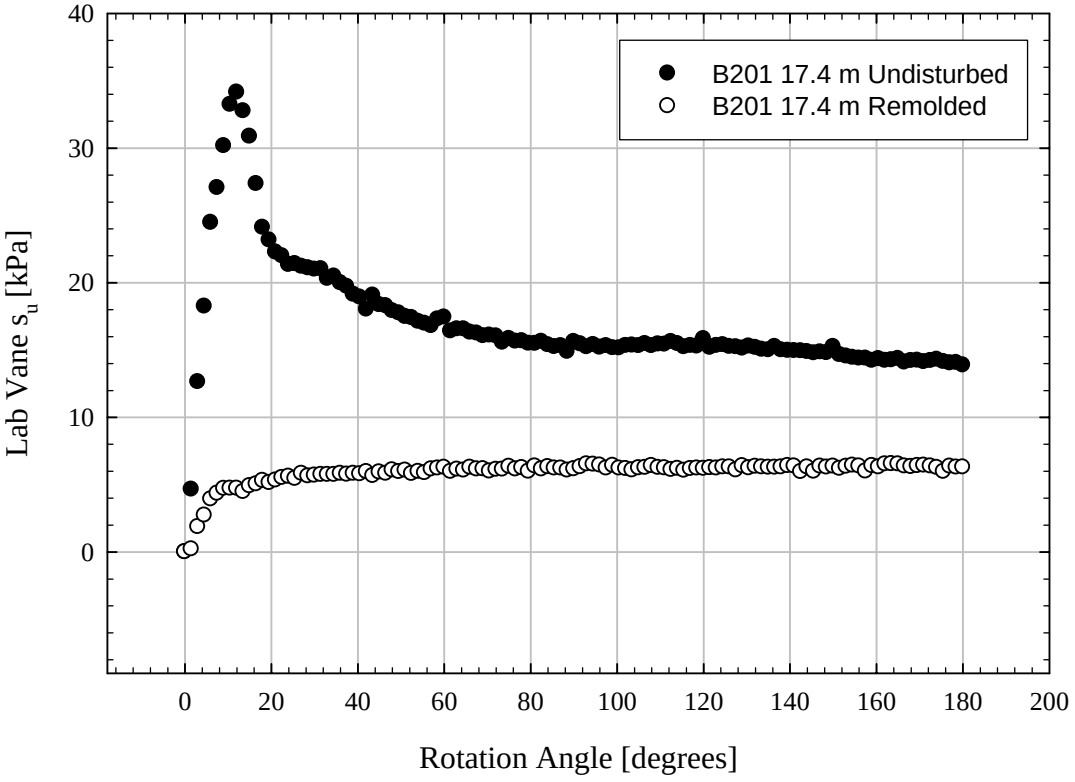
B201 17.4 m Undisturbed
B201 17.4 m Remolded
Lab Vane s_u [kPa]
Rotation Angle [degrees]
0
10
20
30
40
0
20
40
60
80
100
120
140
160
180
200

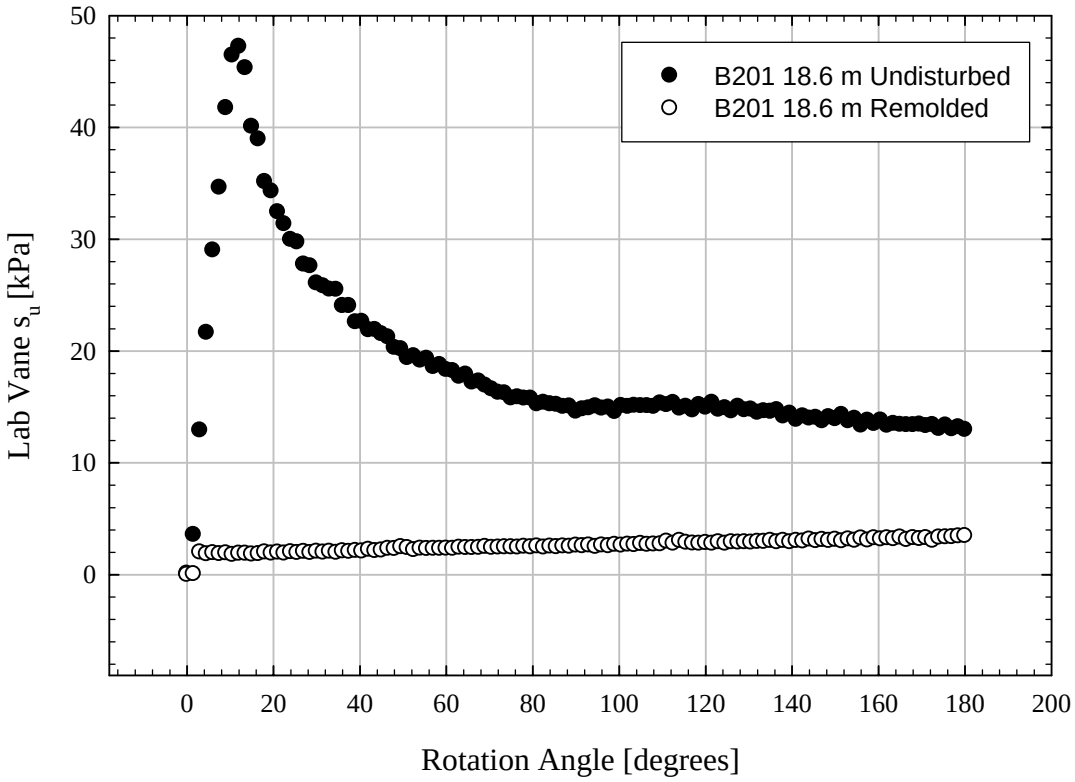
B201 18.6 m Undisturbed
B201 18.6 m Remolded
Lab Vane s_u [kPa]
Rotation Angle [degrees]
0
10
20
30
40
50
0
20
40
60
80
100
120
140
160
180
200

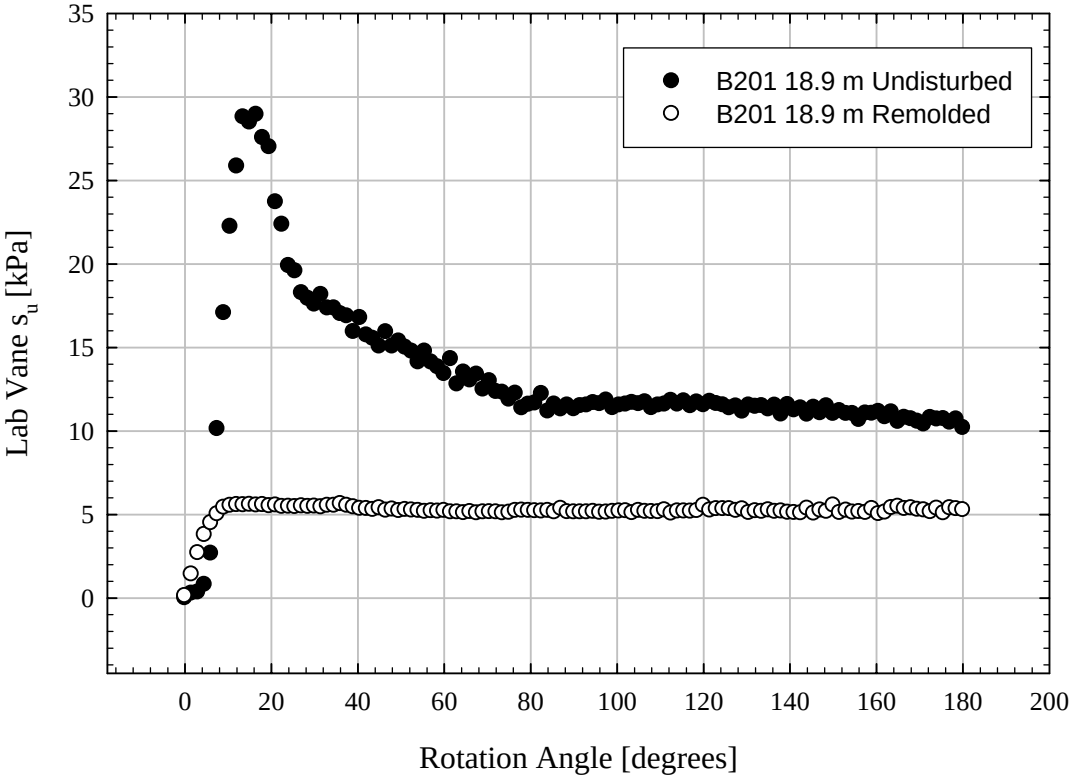
B201 18.9 m Undisturbed
B201 18.9 m Remolded
Lab Vane s_u [kPa]
Rotation Angle [degrees]
0
5
10
15
20
25
30
35
0
20
40
60
80
100
120
140
160
180
200

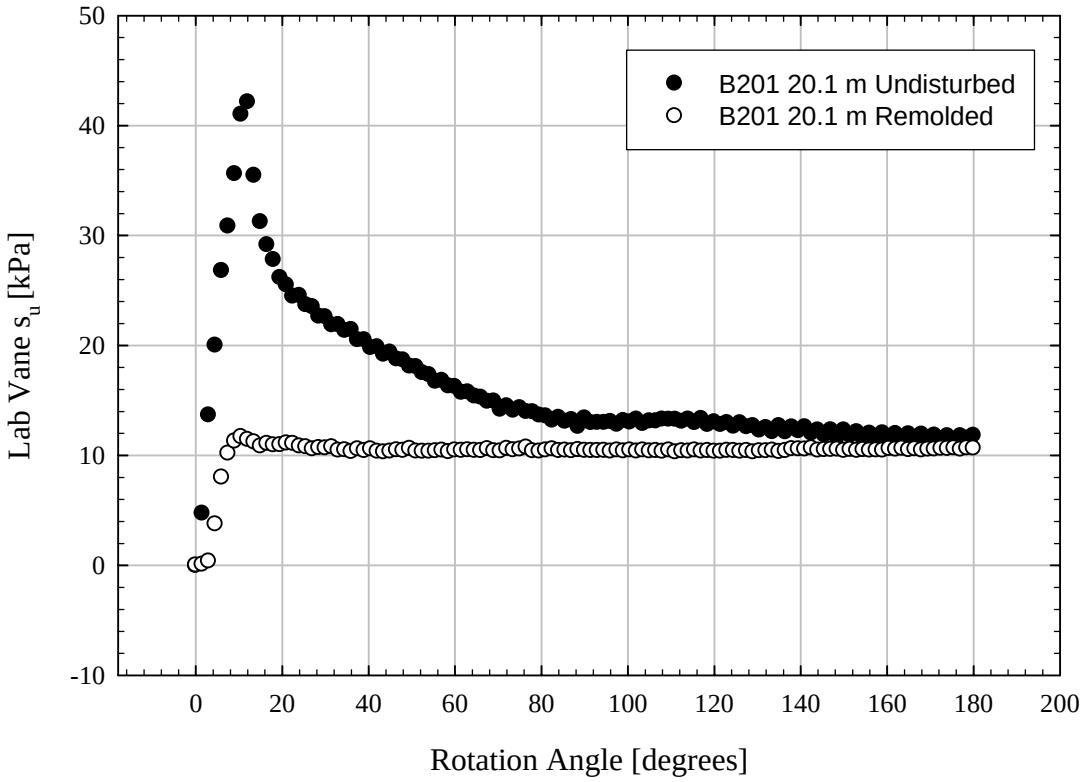
B201 20.1 m Undisturbed
B201 20.1 m Remolded
Lab Vane s_u [kPa]
Rotation Angle [degrees]
50
40
30
20
10
0
-10
0
20
40
60
80
100
120
140
160
180
200

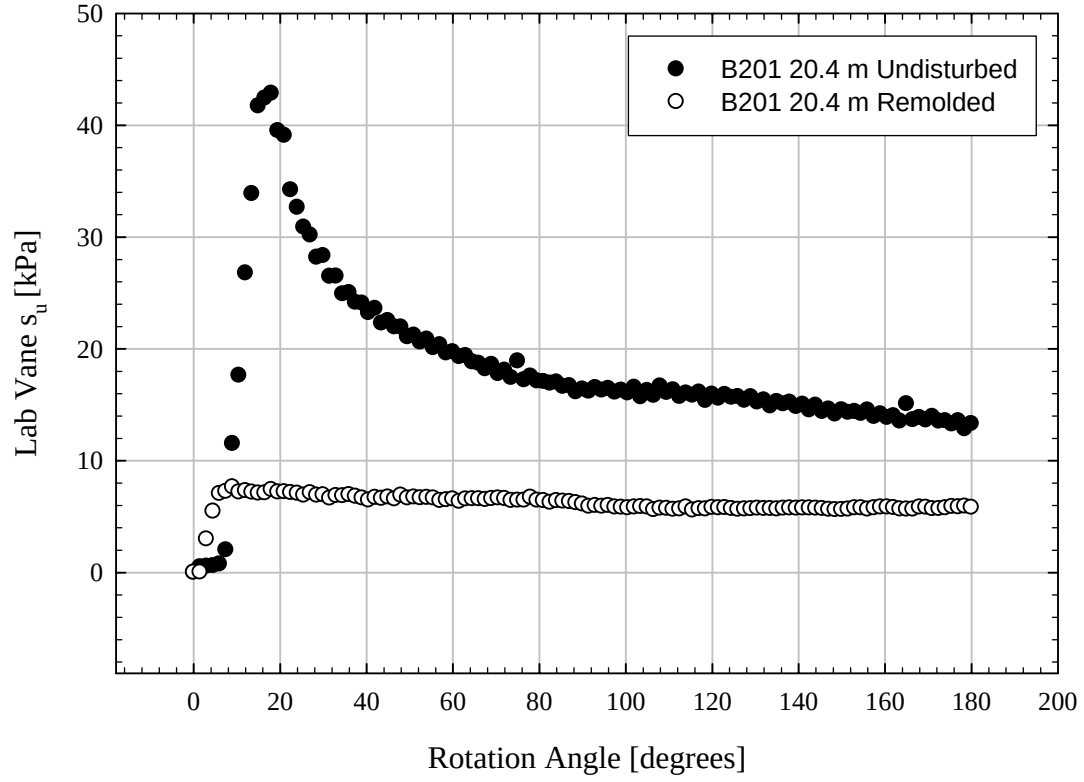
B201 20.4 m Undisturbed
B201 20.4 m Remolded
Lab Vane s_u [kPa]
Rotation Angle [degrees]
50
40
30
20
10
0
0
20
40
60
80
100
120
140
160
180
200

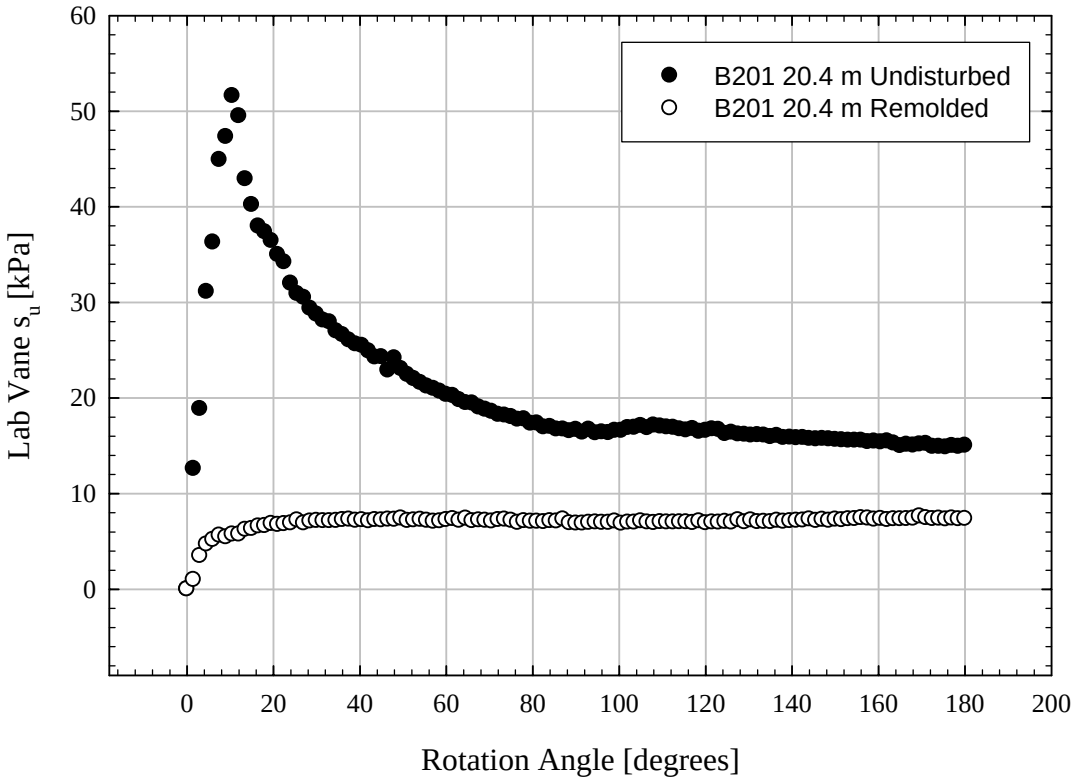
B201 20.4 m Undisturbed
B201 20.4 m Remolded
Lab Vane s_u [kPa]
Rotation Angle [degrees]
0
10
20
30
40
50
60
0
20
40
60
80
100
120
140
160
180
200

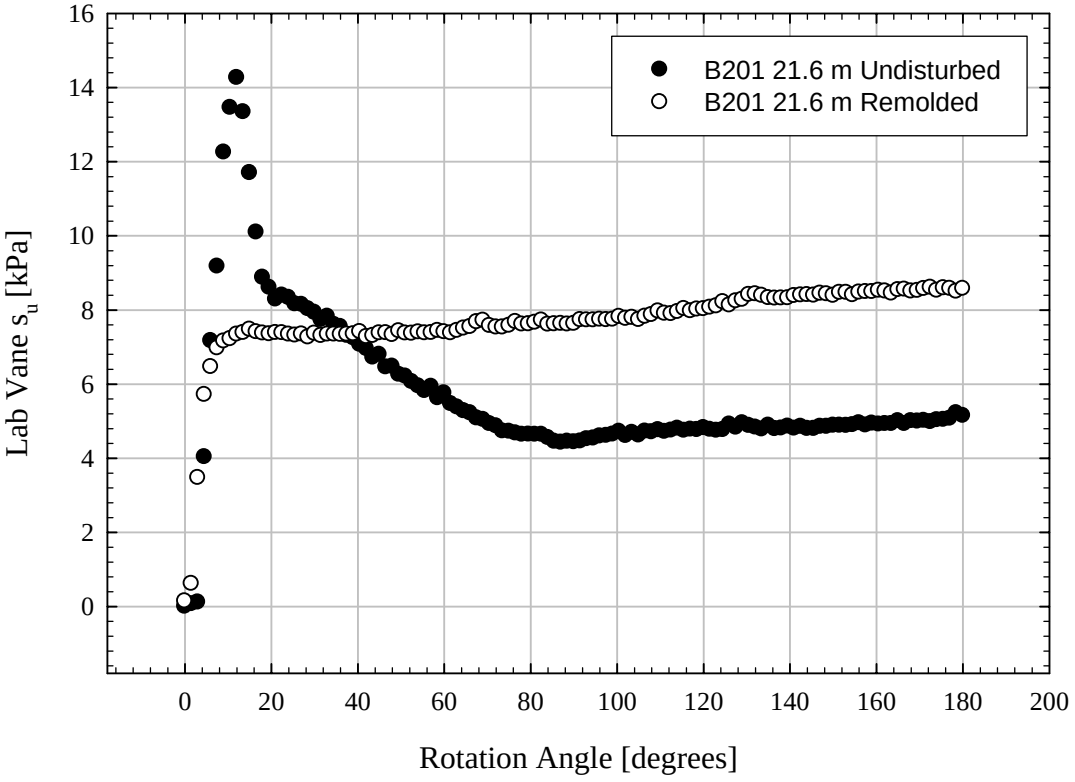
B201 21.6 m Undisturbed
B201 21.6 m Remolded
Lab Vane s_u [kPa]
Rotation Angle [degrees]
0
2
4
6
8
10
12
14
16
0
20
40
60
80
100
120
140
160
180
200

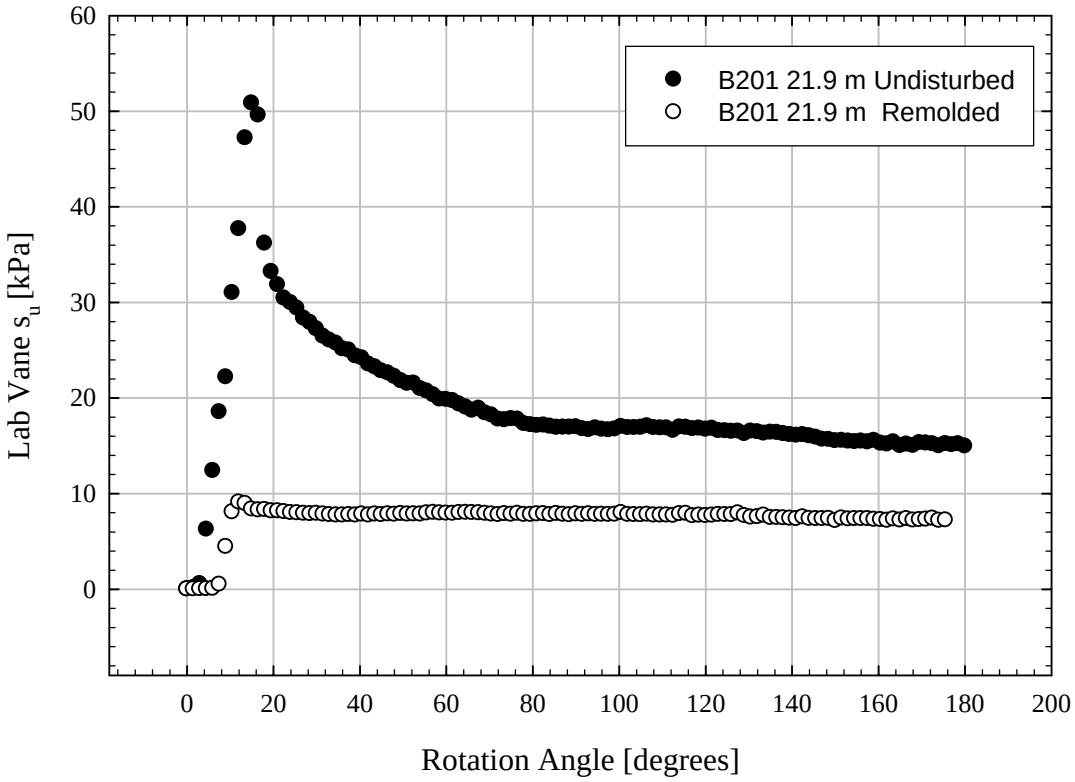
B201 21.9 m Undisturbed
B201 21.9 m Remolded
Lab Vane s_u [kPa]
Rotation Angle [degrees]
0
10
20
30
40
50
60
0
20
40
60
80
100
120
140
160
180
200

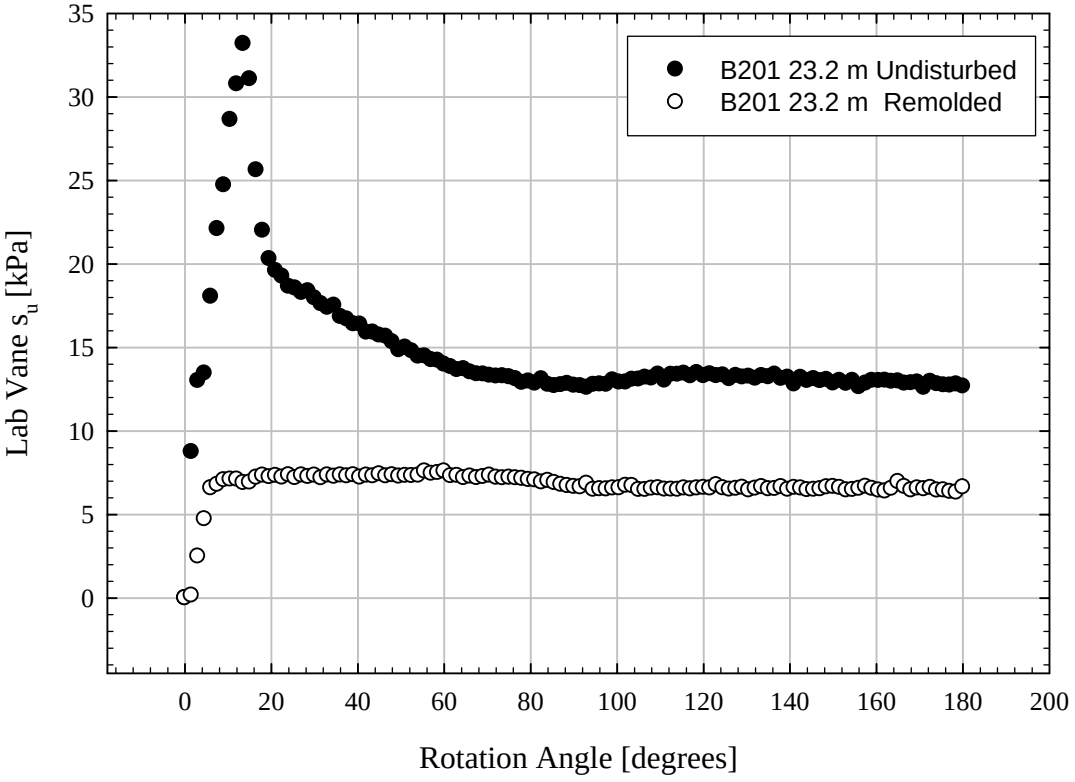
B201 23.2 m Undisturbed
B201 23.2 m Remolded
Lab Vane s_u [kPa]
Rotation Angle [degrees]
0
5
10
15
20
25
30
35
0
20
40
60
80
100
120
140
160
180
200

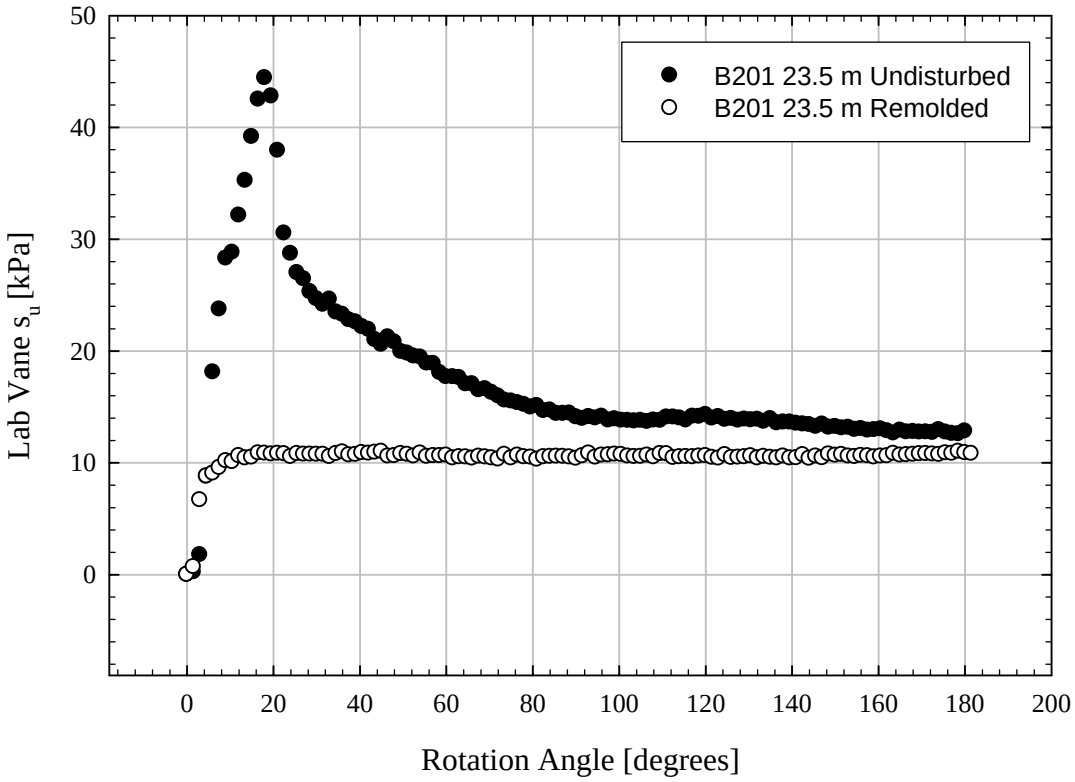
B201 23.5 m Undisturbed
B201 23.5 m Remolded
Lab Vane s_u [kPa]
Rotation Angle [degrees]
0
10
20
30
40
50
0
20
40
60
80
100
120
140
160
180
200

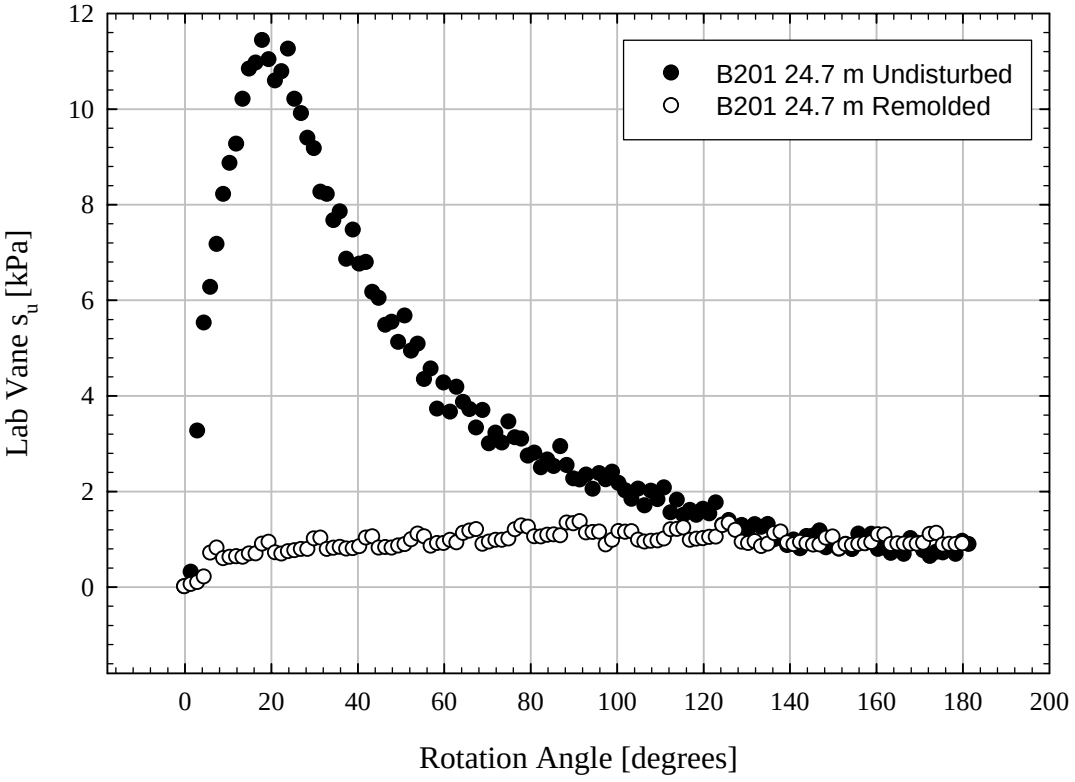
B201 24.7 m Undisturbed
B201 24.7 m Remolded
Lab Vane s_u [kPa]
Rotation Angle [degrees]
0
2
4
6
8
10
12
0
20
40
60
80
100
120
140
160
180
200

Figure

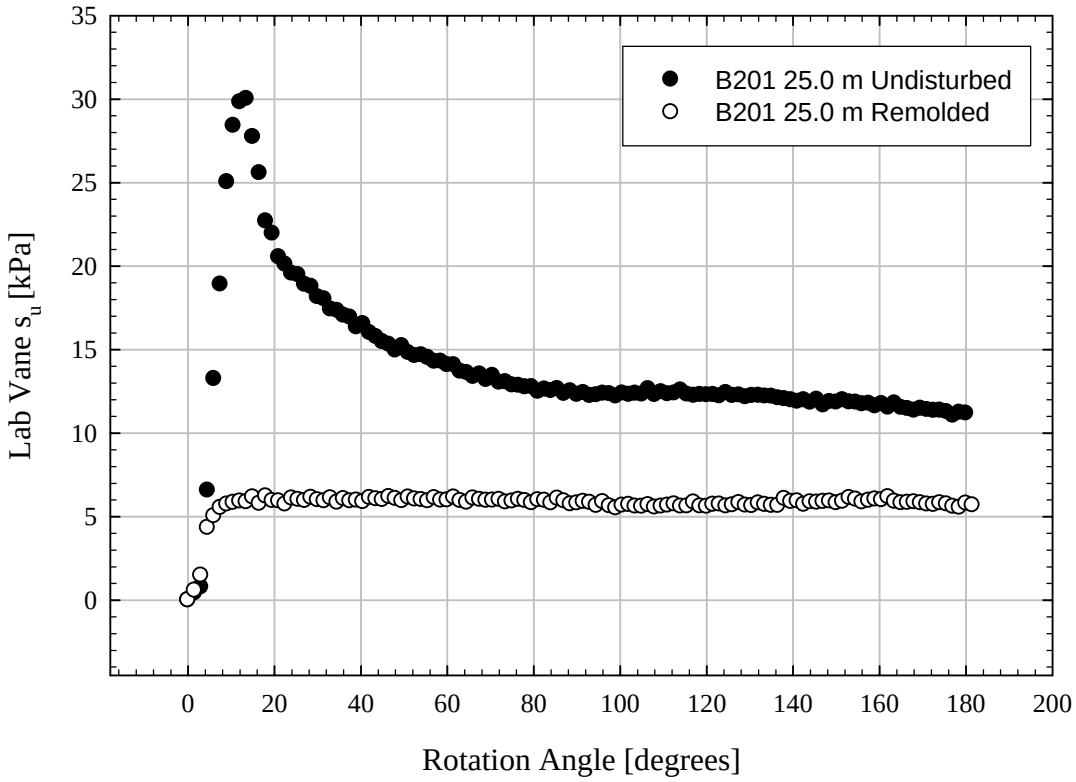
B201 25.0 m Undisturbed
B201 25.0 m Remolded
Lab Vane s_u [kPa]
Rotation Angle [degrees]
0
5
10
15
20
25
30
35
0
20
40
60
80
100
120
140
160
180
200

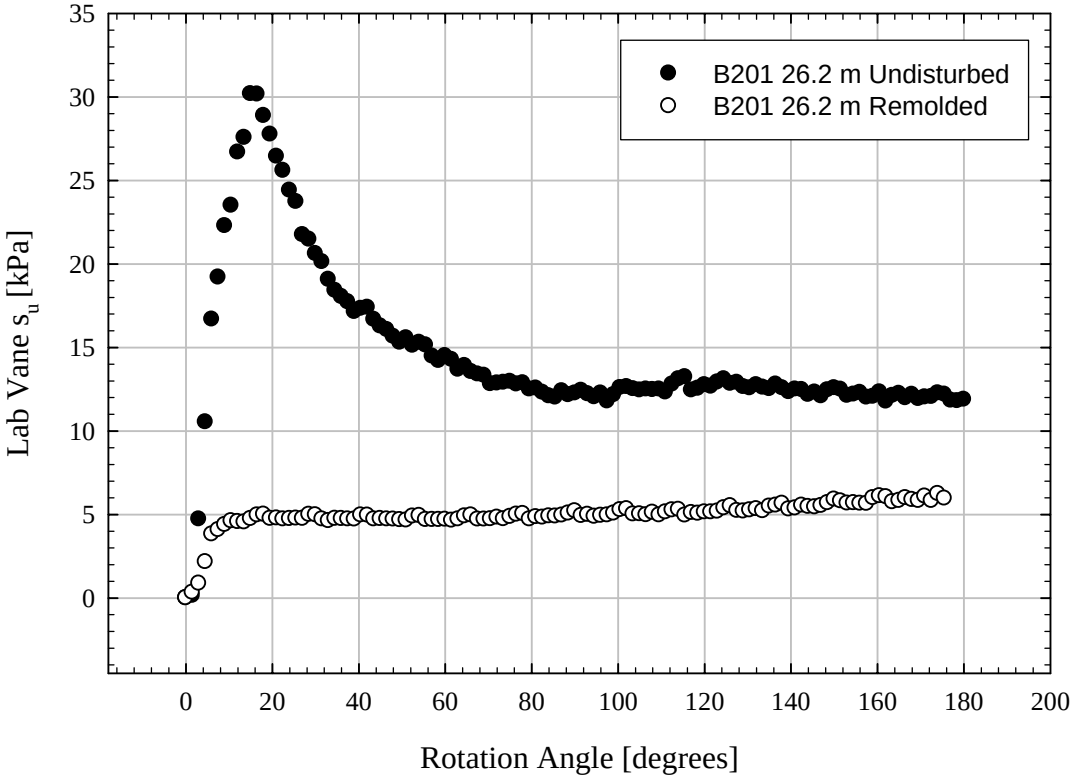
B201 26.2 m Undisturbed
B201 26.2 m Remolded
Lab Vane s_u [kPa]
Rotation Angle [degrees]
0
5
10
15
20
25
30
35
0
20
40
60
80
100
120
140
160
180
200

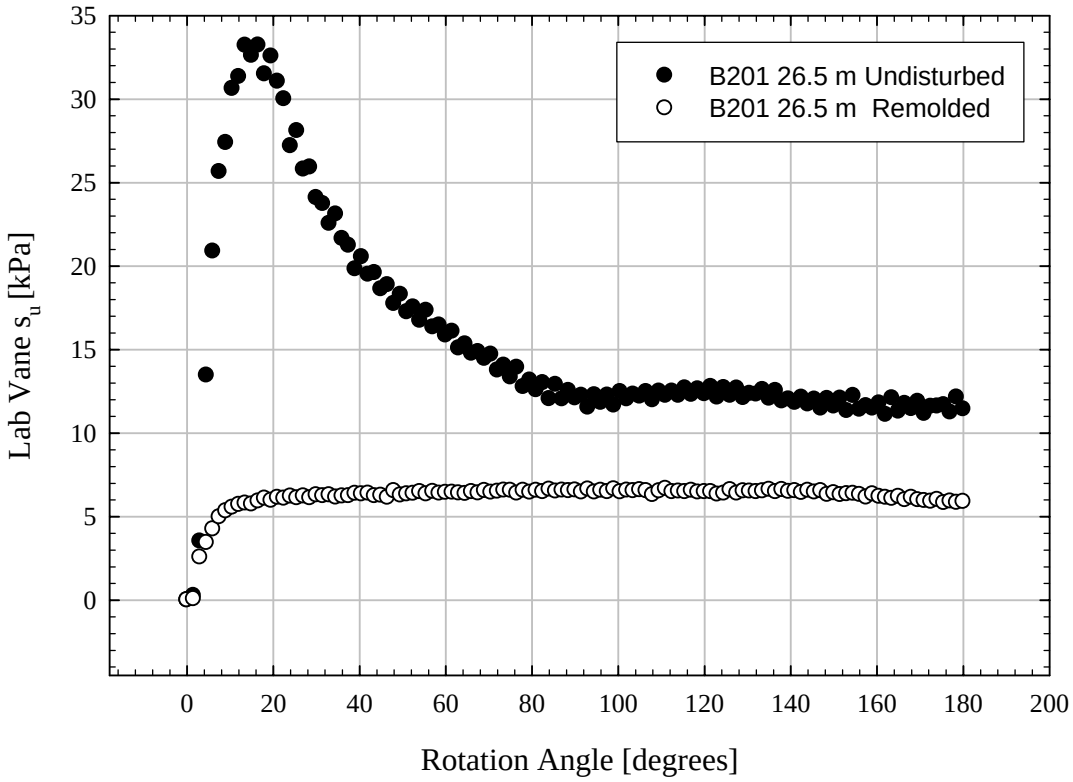
B201 26.5 m Undisturbed
B201 26.5 m Remolded
Lab Vane s_u [kPa]
Rotation Angle [degrees]
0
5
10
15
20
25
30
35
0
20
40
60
80
100
120
140
160
180
200

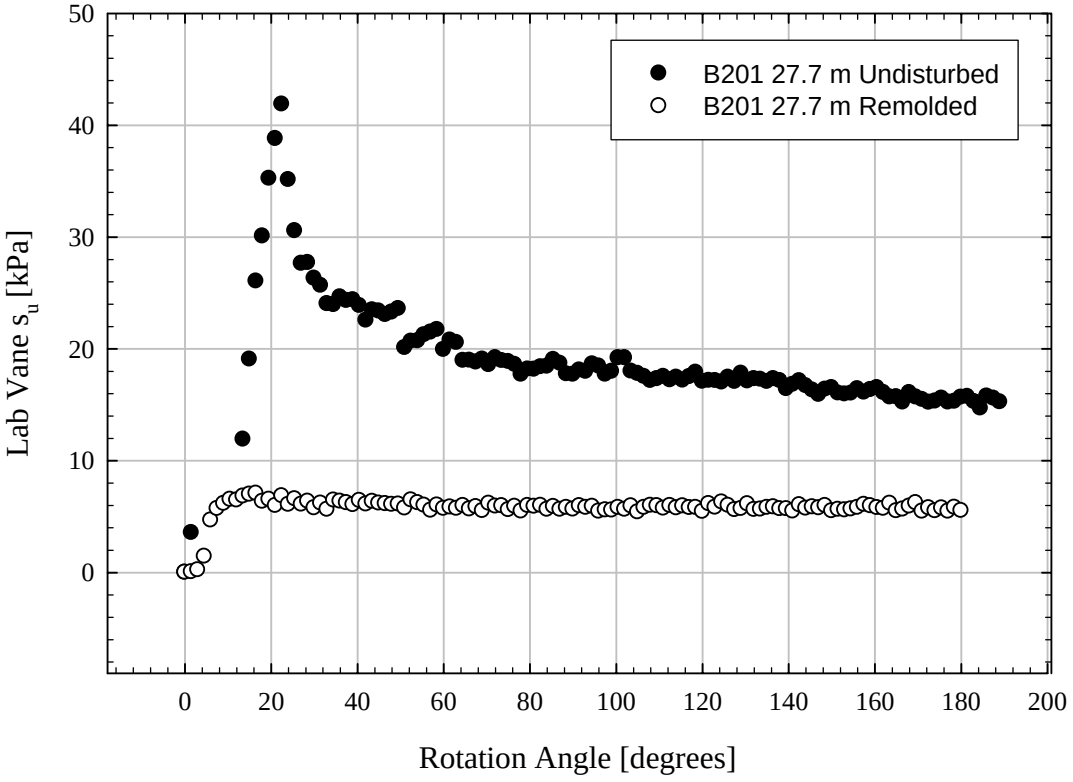
B201 27.7 m Undisturbed
B201 27.7 m Remolded
Lab Vane s_u [kPa]
Rotation Angle [degrees]
0
10
20
30
40
50
0
20
40
60
80
100
120
140
160
180
200

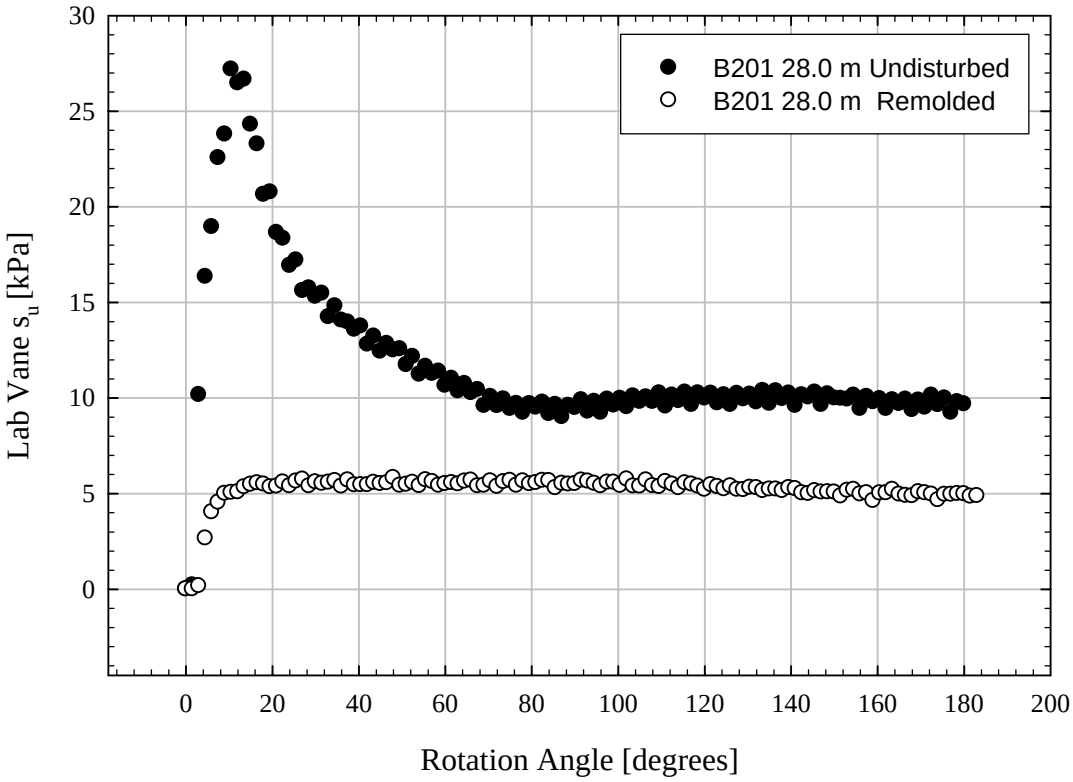
B201 28.0 m Undisturbed
B201 28.0 m Remolded
Lab Vane s_u [kPa]
Rotation Angle [degrees]
0
5
10
15
20
25
30
0
20
40
60
80
100
120
140
160
180
200

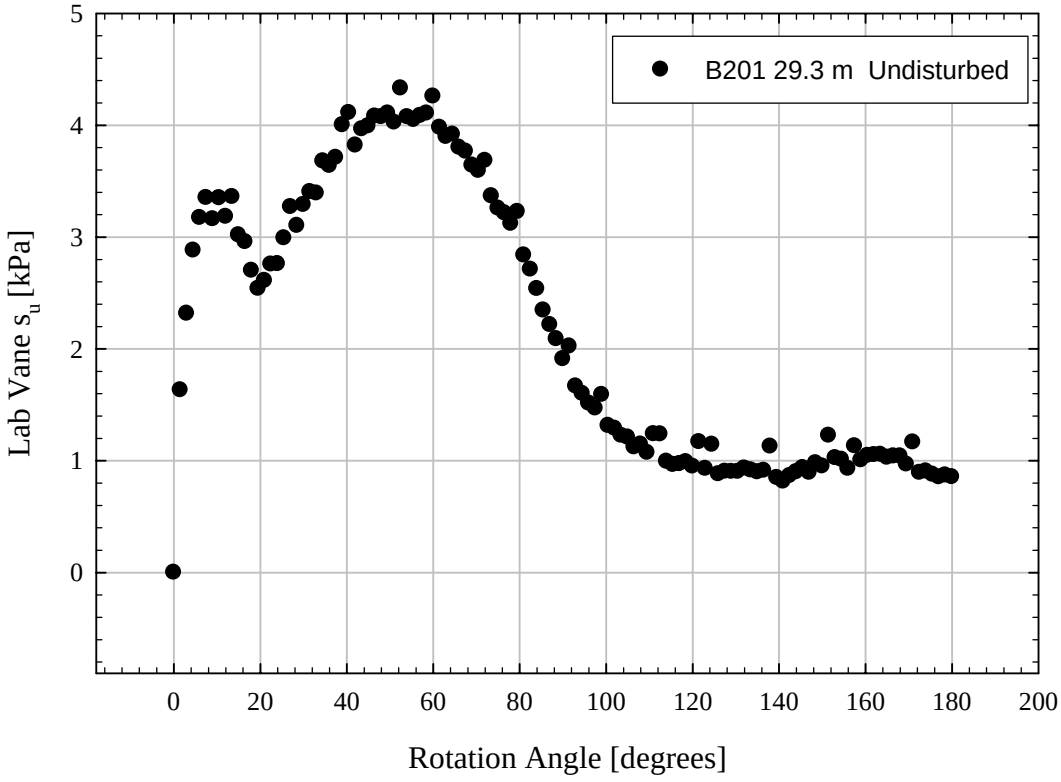
B201 29.3 m Undisturbed
Lab Vane s_u [kPa]
Rotation Angle [degrees]
0
1
2
3
4
5
0
20
40
60
80
100
120
140
160
180
200

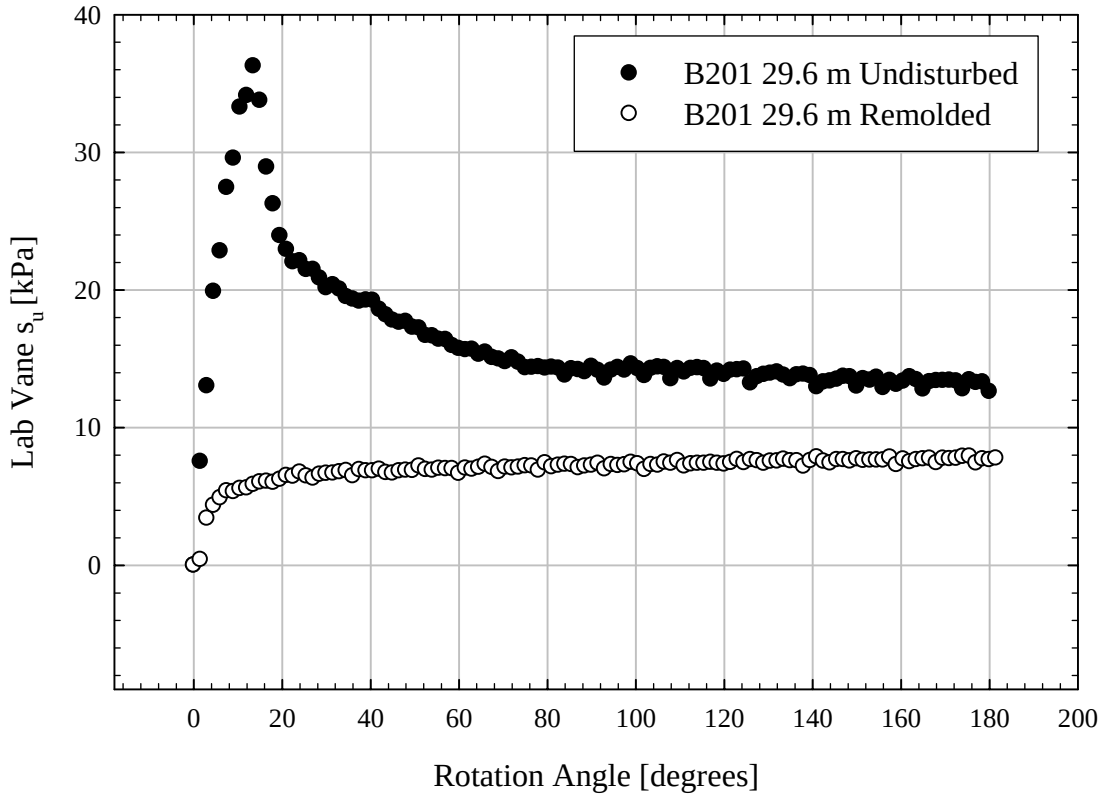
B201 29.6 m Undisturbed
B201 29.6 m Remolded
Lab Vane s_u [kPa]
Rotation Angle [degrees]
40
30
20
10
0
0
20
40
60
80
100
120
140
160
180
200

APPENDIX C: Earth Pressure Cell Readings

Registered Pressures, Earth Pressure Cell 1A1

Date	Temp. (C°)	Digits	Stress (kPa)	Stress (psi)
8/25/2006	19.4	8830.6	0.0	0.0
8/25/2006	20.5	8794.6	1.0	0.1
8/30/2006	14.8	8824.5	-0.2	0.0
8/30/2006	14.5	8826.0	-0.3	0.0
9/6/2006	12.2	8804.8	0.0	0.0
9/6/2006	12.2	8802.7	0.1	0.0
9/7/2006	12.1	8785.6	0.5	0.1
9/7/2006	12.2	8783.6	0.6	0.1
9/7/2006	12.1	8784.2	0.5	0.1
9/7/2006	12.0	8781.8	0.6	0.1
9/7/2006	12.0	8783.5	0.6	0.1
9/7/2006	12.1	8786.2	0.5	0.1
9/7/2006	11.9	8794.2	0.3	0.0
9/7/2006	12.0	8795.3	0.3	0.0
9/14/2006	17.1	8206.1	15.1	2.2
9/19/2006	14.3	8279.5	13.1	1.9
10/5/2006	14.3	7773.3	25.5	3.7
11/16/2006	13.2	7463.2	33.0	4.8
12/14/2006	12.3	7572.0	30.2	4.4
1/18/2007	10.6	7256.7	37.8	5.5
5/24/2007	8.4	7467.7	32.5	4.7
7/27/2007	11.1	7604.2	29.4	4.3
8/29/2007	11.0	7638.0	28.5	4.1

Registered Pressures, Earth Pressure Cell 1A2

Date	Temp. (C°)	Digits	Stress (kPa)	Stress (psi)
8/25/2006	18.5	8915.5	0.0	0.0
8/30/2006	18.5	8921.5	-0.1	0.0
8/30/2006	24.8	8960.0	-0.7	-0.1
9/6/2006	17.6	8700.8	4.9	0.7
9/6/2006	17.5	7665.7	28.9	4.2
9/7/2006	17.6	7836.5	25.0	3.6
9/7/2006	17.6	7999.7	21.2	3.1
9/7/2006	17.8	7883.7	23.9	3.5
9/7/2006	17.6	7859.4	24.5	3.5
9/7/2006	17.6	7696.0	28.2	4.1
9/7/2006	17.6	7509.5	32.6	4.7
9/7/2006	17.6	7380.9	35.6	5.2
9/14/2006	19.2	8045.0	20.2	2.9
9/19/2006	17.3	8473.3	10.2	1.5
10/5/2006	15.0	7277.7	37.8	5.5
11/16/2006	10.7	5371.9	81.8	11.9
12/14/2006	7.3	5651.1	75.1	10.9
1/18/2007	5.6	5991.5	67.1	9.7
5/24/2007	9.5	5732.2	73.4	10.6
7/27/2007	15.4	5716.0	74.1	10.7
8/29/2007	16.5	4558.2	101.0	14.7

Registered Pressures, Earth Pressure Cell 1A3

Date	Temp. (C°)	Digits	Stress (kPa)	Stress (psi)
8/25/2006	23.7	8936.6	0.0	0.0
8/30/2006	19.7	8929.4	-0.1	0.0
8/30/2006	23.7	8991.1	-1.3	-0.2
9/6/2006	19.9	8916.8	0.3	0.0
9/6/2006	20.2	8913.1	0.4	0.1
9/7/2006	19.2	8894.7	0.7	0.1
9/7/2006	19.2	8841.1	2.0	0.3
9/7/2006	19.2	8760.6	3.9	0.6
9/7/2006	19.2	8791.7	3.1	0.5
9/7/2006	19.2	8763.5	3.8	0.6
9/7/2006	19.1	8769.9	3.6	0.5
9/7/2006	19.1	8767.6	3.7	0.5
9/7/2006	19.1	8740.5	4.3	0.6
9/14/2006	21.1	8928.7	0.0	0.0
9/19/2006	20.8	8974.3	-1.0	-0.2
10/5/2006	13.9	8884.1	0.7	0.1
11/16/2006	9.5	8954.8	-1.2	-0.2
12/14/2006	4.2	8938.2	-1.1	-0.2
1/18/2007	-0.4	8762.7	2.7	0.4
5/24/2007	12.5	8872.5	0.9	0.1
7/27/2007	21.5	8796	3.2	0.5
8/29/2007	21.6	8780	3.6	0.5

Registered Pressures, Earth Pressure Cell 1A4.

Date	Temp. (C°)	Digits	Stress (kPa)	Stress (psi)
9/6/2006	25.5	8963.0	0.0	0.0
9/6/2006	21.8	8872.5	2.0	0.3
9/6/2006	26.7	8863.6	2.6	0.4
9/7/2006	16.9	8625.7	7.8	1.1
9/7/2006	17.1	6355.0	65.8	9.5
9/7/2006	17.3	8413.4	13.3	1.9
9/7/2006	17.4	8131.6	20.5	3.0
9/7/2006	17.7	7915.3	26.0	3.8
9/7/2006	17.9	7794.4	29.2	4.2
9/14/2006	18.8	7193.4	44.6	6.5
9/19/2006	18.5	7278.4	42.4	6.1
10/5/2006	14.5	7039.5	48.1	7.0
11/16/2006	11.0	6228.1	68.5	9.9
12/14/2006	7.1	6322.4	65.8	9.5
1/18/2007	3.6	6206.6	68.4	9.9
5/24/2007	10.3	6086.5	72.1	10.5
7/27/2007	23.1	5928.6	77.3	11.2
8/29/2007	24.9	5972.9	76.3	11.1

Registered Pressures, Earth Pressure Cell 1A5.

Date	Temp. (C°)	Digits	Stress (kPa)	Stress (psi)
9/6/2006	24.3	8833.7	0.0	0.0
9/6/2006	23.9	8732.8	2.6	0.4
9/6/2006	28	8537.6	8.0	1.2
9/7/2006	17.8	5576.8	84.0	12.2
9/7/2006	17.8	8497.9	8.1	1.2
9/7/2006	17.7	8355.5	11.8	1.7
9/7/2006	17.7	8310.6	13.0	1.9
9/7/2006	17.7	8159.8	16.9	2.5
9/7/2006	18.1	8154.3	17.1	2.5
9/7/2006	18.1	7805.5	26.1	3.8
9/14/2006	18.1	7193.4	42.0	6.1
9/14/2006	18.4	7249.0	40.6	5.9
10/5/2006	14.6	7334.7	38.0	5.5

11/16/2006	9.4	6649.4	55.4	8.0
12/14/2006	8.5	6770.4	52.1	7.6
1/18/2007	4.9	6864.1	49.4	7.2
5/24/2007	10.1	6493.0	59.5	8.63
7/27/2007	23.3	6104.9	70.8	10.3
8/29/2007	26.0	6019.1	73.3	10.6

Registered Pressures, Earth Pressure Cell 1A6.

Date	Temp. (C°)	Digits	Stress (kPa)	Stress (psi)
9/6/2006	25.0	8834.2	0	0
9/6/2006	25.8	8771.9	1.7	0.2
9/6/2006	31.4	8611.8	6.5	0.9
9/7/2006	17.8	7082.1	45.2	6.5
9/7/2006	17.6	8570.7	6.2	0.9
9/7/2006	17.6	7026.6	46.6	6.8
9/7/2006	17.6	8512.6	7.7	1.1
9/7/2006	17.7	8447.3	9.4	1.4
9/7/2006	17.8	8336.7	12.3	1.8
9/7/2006	18.1	8154.3	17.1	2.5
9/7/2006	18.2	8118.4	18.1	2.6
9/14/2006	18.5	7130.4	44.0	6.4
9/19/2006	19.2	7394.2	37.1	5.4
10/5/2006	14.7	7037.0	46.0	6.7
11/16/2006	9.2	6740.3	53.3	7.7
12/14/2006	8.7	6837.6	50.7	7.3
1/18/2007	5.1	6923.2	48.1	7.0
5/24/2007	10	6722.0	53.8	7.8
7/27/2007	23.2	6384.6	64	9.3
8/29/2007	26.3	6273.1	67.2	9.7

Registered Pressures, Earth Pressure Cell 2A1.

Date	Temp. (C°)	Digits	Stress (kPa)	Stress (psi)
9/14/2006	16.7	7753.0	0.0	0.0
9/19/2006	15.7	7829.0	-2.1	-0.3
9/19/2006	15.7	7892.6	-3.8	-0.5
9/19/2006	15.8	7181.0	14.9	2.2
10/5/2006	15.8	5189.1	67.3	9.8
11/16/2006	14.2	3957.4	99.5	14.4
12/14/2006	13.2	4138.8	94.6	13.7
1/18/2007	11.7	4287.0	90.5	13.1
5/24/2007	8.8	4734.1	78.5	11.4
7/27/2007	9.9	4228.8	91.9	13.3
8/29/2007	10.7	4289.3	90.4	13.1

Registered Pressures, Earth Pressure Cell 2A2.

Date	Temp. (C°)	Digits	Stress (kPa)	Stress (psi)
9/14/2006	17.0	8689.5	0.0	0.0
9/19/2006	19.1	8982.5	-6.6	-1.0
9/19/2006	19.3	8730.6	-0.8	-0.1
10/5/2006	16.9	8338.9	8.1	1.2
11/16/2006	11.2	8138.8	12.4	1.8
12/14/2006	10.6	8363.8	7.1	1.0
1/18/2007	5.4	7963.2	16.1	2.3
5/24/2007	9.6	8250.3	9.7	1.4
7/27/2007	14.4	8473.0	4.9	0.7
8/29/2007	15.6	8623.0	1.4	0.2

Registered Pressures, Earth Pressure Cell 2A3.

Date	Temp. (C°)	Digits	Stress (kPa)	Stress (psi)
9/14/2006	22.2	8878.8	0.0	0.0
9/19/2006	19.1	8729.2	3.3	0.5
9/19/2006	21.7	8904.6	-0.6	-0.1
10/5/2006	14.6	8864.9	0.0	0.0
11/16/2006	9.2	8978.6	-2.8	-0.4
12/14/2006	4.4	8981.1	-3.1	-0.4
1/18/2007	2.5	8908.4	-1.5	-0.2
5/24/2007	10.9	8886.2	-0.6	-0.1
7/27/2007	19	8862.0	0.3	0.0
8/29/2007	19.4	8874.1	0.0	0.0

Registered Pressures, Earth Pressure Cell 2A4.

Date	Temp. (C°)	Digits	Stress (kPa)	Stress (psi)
9/19/2006	16.6	9016.5	0	0
9/19/2006	22.3	8982.5	1.4	0.2
9/19/2006	20.4	8070.4	24.5	3.6
10/5/2006	14.2	7696.1	33.6	4.9
11/16/2006	11.9	6850.8	55.0	8.0
12/14/2006	7.6	6999.2	50.8	7.4
1/18/2007	3.7	6915.7	52.6	7.6
5/24/2007	9.8	6802.8	56.0	8.1
7/27/2007	23.3	6686.5	60.2	8.7
8/29/2007	25.3	6718.5	59.5	8.6

Registered Pressures, Earth Pressure Cell 2A5.

Date	Temp. (C°)	Digits	Stress (kPa)	Stress (psi)
9/19/2006	16.9	8949.2	0.0	0.0
9/19/2006	21.3	7873.4	28.0	4.1
9/19/2006	19.4	8033.8	23.7	3.4
10/5/2006	13.9	6518	62.0	9.0
11/16/2006	10.2	5845.3	78.9	11.4
12/14/2006	9.1	6052.4	73.5	10.7
1/18/2007	5.6	6214.2	69.1	10.0
5/24/2007	10.6	5769.8	80.9	11.7
7/27/2007	22.9	5424.2	90.9	13.2
8/29/2007	25.6	5409.8	91.5	13.3

Registered Pressures, Earth Pressure Cell 2A6.

Date	Temp. (C°)	Digits	Stress (kPa)	Stress (psi)
9/19/2006	17.3	8768.5	0.0	0.0
9/19/2006	20.5	7381.9	31.2	4.5
9/19/2006	19.1	7736.3	23.2	3.4
10/5/2006	13.9	6706.7	46.1	6.7
11/16/2006	10	5859.3	64.9	9.4
12/14/2006	9.1	6019.7	61.3	8.9
1/18/2007	5.8	6137.8	58.5	8.5
5/24/2007	10.2	5767.7	67.0	9.7
7/27/2007	22.2	5340.2	77.0	11.2
8/29/2007	24.8	5304.2	78.0	11.3